Thermodynamic optimisation of ORC systems using hybrid renewable energy sources and nanofluid-zeotropic mixtures

by

EBENEZER NYARKO KUMI

submitted in accordance with the requirements
for the degree of

DOCTOR OF PHILOSOPHY

at the

UNIVERSITY OF SOUTH AFRICA

SUPERVISOR: PROFESSOR CHRISTOPHER CHINTUA ENWEREMADU

CO-SUPERVISOR: PROFESSOR VASUDEVA RAO VEEREDHI

JANUARY 2026

Abstract

This study examines the thermodynamic performance of a hybrid solar–biomass Organic Rankine Cycle system, focusing on the selection of the working fluid and the integration of nanoparticle-enhanced zeotropic mixtures. The work is motivated by the need for decentralised renewable energy systems in regions such as sub-Saharan Africa, where solar potential is high but inconsistent, and biomass provides a reliable complementary resource.

A simulation framework was developed using ASPEN Plus V14, with the Peng–Robinson Equation of state used to estimate thermophysical properties. The hybrid heat source configuration combines evacuated-tube solar collectors with a biomass-fired boiler, stabilised by a buffer tank to ensure a consistent thermal input to the ORC evaporator. System performance was assessed under solar-dominant, balanced, and biomass-dominant scenarios, with operating temperatures ranging from 120 to 200 °C.

Two sets of zeotropic mixtures were evaluated; transitional refrigerants (R245fa/R123, R245fa/R1233zd(E), and R1233zd(E)/R123) and newer low-GWP alternatives (R1224yd(Z)/R1233zd(E), R1224yd(Z)/R1336mzz(Z), and R1233zd(E)/R1336mzz(Z)). Performance metrics included thermal efficiency, net power output, and heat absorption, supported by system-level indicators such as condenser load and specific work. Nanoparticles of Ag, Al_2O_3, CuO, TiO_2, and ZnO were introduced at varying concentrations to examine their effect on thermal conductivity and cycle stability.

Results show that zeotropic mixtures significantly improve thermal matching in heat exchangers through temperature glide, thereby reducing irreversibility and enhancing cycle efficiency. Among the tested fluids, R1233zd(E)/R123 and R1224yd(Z)/R1233zd(E) demonstrated the best performance, delivering higher net power and efficiency across a range of conditions. Ag nanoparticles provided the most substantial enhancement, achieving up to a 16% efficiency improvement at optimal concentrations; however, higher mass fractions introduced viscosity penalties and stability concerns. Oxide nanoparticles yielded modest but more stable performance.

The findings demonstrate the technical feasibility of hybrid solar–biomass ORC systems using advanced fluid formulations. While the study is limited to thermodynamic modelling, it provides a reproducible foundation for future experimental validation and techno-economic assessments. The work contributes to ongoing efforts to develop sustainable, decentralised energy systems suitable for regions with variable renewable resources.

Key Terms:
Organic Rankine Cycle (ORC), Zeotropic Mixtures, Nanoparticle-Enhanced Fluids, Aspen Plus, Thermal Efficiency, Hybrid Energy Systems, Solar-Biomass Integration, Low-Grade Heat Recovery, Sustainable Power Generation, Renewable Energy Modelling

Declaration

Name: Ebenezer Nyarko Kumi

Student number: 10127674

Degree: Doctor of Philosophy (90040)

Exact wording of the title of the thesis as appearing on the electronic copy submitted for examination:

Thermodynamic Optimisation of ORC Systems Using Hybrid Renewable Energy Sources and Nanofluid-Zeotropic Mixtures

I declare that ***Thermodynamic Optimisation of ORC Systems Using Hybrid Renewable Energy Sources and Nanofluid-Zeotropic Mixtures*** is my own work and that all the sources that I have used or quoted have been indicated and acknowledged by means of complete references, and that any use of Artificial Intelligence (AI) has been fully disclosed.

I further declare that I submitted the thesis/dissertation to the appropriate originality detection system which is endorsed by UNISA and that it falls within the accepted requirements for originality.

I further declare that I have not previously submitted this work, or part of it, for examination at UNISA for another qualification or at any other higher education institution.

I further declare that where Artificial Intelligence (AI) tools have been used in the preparation of this thesis/dissertation, their use has been limited to ethical permissible support, has been fully disclosed, and does not replace my own original research, my independent critical thinking and analysis, or authorship responsibilities.

I understand that failure to disclose AI use, plagiarism and/or lack of academic integrity may constitute academic misconduct under UNISA's policies.

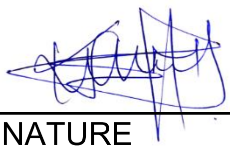

3rd July 2026

SIGNATURE DATE

Publications

This section presents research articles that are directly linked to the work undertaken in this thesis. Three papers have been produced to date. One has been published in a peer-reviewed journal, while the remaining two are at various stages of the review process. Additionally, one of these papers has been presented at an international conference.

Published Academic Journal Papers

1. **Kumi, E., Veeredhi, V. R., & Enweremadu, C. (2024).** Innovative Approaches for Improving ORC Performance: A Review of Pure Fluids, Zeotropic Mixtures, and Nanoparticles. Journal of Mechanical Engineering Science and Technology, 8(2), 253–270. http://dx.doi.org/10.17977/10.17977/um016v8i22024p253
2. **Kumi, E.N., Enweremadu, C.C. (2026).** Thermodynamic exploration of hybrid renewable ORC systems using HFO-based nanofluid zeotropic mixtures. *J Therm Anal Calorim* 151, 2651–2668. https://doi.org/10.1007/s10973-025-15230-4

Manuscript Accepted for Publication

1. **Kumi, E. N., Veeredhi, V. R., & Enweremadu, C. C. (2025)**. Optimising Organic Rankine Cycle Operations with Nanoparticle-Enhanced Zeotropic Mixtures: Modelling and Performance Evaluation. Manuscript accepted for publication in the Journal of Thermal Engineering (Manuscript No.: JTEN-2025-262)

Presented Conference Papers

1. **Kumi, E. N., Veeredhi, V. R., & Enweremadu, C. C**. (2024). Optimising Organic Rankine Cycle Operations with Nanoparticle-Enhanced Zeotropic Mixtures: Modelling and Performance Evaluation. In Proceedings of the Sustainable, Clean & Emerging Energy Technologies Conference 2024, University of Nigeria, Nsukka.

Dedication

This work is lovingly dedicated to my mother, Madam Grace Tettey, whose unwavering support and sacrifices laid the foundation for all my pursuits; my siblings (Isaac, Gabriel and Dorothy) for their encouragement and belief in my journey; and to my wife, Helena Afua Dogbey Karde, whose love, patience, and strength have been my constant source of inspiration.

Your faith in me has made this achievement possible.

Acknowledgments

"Being confident of this, that He who began a good work in you will carry it on to completion until the day of Christ Jesus." **- Philippians 1:6**

I begin by giving all glory to God Almighty, whose presence has been my anchor throughout this challenging journey. In moments of uncertainty, fatigue, and doubt, His grace sustained me. Intense intellectual demands and personal sacrifices marked the path to completing this thesis, yet through it all, God provided clarity, strength, and resilience. I am deeply grateful for His divine guidance, which illuminated each step and gave me the courage to persevere.

I would like to express my deepest gratitude to my supervisor, Professor Christopher Chintua Enweremadu, for his invaluable guidance, mentorship, and unwavering support throughout this research project. His insights and encouragement have been instrumental in shaping both the technical and academic rigour of this work.

I am equally grateful to my co-supervisor, Professor Vasudeva Rao Veeredhi, for his thoughtful feedback, constructive criticism, and commitment to excellence. His contributions have enriched the quality and clarity of this thesis.

Special thanks are due to the Department of Mechanical, Bioresources, and Biomedical Engineering at the University of South Africa, Science Campus, Florida, whose academic environment and resources provided the ideal platform for this research. I also acknowledge the administrative and technical staff for their assistance and professionalism.

Professor Emmanuel Kobla Glakpe provided a lot of inspiration for this work, and I greatly appreciate his support.

I am indebted to my family for their patience, understanding, and unwavering belief in my vision. Their emotional support made the long hours and challenges bearable.

Finally, I thank God Almighty for the strength, wisdom, and grace that enabled me to complete this work. Without divine guidance, none of this would have been possible.

Table of Contents

List of Figures

List of Tables

List of Abbreviations

Abbreviation	Description
ORC	Organic Rankine Cycle
HFO	Hydrofluoroolefin
GWP	Global Warming Potential
ODP	Ozone Depletion Potential
NPF	Nanoparticle Mass Fraction
Tglide	Temperature Glide
HTF	Heat Transfer Fluid
DNI	Direct Normal Irradiance
CFD	Computational Fluid Dynamics
LMTD	Log Mean Temperature Difference
HX	Heat Exchanger
Ts	Source Temperature
Tc	Condensation Temperature
Tevap	Evaporation Temperature
Wnet	Net Work Output
Qin	Heat Input
Qout	Heat Rejection
Ag	Silver
Al_2O_3	Aluminium Oxide
TiO_2	Titanium Dioxide
ZnO	Zinc Oxide
CuO	Copper Oxide
Aspen Plus	Process Simulation Software

List of Symbols

Symbol	Description	Units
η	Thermal efficiency	%
ηex	Exergy efficiency	%
$\dot{m}$	Mass flow rate	kg/s
$\dot{Q}$	Heat transfer rate	kW
$\dot{W}$	Power output	kW
T	Temperature	°C or K
P	Pressure	bar or Pa
h	Specific enthalpy	kJ/kg
s	Specific entropy	kJ/kg·K
c_p	Specific heat capacity at constant pressure	kJ/kg·K
M	Dynamic viscosity	Pa·s
K	Thermal conductivity	W/m·K
ρ	Density	kg/m^3
Φ	Nanoparticle volume fraction	–
ΔT	Temperature difference	K
ε	Effectiveness (e.g., of heat exchanger)	–

Chapter One

1 General Introduction

1.1 Background Information

Electricity has consistently been a fundamental driver of economic development, with a strong correlation between energy access and national prosperity. Countries with low electricity access rates have historically ranked among the poorest globally. Although the global electricity access rate rose to 90% by 2018, approximately 789 million people remained without access to electricity, with Sub-Saharan Africa (SSA) accounting for the largest share of this deficit (IEA, 2020). The average electricity access rate across SSA was 47%, as shown in Figure 1.1. More than half of the countries in the region had less than 50% of their populations connected to electricity, and only three had achieved universal access.

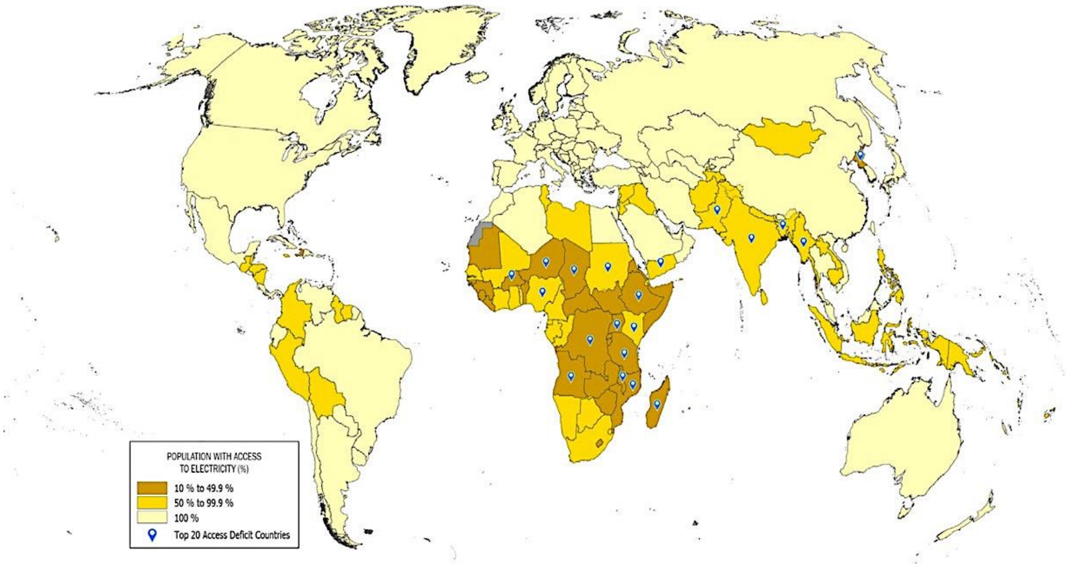

Figure 1.1: Global Electricity Access For 2018

Source: (IEA, 2020)

The global electricity generation sector has remained predominantly reliant on fossil fuels, including coal, natural gas, and crude oil, which together accounted for over 60% of total electricity production in 2019 (REN21, 2020). While the share of renewable energy (RE) in the global electricity mix has steadily increased, reaching

27.3% in 2019, its composition remains uneven. According to REN21 (2020), solar, biomass, and other non-hydro renewable energy systems contributed only 11.4% of global electricity generation. Hydropower alone represented more than half of the total RE share during the same period, as illustrated in

. Technologies such as solar photovoltaics (PV), geothermal energy, concentrated solar power (CSP), and ocean energy collectively accounted for a mere 3.2% of total electricity generation, while bio-power contributed only 2.2%. This underutilisation of renewable energy resources is not due to a lack of resource potential but rather to persistent technological and economic constraints that hinder their widespread adoption and integration. Among renewable energy technologies, solar energy stands out for its widespread availability, scalability, and relevance to regions with limited grid infrastructure.

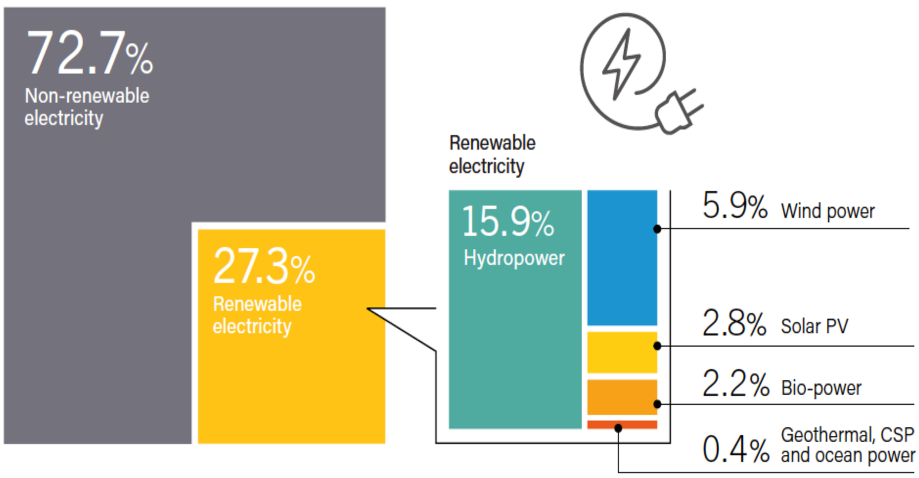

Figure 1.2: Global Electricity Generation Mix For 2019

Source: (REN21, 2020)

Solar energy serves as a primary energy source for both thermal and photovoltaic applications, supporting heating and electricity generation across various sectors. It is also widely regarded as an indirect source of energy for nearly all other terrestrial energy forms, except for geothermal and nuclear energy (Quaschning, 2014). Solar radiation plays a pivotal role in the formation of fossil fuels. It significantly influences weather and climate patterns, thereby affecting other renewable energy sources such as wind, wave, hydro, and biomass. As illustrated in Source: *(*ESMAP et al., 2019)

, all countries with electricity access rates below 50% (as shown in Figure 1.1) are in SSA, a region that receives substantial solar radiation (ESMAP *et al*., 2019). Average values for Global Horizontal Irradiance (GHI) and Direct Normal Irradiance (DNI) in SSA are approximately 6.2 kWh/m²/day and 6.0 kWh/m²/day, respectively. These figures underscore the region's considerable solar potential, providing a compelling rationale for increased investment in solar power infrastructure to enhance electricity access. Despite the abundance of solar radiation in SSA, solar energy remains intermittent due to diurnal and seasonal variations. Biomass, on the other hand, offers a more stable and dispatchable thermal resource, particularly in rural areas where agricultural residues are readily available. By integrating solar and biomass heat sources within a hybrid configuration, the system can achieve greater thermal continuity, reduce reliance on fossil-based backup systems, and enhance overall energy resilience. This hybrid approach is particularly suited to decentralised energy systems in off-grid communities.

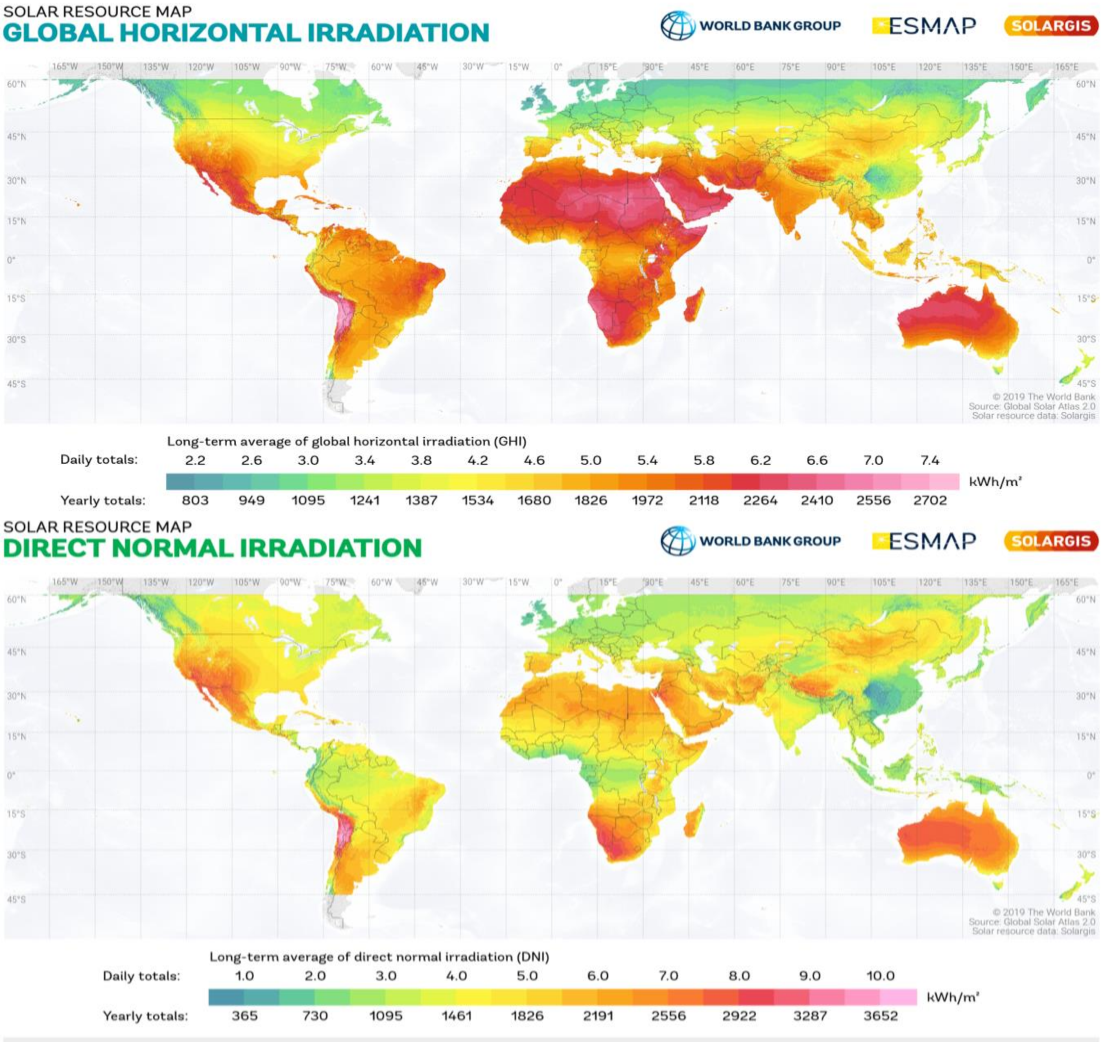

Figure 1.3: Global Solar Resource Map

Source: (ESMAP *et al*., 2019)

Thermal energy derived from sources such as biomass, solar radiation, industrial waste heat, and geothermal reservoirs typically has low temperatures but contains substantial energy. Despite this potential, the relatively low temperatures make these sources commercially unviable for conventional power generation systems. To address this limitation, several thermodynamic cycles have been developed to convert low-grade heat into mechanical work. These include the Rankine Cycle, Stirling Cycle, Kalina Cycle, Inverted Brayton Cycle, and Thermoelectric Energy Conversion systems (Cipollone *et al*., 2014). Among these, the Organic Rankine Cycle (ORC) has emerged as the most effective heat-driven technology for harnessing low-grade thermal energy to generate mechanical and electrical power. Its adaptability to a wide range of heat sources and working fluids has positioned it as a promising solution for sustainable energy conversion (Desideri *et al*., 2016; Vélez *et al*., 2012).

The Organic Rankine Cycle (ORC) differs from the conventional Rankine Cycle in two principal aspects: the temperature range of the heat source and the nature of the working fluid. While the conventional Rankine Cycle typically employs water and operates at temperatures exceeding 300 °C, the ORC is designed to utilise low-grade heat sources, often below 150 °C, and therefore requires organic fluids such as refrigerants and hydrocarbons with low boiling points and critical temperatures (Jiménez-García *et al*., 2023; Liang & Yu, 2021).

A basic ORC system comprises four main thermodynamic processes: pressurisation, evaporation, expansion, and condensation. Initially, the working fluid is pressurised by a pump and then heated at constant pressure in the evaporator until it vaporises. The vapour enters the expander (typically a turbine or scroll expander), where it expands and performs mechanical work that may be converted into electricity. The expanded vapour is subsequently condensed into a subcooled liquid in the condenser, and the cycle is completed as the fluid is recirculated to the pump (Wei *et al*., 2019; Yang *et al*., 2021).

Recent studies emphasise the importance of selecting appropriate working fluids based on thermophysical properties, environmental impact, and compatibility with low-temperature heat sources. Fluids such as R245fa, R1233zd(E), and zeotropic mixtures have demonstrated favourable performance in subcritical and regenerative ORC configurations, particularly when enhanced with nanoparticles or integrated into hybrid systems (Faghih & Pourshaghaghy, 2022; Herath *et al*., 2020).

ORC systems have gained prominence as a viable means of converting low-grade thermal energy into mechanical and electrical power. However, their efficiency remains constrained by the modest temperature levels of renewable heat sources such as solar and biomass. According to the second law of thermodynamics, the limited temperature differential between the heat source and sink inherently restricts the cycle's thermal efficiency (Yang *et al*., 2021). The selection of appropriate working fluids is, therefore, critical to enhancing ORC performance. Fluorine-based refrigerants, which are commonly used due to their environmental acceptability, often exhibit low critical temperatures, further limiting the efficiency of the refrigeration cycle. Although chlorine-based refrigerants historically offered superior thermodynamic properties, their adverse environmental impact led to their global phase-out.

To address these limitations, recent research has explored the use of zeotropic mixtures and nanoparticle-enhanced fluids (nanofluids) to enhance heat transfer and improve thermodynamic stability. Zeotropic mixtures enable temperature glide during phase transitions, enhancing thermal matching with variable heat sources and reducing irreversibilities in heat exchangers (Fergani *et al*., 2021; Zhang *et al*., 2020). Nanofluids, which are colloidal suspensions of nanoparticles in base fluids, have demonstrated improved thermal conductivity and exergy performance in ORC applications (Howard, 2022; Mondejar *et al*., 2017). These enhancements have shown potential to increase system efficiency by up to 17% compared to conventional fluids (Sami, 2020).

This study focused on the thermodynamic optimisation of a hybrid ORC system powered by solar and biomass heat sources, employing nanofluid-enhanced zeotropic mixtures as working fluids. The objective was to evaluate the performance of various fluid combinations and nanoparticle concentrations via simulation and to identify optimal configurations to improve efficiency and system-level resilience. To achieve meaningful performance improvements, this study employed thermodynamic optimisation techniques, including parametric analysis and multi-objective evaluation. Key performance indicators, including thermal efficiency, net power output, and pumping losses, were evaluated across various fluid compositions and nanoparticle concentrations. The optimisation framework was designed to identify configurations that balance energy conversion efficiency with system stability and environmental acceptability.

1.2 Justification

ORC systems are widely recognised as one of the most promising technologies for recovering low-grade thermal energy for electricity generation and other applications. Despite their potential, ORC systems continue to face significant challenges related to low thermal efficiencies. These limitations are primarily attributed to the modest operating temperatures of renewable heat sources and the physicochemical constraints of organic working fluids. Solar thermal energy has emerged as a key renewable heat source for ORC systems; however, its intermittent nature necessitates integration with complementary sources such as biomass to ensure continuous and reliable operation.

The search for more suitable organic working fluids has become increasingly important following the global phase-out of chlorine-based refrigerants due to their environmental hazards. Fluorine-based refrigerants, which replaced them under international protocols such as the Kyoto Protocol, are more environmentally acceptable but typically possess lower critical temperatures. This thermodynamic limitation results in reduced cycle efficiencies and, consequently, higher overall installation and operational costs. Collings (2018) notes that ORC systems tend to have higher capital costs compared to conventional power generation technologies. This is primarily due to the low driving temperatures, which result in smaller specific enthalpy drops across the turbine, necessitating larger components to achieve a comparable power output.

The temperature of the heat source is, therefore, a critical parameter in the design and optimisation of ORC systems. Liu *et al*. (2017) reported a maximum efficiency of 6.37% for an ORC system powered by a modelled waste-heat source at 200 °C. Wang *et al*. (2017) demonstrated that increasing the heat source temperature from 75 to 100 °C improved energy efficiency from 11.3 to 12.6% and exergy efficiency from 45.8 to 51.3%. Similarly, Dai *et al*. (2009) observed efficiency improvements of 11.5-13% through parametric optimisation at a heat source temperature of 145 °C. Biomass-fired ORC systems have achieved temperatures up to 300 °C, while solar-driven ORC systems have exhibited varying performance depending on the type of collector used (Ismail *et al*., 2016). Manolakos *et al*. (2009) reported low efficiencies in a solar-powered desalination plant using ORC, and comparative studies showed that parabolic trough collectors yielded efficiencies of 7.5 to 12.1%, outperforming evacuated tube collectors (4.2%) and flat-plate collectors (3.2%) (Canada *et al*., 2005; Freeman *et al*., 2015; Quoilin *et al*., 2010).

Hybridisation of solar and biomass heat sources offers a practical solution to the intermittency challenge, enabling more stable thermal input and improved system reliability. Biomass, being locally available and dispatchable, complements solar energy and enhances the feasibility of continuous ORC operation, particularly in off-grid and rural contexts. Combined heat and power systems based on ORC technology and solar thermal input have also demonstrated the advantage of incorporating inexpensive thermal energy storage to buffer fluctuations in solar irradiance (Freeman *et al*., 2017).

The selection of working fluid remains a pivotal factor in ORC system design and optimisation. Tocci *et al*. (2017) identified the choice of working fluid and expander design as major limitations to the widespread adoption of ORC technology. The transition from chlorine-containing refrigerants, such as R-11 and R-12, to fluorine-based alternatives, such as R-134a, has led to lower critical temperatures and, by extension, lower efficiencies. More suitable fluids such as R245fa and pentane have been employed in both experimental and commercial ORC systems (Liu *et al*., 2017; Muratori *et al*., 2017). Furthermore, Bellos and Tzivanidis (2017) reported a system efficiency of 20.11% for a solar-driven ORC using nanofluids in a parabolic trough collector. Andreasen *et al*. (2014) observed an increase in net power output when zeotropic mixtures were used instead of pure fluids.

Zeotropic mixtures offer distinct thermodynamic advantages due to their temperature glide during phase transitions. This property enables improved thermal matching with variable heat sources, thereby reducing exergy losses and enhancing overall cycle efficiency. Their application in ORC systems has shown promise in improving performance under fluctuating thermal conditions, such as those encountered in hybrid solar–biomass configurations. In parallel, nanofluids (colloidal suspensions of nanoparticles in base fluids) have demonstrated potential to enhance heat transfer and thermodynamic stability. Papadopoulos *et al*. (2010) proposed using computer-aided molecular design (CAMD) and process optimisation techniques to select optimal working fluids, a methodology later expanded by Mavrou *et al*. (2015) through multi-criteria evaluation frameworks.
Mondejar *et al*. (2017) reported a 4% reduction in heat exchanger size when using a 1% nanoparticle concentration, without adverse effects on pump power consumption, despite an 18% increase in pressure drop. Saadatfar *et al*. (2014) similarly reported improved cycle efficiency and reduced component sizing when nanoparticle-infused pentane was used as the working fluid. These findings underscore the potential of nanofluids not only to improve heat transfer but also to enable thermodynamic optimisation of ORC systems. By adjusting the nanoparticle type and concentration, it becomes possible to fine-tune fluid properties, such as thermal conductivity, viscosity, and stability, which are key parameters in maximising efficiency and minimising component size and cost.

In addition to possessing favourable thermophysical properties, suitable working fluids must also be safe, non-hazardous, and environmentally benign (Deniz, 2015). Considering the above, this research seeks to address the limitations of conventional ORC systems by exploring the thermodynamic optimisation of hybrid solar-biomass ORC configurations using nanofluid-enhanced zeotropic mixtures. Through simulation and parametric analysis, the study aims to identify fluid combinations and operating conditions that improve efficiency, reduce component sizing, and enhance system-level resilience, particularly for deployment in energy-constrained regions.

1.3 Problem Statement

Organic Rankine Cycle (ORC) systems have emerged as a promising technology for converting low-grade thermal energy into mechanical and electrical power. However, their widespread adoption remains limited due to inherently low thermal efficiencies (Lecompte *et al.*, 2015). These inefficiencies stem primarily from the modest temperatures of renewable heat sources such as solar and biomass, which result in low Carnot efficiencies and, by extension, reduced actual cycle efficiencies as dictated by the second law of thermodynamics.

A critical factor influencing ORC performance is the selection of the working fluid. While fluorine-based refrigerants are favoured for their environmental acceptability, having replaced chlorine-based refrigerants due to concerns about ozone depletion, they typically possess lower critical temperatures (Bederna *et al.*, 2021). This thermophysical limitation further reduces the efficiency of ORC systems, especially at low temperatures. Consequently, ORC systems often require larger components and more complex configurations to achieve comparable power output, resulting in higher installation and operational costs compared to conventional power generation technologies (Lemmens, 2016).

Moreover, the intermittent nature of solar energy necessitates integrating complementary heat sources, such as biomass, to ensure continuous operation. While hybridisation improves thermal reliability, it also introduces complexity in system design and fluid compatibility (Manente *et al.*, 2017). Recent advances suggest that zeotropic mixtures, fluids exhibiting non-isothermal phase change behaviour, can enhance thermal matching and reduce exergy losses. Additionally, nanoparticle doping has shown potential to enhance the thermophysical properties of working fluids, particularly thermal conductivity and heat capacity (Cao *et al*., 2023; Said *et al*., 2015).

Despite these promising developments, the combined use of zeotropic mixtures and nanoparticles in ORC systems remains underexplored. There is a lack of comprehensive studies evaluating how these enhancements impact system-level performance, particularly in hybrid configurations that utilise solar and biomass energy sources. This gap presents a significant barrier to optimising ORC systems for low-grade heat recovery and sustainable power generation.

1.4 Research Questions

The study sought to answer the following research questions:

i. What combination of solar thermal and biomass thermal sources can reliably provide adequate temperatures to operate an ORC power system?
ii. Can mixtures of existing organic working fluids be engineered to improve critical temperatures and other thermodynamic properties, thereby enhancing ORC cycle efficiency?
iii. To what extent can nanoparticles improve the thermophysical properties, including thermal conductivity, of organic working fluid mixtures used in ORC systems?
iv. How do variations in working fluid composition, nanoparticle concentration, and heat source temperature affect the overall thermal efficiency and net power output of hybrid ORC systems?

1.5 Research Objectives

The main objective of the study was to optimise the performance of a hybrid solar–biomass Organic Rankine Cycle system using nanoparticle-enhanced zeotropic mixtures as working fluids.

The specific objectives include;

i. To evaluate the thermal suitability of solar and biomass heat sources for hybrid ORC operation.

ii. To assess the impact of zeotropic working fluid mixtures on cycle efficiency and critical temperature.
iii. To investigate the effect of nanoparticle doping on the thermophysical properties of zeotropic mixtures.
iv. To simulate and optimise ORC system performance under varying fluid compositions and operating conditions.

1.6 Scope And Research Focus

The study focused on modelling and simulating a hybrid ORC system under various operating conditions, including different heat-source configurations, working-fluid compositions, and system configurations. Specifically, it examined the integration of solar thermal and biomass heat sources to ensure adequate and continuous thermal input for ORC operation.

The research investigated the thermodynamic performance of zeotropic mixtures formulated from selected organic fluids, and explored the potential of nanoparticle doping to enhance their thermophysical properties. While nanoparticle-infused pure fluids have been studied in previous literature, their application within zeotropic mixtures remains largely unexplored. This study, therefore, extended existing knowledge by simulating the effects of nanoparticle doping in zeotropic mixtures and evaluating its impact on ORC performance.

Performance assessments and evaluations were conducted using ASPEN Plus, with the Peng-Robinson equation of state, employed to model non-ideal fluid behaviour. Thermophysical property data were adjusted to account for nanoparticle effects, and sensitivity analyses were conducted to determine the optimal fluid compositions, nanoparticle concentrations, and operating conditions for enhanced cycle efficiency and net power output.

Chapter Two

2 Literature Review

2.1 Overview of Organic Rankine Cycles

The ORC shares its foundational principles with the conventional Rankine Cycle, which uses water as the working fluid. In both systems, a high-pressure fluid in a superheated vapour state expands through a turbine, producing mechanical work. The fluid then exits the turbine as a low-pressure, saturated liquid-vapour mixture, which is fully condensed in the condenser before being pressurised by a pump and returned to the boiler or heat exchanger for heat addition, thus completing the cycle.

A simple ORC system, illustrated in Figure *2.1*, comprises four key components;

i. Evaporator - for heat addition
ii. Expander - for mechanical work output
iii. Condenser - for heat rejection
iv. Pump - to increase fluid pressure before entering the evaporator

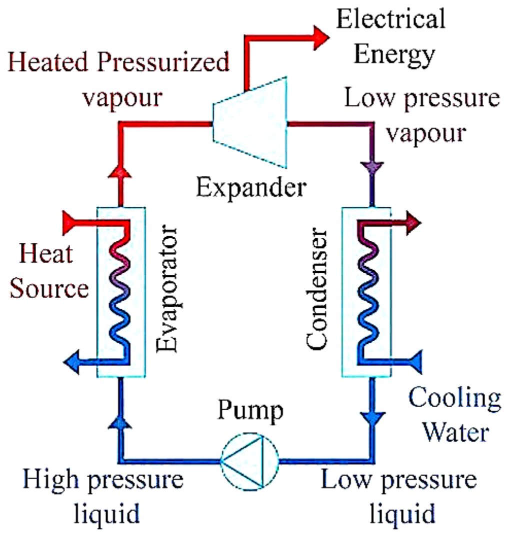

Figure 2.1: The Organic Rankine Cycle

Source: (Shaligram, 2016)

Unlike the conventional Rankine Cycle, which operates at high temperatures and pressures using water, the ORC employs organic fluids, such as refrigerants and hydrocarbons, which boil at significantly lower temperatures. This makes ORC systems particularly suitable for harnessing low-grade heat from renewable sources, such as solar and biomass, as well as industrial waste heat and geothermal energy.

The working fluid in any Rankine-based cycle must be capable of transitioning between liquid and vapour phases under the operating conditions of each component. Organic fluids used in ORC systems are selected for their low boiling points, moderate critical temperatures, and favourable thermophysical properties, enabling efficient operation with heat sources typically below 150 °C.

Due to their modularity and adaptability, ORC systems are well-suited for small-scale, decentralised electricity generation. They are increasingly deployed in biomass-fired plants, concentrated solar power systems, geothermal installations, and waste heat recovery applications.

2.2 ORC Configurations

The performance of ORC systems is primarily influenced by three key variables: the heat source temperature, the turbine or expander operating conditions, and the thermophysical properties of the working fluid. According to Bao *et al*. (2018), the ORC configuration plays a critical role in determining overall system efficiency, making it a central consideration in ORC design.

The basic ORC configuration consists of four core components: a turbine for expansion and work output, a condenser for heat rejection, a pump for fluid pressurisation, and a heat source for energy input. While this setup is sufficient for basic low-grade heat recovery, performance can be significantly enhanced by integrating additional components such as recuperators, regenerators, and ejectors. These devices enhance thermal matching, minimise irreversibilities, and improve cycle efficiency.

Li *et al*. (2021) classified ORC configurations into five distinct categories based on the inclusion or exclusion of specific components:

i. Basic ORC
ii. ORC with Recuperator

iii. Regenerative ORC
iv. ORC with Reheater
v. Ejector ORC

These configurations are summarised in Table 2.1, which presents a comparative overview of their structural variations and corresponding references from the literature.

Table 2.1: Classifications of organic Rankine Cycle Configurations

ORC Configurations in Li *et al*. (2021)	**ORC Configurations in other publications**	**Source**
Basic ORC	i. Basic ORC ii. Simple ORC iii. Subcritical ORC	(Imran *et al*., 2014; Lecompte *et al*., 2015; Li *et al*., 2013; Mago *et al*., 2008; Mahmoudi *et al*., 2018; Safarian & Aramoun, 2015; Shi *et al*., 2018; Tchanche *et al*., 2014; Wang *et al*., 2020; Xu & He, 2011)
ORC with a recuperator	i. ORC with an internal heat exchanger ii. Regenerative ORC iii. ORC with a recuperator Recuperative ORC iv. ORC with a preheater v. Regenerated ORC vi. Internal regenerative ORC vii. Recuperated ORC viii. Others	(Chys *et al*., 2012; Larsen *et al*., 2013; Lecompte *et al*., 2015; Mahmoudi *et al*., 2018; Mazzi *et al*., 2015; Meinel *et al*., 2014; Uusitalo *et al*., 2014; Wang *et al*., 2011a; Yang *et al*., 2014)

Regenerative ORC	i. Single-stage regenerative ORC ii. ORC with integrated feed-fluid heater iii. Two-stage ORC	(Branchini *et al*., 2013; Imran *et al*., 2014; Lecompte *et al*., 2015; G. Li, 2016; Mago *et al*., 2008; Pei *et al*., 2010; Safarian & Aramoun, 2015; Wang *et al*., 2012)
ORC with a reheater	i. ORC with an internal heat exchanger ii. Reheat ORC iii. Reheating ORC	(Li, 2016; Mahmoudi *et al*., 2018)
Ejector ORC	i. Regenerative ORC with vapour ejector ii. ORC with ejector	(Li *et al*., 2012; Peris *et al*., 2013; Xu & He, 2011)

2.2.1 Basic ORC

The basic ORC, illustrated in Figure 2.1, represents the simplest configuration of the ORC system. It comprises four primary components: the evaporator, turbine, condenser, and pump. These components work together to convert thermal energy, typically from low-grade heat sources, into mechanical work, which is subsequently converted into electricity.

The simplicity of the basic ORC system offers several advantages:

i. Cost-effectiveness: Fewer components reduce capital and maintenance costs.

ii. Ease of installation and operation: Its straightforward design makes deployment in diverse industrial settings straightforward.

iii. Suitability for low-grade heat recovery: It is particularly effective in harnessing waste heat from industrial processes and renewable sources with modest power demands.

However, the basic ORC system has inherent limitations. The absence of additional components, such as recuperators or regenerators, limits its ability to optimise heat recovery and improve thermodynamic performance. This results in:

i. Lower thermal efficiency

ii. Higher irreversibilities

iii. Increased exergy losses

Recent comparative studies have reinforced these limitations. For instance, Nondy and Gogoi (2021) conducted a multi-objective optimisation of four ORC configurations (Basic, Recuperative, Regenerative, and Recuperative-Regenerative) and found that the Basic ORC had the lowest exergy efficiency and net power output under optimal conditions. Similarly, Zhu *et al*. (2015) demonstrated that regenerative ORCs consistently outperform basic cycles in terms of thermal efficiency, especially when optimised for working fluid selection and operating conditions.

In a study published in 2023 by Mana *et al*., the basic ORC was compared with a recuperative configuration for waste heat recovery and geothermal applications. The recuperative system achieved a net efficiency 7.29% higher and an improved exergy efficiency of 20.54%, highlighting the performance gap between basic and enhanced designs.

While the basic ORC remains a practical and economical solution for low-grade heat recovery, its performance can be significantly improved by integrating regenerative or recuperative components. These enhancements are increasingly relevant to applications requiring higher efficiency, such as hybrid renewable energy systems and industrial waste heat recovery.

2.2.2 ORC with a Recuperator

A recuperator is a heat exchanger that, when integrated into the basic ORC, significantly enhances system performance. As illustrated in

Figure 2.**2**, the recuperator is positioned between the turbine outlet and the evaporator inlet. It recovers residual thermal energy from the turbine exhaust and transfers it to the working fluid before it enters the evaporator. This preheating process increases the working fluid's temperature and enthalpy, thereby reducing

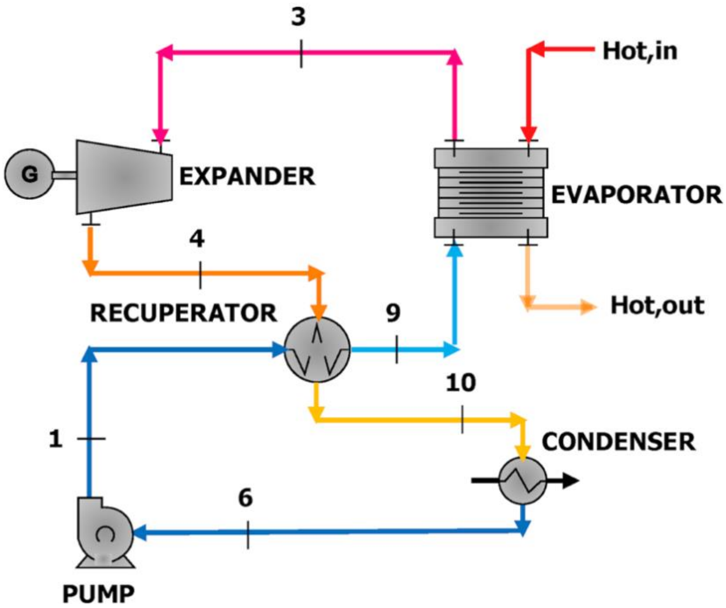

the external heat input required to reach the desired evaporation temperature.

Figure 2.2: Schematic Diagram of an Organic Rankine Cycle with Recuperator

Source: (Benato & Macor, 2017)

The inclusion of a recuperator improves the thermodynamic efficiency of the ORC by narrowing the temperature gradient between the heat source and the working fluid. This results in reduced irreversibilities and enhanced exergy utilisation, ultimately leading to higher net power output from the same heat source. Benato and Macor (2017) demonstrated that recuperative ORCs applied to a biogas engine waste-heat recovery can achieve up to 30% more net electric power than basic configurations.

Moreover, ORCs with recuperators offer greater flexibility in selecting the working fluid. This enables the optimisation of heat transfer characteristics based on the thermophysical properties of various fluids. Doninelli and Di Marcoberardino (2024) emphasised the importance of accurately predicting transport properties in designing recuperators for trans-critical cycles using CO_2-based mixtures. Similarly, Liu *et al*. (2022) showed that recuperator-equipped ORCs exhibit improved transient performance and thermal stability under dynamic operating conditions.

Pourahmad *et al*. (2018), further validated the benefits of recuperator integration in biomass-powered ORCs, reporting a 7.91% increase in system efficiency from 6.84%. These findings underscore the recuperator's role in enhancing energy recovery, reducing fuel consumption, and improving overall system sustainability.

2.2.3 Regenerative ORC

The regenerative ORC is an advanced configuration of the basic ORC that incorporates a regenerator, a heat exchanger that improves thermal efficiency by facilitating internal heat recovery between different stages of the working fluid (Braimakis & Karellas, 2018). This component transfers residual heat from the expander outlet stream to the pre-evaporator inlet stream, preheating the working fluid before it enters the evaporator. This internal heat exchange reduces the external heat input required from the primary heat source.

Depending on the configuration, the regenerator may be implemented as either a closed-feed or open-feed system:

i. In a closed-feed regenerator, the heat exchange occurs between two fluid streams without mixing, maintaining separation between the high-pressure and low-pressure sides.

ii. In an open-feed regenerator, partial mixing of streams may occur, typically involving extraction and reinjection points within the cycle.

These configurations are illustrated in Figure 2.3 and Figure 2.4

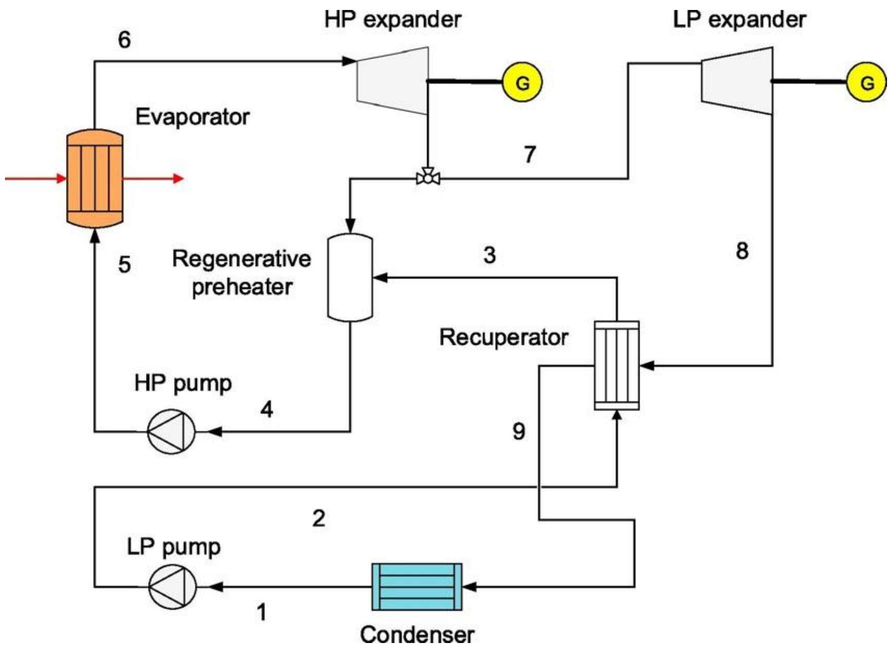

Figure 2.3: ORC With Open-Feed Organic Fluid Heater

Source: (Braimakis & Karellas, 2018)

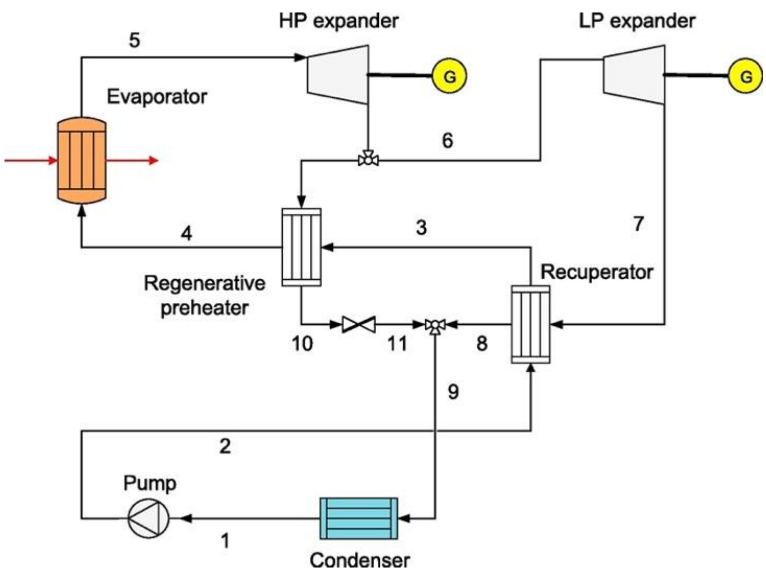

Figure 2.4: ORC With a Closed-Feed Organic Fluid Heater

Source: (Braimakis & Karellas, 2018)

The regenerative ORC achieves a higher thermal efficiency than the basic ORC by recycling internal thermal energy, thereby reducing the demand on external heat sources. This internal recovery mechanism also enhances the flexibility of the working fluid, enabling the selection of fluids tailored to specific heat-source characteristics and operating conditions (Kindra *et al*., 2022; Pikra *et al*., 2020).

However, integrating a regenerator introduces design and operational complexities. Key considerations include:

i. Heat transfer effectiveness: Influences the degree of preheating and overall cycle efficiency.

ii. Pressure-drop penalties: Can offset efficiency gains if not properly managed.

iii. Size and cost constraints: Affect system compactness and economic viability.

iv. Control strategies: Required to manage transient behaviour and ensure stable operation under varying load conditions (Lopes *et al*., 2021; Omosehin *et al*., 2022).

Despite these challenges, regenerative ORC systems remain a promising pathway for enhancing energy recovery in low- to medium-grade heat applications, particularly where system efficiency and fuel savings are critical.

2.2.4 Reheat ORC

The Reheat ORC is a variation of the Basic ORC that incorporates a reheater to enhance the system's energy conversion efficiency. In the configuration illustrated in *Figure 2.5*, the working fluid is reheated by an external heat source after expansion in the first stage of the turbine before entering the second stage. After the initial expansion, the temperature of the working fluid drops significantly; the reheating process raises it back to a higher level, thereby increasing the temperature and enthalpy of the fluid before it undergoes further expansion in the second turbine stage (Ma *et al*., 2023; Pambudi *et al*., 2021; Zhou *et al*., 2022).

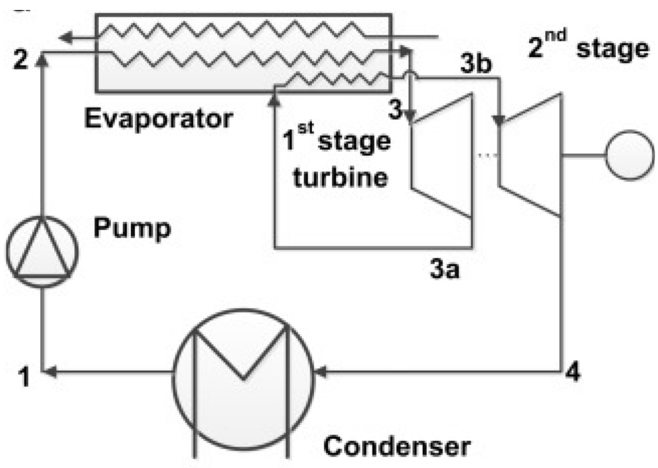

Figure 2.5: Reheat ORC

Source: (G. Li, 2016)

The inclusion of a reheater helps to maximise the utilisation of available thermal energy by extracting additional work from the working fluid. This process increases the fluid's temperature, improving thermodynamic efficiency and increasing power output. Additionally, the Reheat ORC allows a broader range of working fluids. The reheater compensates for the temperature drop during expansion, enabling the use of low-temperature heat sources that may not be suitable for traditional ORCs (Daniarta & Kolasiński, 2022; Faghih & Pourshaghaghy, 2022; Jafarmadar & Habibzadeh, 2017).

However, the design of the reheater must ensure efficient heat transfer and a controlled temperature rise while minimising pressure losses. The addition of a reheater also increases system complexity, necessitating additional components and meticulous thermal integration to ensure stable, efficient operation.

2.2.5 Ejector ORC

The Ejector ORC is an innovative configuration of the Organic Rankine Cycle that incorporates an ejector to enhance energy conversion and fluid dynamics. As illustrated in Figure 2.6, the high-pressure vapourised working fluid exiting the evaporator enters the ejector, where it mixes with a motive fluid, typically high-pressure steam or refrigerant. This mixing process generates a high-velocity jet, which increases the pressure and temperature of the working fluid (Mariani *et al.*, 2022). The resulting high-energy mixture is then directed into the turbine to produce mechanical power. After expansion, the working fluid is cooled in the condenser and pumped back to the evaporator to complete the cycle.

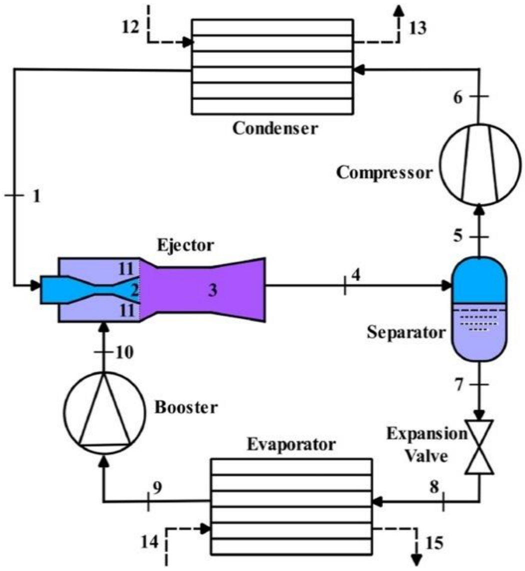

Figure 2.6: ORC with an Ejector

Source: (Rostamnejad & Zare, 2019)

The inclusion of an ejector enhances system performance by using the motive fluid to compress the working fluid, thereby eliminating the need for a mechanical compressor (Almehmadi *et al*., 2022; Kumar *et al*., 2021; Rak *et al*., 2018). This approach results in a more efficient, cost-effective design than conventional ORCs. Moreover, the absence of moving parts in the ejector simplifies the system architecture, reduces maintenance requirements, and improves overall reliability.

However, the design and optimisation of the ejector require careful consideration of fluid dynamics and thermodynamic parameters to achieve optimal performance (Rak *et al*., 2018). The selection of working fluids must closely match the operating conditions to ensure efficient mixing, entrainment, and pressure recovery.

2.2.6 Other Complex ORC Configurations

2.2.6.1 Cascade ORC

The Cascade ORC, illustrated in Figure 2.7, is particularly suitable for applications involving a wide temperature range between the heat source and the cooling medium. It employs multiple stages of ORCs arranged in cascaded loops, with each loop operating at a distinct temperature level (Rashwan *et al*., 2019). The higher-temperature loop extracts energy from a high-grade heat source, while the lower-temperature loop utilises residual or low-grade heat. This configuration allows each loop to operate within its optimal temperature range, thereby improving the overall energy conversion efficiency.

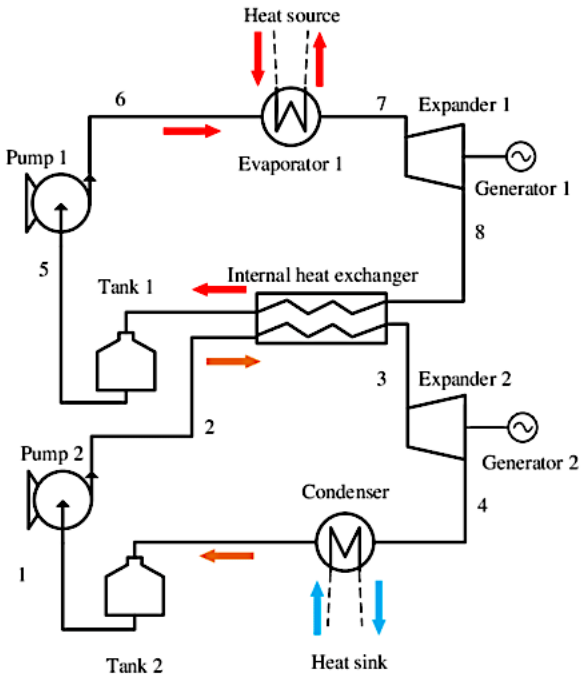

Figure 2.7: Cascade ORC

Source: (Zhao *et al*., 2020a)

Cascade ORC can accommodate heat sources with varying temperature profiles by using multiple loops, ensuring effective heat recovery and utilisation. However, this configuration requires additional components, such as turbines, condensers, and heat exchangers, thereby increasing system complexity. The design and optimisation of a Cascade ORC system involve careful selection of working fluids, appropriate temperature zoning for each loop, and efficient integration of heat exchangers and expansion devices (Allison *et al*., 2022; Ancona *et al*., 2021; Kiliç, 2020). Advanced control strategies and optimisation algorithms can further enhance system performance and energy conversion efficiency.

2.2.6.2 Dual-Loop Vaporisation ORC

The dual-loop vaporisation system is an advanced ORC configuration that incorporates two distinct thermodynamic loops, each utilising a separate working fluid tailored to specific temperature ranges. As illustrated in Figure 2.8, this arrangement enhances heat transfer and energy conversion efficiency by dividing the heat source into two stages (Civgin & Deniz, 2021).

In the primary loop, a high-boiling-point working fluid absorbs thermal energy from a high-temperature source. This fluid undergoes phase change in the evaporator, producing high-pressure vapour that drives a turbine to generate mechanical power. The vapour is subsequently condensed and recirculated. The secondary loop operates at lower temperatures and employs a low-boiling-point working fluid. It extracts residual heat from the lower-temperature stage of the source, vaporises in a separate evaporator, and drives a second turbine before being condensed and returned to the cycle (Civgin & Deniz, 2021; Vallis *et al.*, 2020).

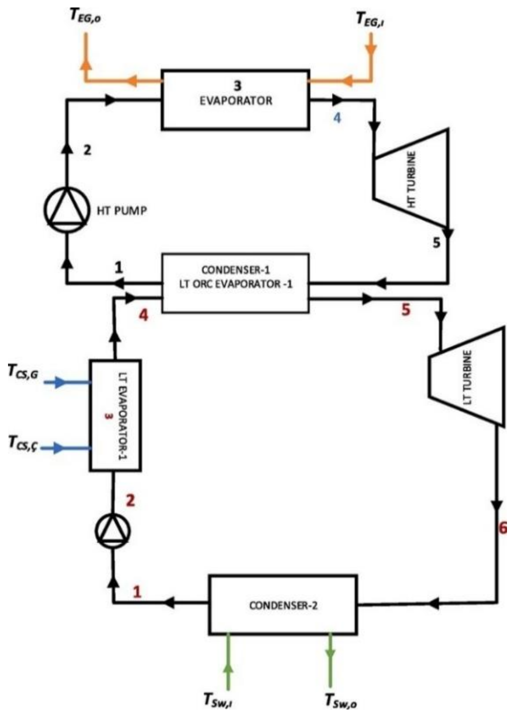

Figure 2.8: Dual-Loop Vaporisation ORC

Source: (Civgin & Deniz, 2021)

This dual-loop configuration enables effective utilisation of heat sources at varying temperatures, thereby improving the overall thermal efficiency of the ORC system. The strategic selection of working fluids for each loop enables optimal thermodynamic performance across the entire temperature spectrum. Studies have shown that such systems can significantly increase net power output while reducing fuel consumption and emissions, particularly in marine and industrial waste heat recovery applications (Civgin & Deniz, 2021; Vallis *et al*., 2020).

However, the system's complexity and associated costs are considerable. The requirement to manage two distinct working fluids introduces operational challenges, including fluid compatibility, control strategies, and maintenance demands. These factors must be carefully weighed against the potential efficiency gains when considering the deployment of dual-loop ORC systems.

2.3 Heat Source

Organic Rankine Cycle systems are designed to harness thermal energy from a wide range of heat sources, particularly low-grade ones. These include waste heat from industrial processes, renewable energy sources such as geothermal, solar, and biomass, and exhaust gases from internal combustion engines. As illustrated in Figure 2.9, Vélez *et al*. (2012) categorise these sources into high- and low-temperature groups based on their suitability for different thermodynamic cycles.

i. High-temperature sources: Fossil fuels, biomass via gasification or anaerobic digestion.
ii. Low-temperature sources: Solar energy, geothermal energy, and biomass combustion.

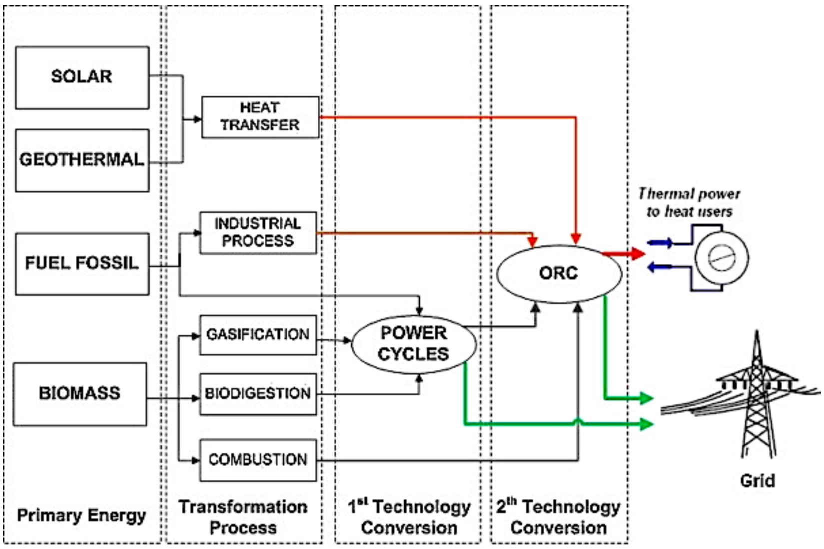

Figure 2.9: Potential Application of ORC Based on Heat Sources

(Adapted from (Vélez *et al*., 2012))

The temperature range of these sources significantly influences the design and performance of ORC systems. Table 2.2 presents a summary of operating temperatures for various heat sources used in ORC operations. Low-temperature sources typically operate between 80 and 200°C, although some configurations, such as concentrated solar thermal systems, can reach higher temperatures. High-temperature sources, including industrial waste heat and engine exhaust gases, may exceed 500 °C, offering greater thermodynamic potential. Recent studies provide detailed insights into the operating temperature ranges of various heat sources:

Table 2.2: Typical Operating Temperatures of Various Heat Sources for ORC Operations

Heat Source	Temperature Range
Waste heat from industrial processes	100 - 500 °C
Exhaust gases from internal combustion engines	100 - 500 °C
Geothermal energy	80 - 350 °C
Solar energy	80 - 500 °C
Biomass combustion	200 - 450 °C

Source: (Hui-Xing *et al*., 2022; Zhai *et al*., 2016)

These ranges underscore the versatility of ORC systems in adapting to diverse thermal environments. Notably, Concentrated Solar Power (CSP) and geothermal reservoirs can be engineered to deliver heat at temperatures suitable for both subcritical and supercritical ORC configurations.

The selection of appropriate working fluids and cycle architectures is closely tied to the heat source's temperature characteristics. For instance, low-boiling-point fluids are preferred for low-temperature sources to ensure efficient vaporisation, while high-boiling-point fluids are used for high-temperature sources to maximise energy extraction.

2.3.1 Waste Heat

Industrial processes such as power generation, oil refining, and chemical manufacturing often produce substantial amounts of waste heat. Similarly, internal combustion engines, commonly used in vehicles and marine vessels, emit significant thermal energy as a byproduct of their operation. This waste heat is typically classified into three categories based on temperature: low-temperature waste heat (below 200°C), medium-temperature waste heat (between 200°C and 500°C), and high-temperature waste heat (above 500°C). Technologies for recovering medium- and high-temperature waste heat are well developed. For instance, heat from exhaust gases at 350 °C emitted by the kiln hood, clinker coolers, and kiln tail preheaters can be captured by boilers. Likewise, Coke Dry Quenching (CDQ) technology enables the recovery of high-temperature heat up to 1000 °C from hot coke (Cheng *et al.*, 2020).

To optimise the utilisation of waste heat in industrial settings, Weng *et al*. (2013) proposed an energy flow diagram that evaluates the recovery potential across various sectors, as illustrated in Figure 2.10. The potential for waste heat recovery is categorised into three distinct classifications. The first involves waste heat that can be conserved by improving manufacturing process efficiency. The second pertains to waste heat that can be reused within the facility to meet local thermal demands. The third classification refers to waste heat that can be repurposed externally, such as for electricity generation or supplying heat to district heating networks.

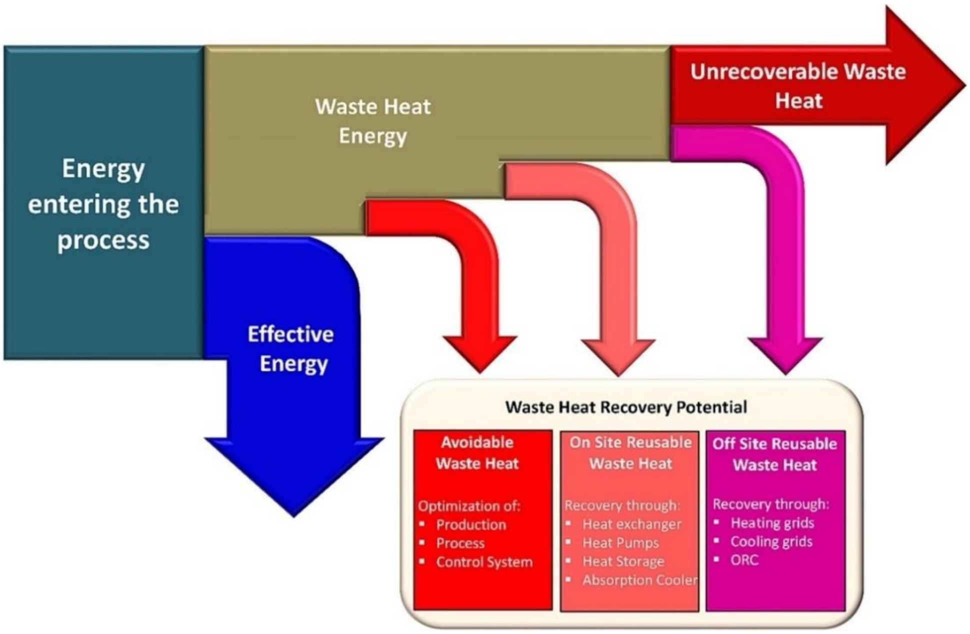

Figure 2.10: Potential for Recovering Waste Heat

Source: (Weng *et al.*, 2013)

Waste heat can exist in gaseous, liquid, or solid forms. A common example of solid-state waste heat is hot steel, while flaring gases, low-quality steam, and exhaust gases represent waste heat in the gaseous state. In liquid form, waste heat is often found in hot oil and water used for industrial cooling purposes (Hui-Xing *et al*., 2022; Zhai *et al*., 2016). These diverse forms and temperature ranges make waste heat a valuable resource for energy recovery systems, particularly ORC configurations, which are designed to efficiently harness low- to medium-grade thermal energy.

2.3.2 Renewable Energy

Renewable energy heat sources commonly used in ORC systems include solar thermal, biomass combustion, and geothermal energy. These sources are particularly suitable for low- to medium-temperature applications and offer sustainable alternatives to fossil-based heat inputs.

Geothermal energy generates electricity by extracting heat from the Earth's crust. ORC systems are often employed in geothermal plants to enhance overall efficiency by recovering additional energy from the geothermal fluid, particularly in binary-cycle configurations, where the geothermal brine is utilised to vaporise a secondary working fluid.

Solar thermal energy can be harnessed using various concentrating technologies, including central receiver systems (solar towers), parabolic troughs, parabolic dishes, and Linear Fresnel Reflectors. These systems focus solar radiation onto a receiver, where it transfers heat to the working fluid, which then drives the ORC. The temperature achieved depends on the concentration ratio and collector type, with solar towers and parabolic dishes reaching the highest temperatures.

Biomass combustion is another viable renewable heat source for ORC systems. It utilises agricultural residues, wood chips, and dedicated energy crops to produce heat through combustion. This heat is then transferred to the working fluid in the ORC system, generating electricity. Biomass is often paired with solar thermal energy in hybrid configurations to improve reliability and extend operational hours.
Hybrid systems combining biomass and solar thermal energy have shown promising

results in terms of efficiency and flexibility. Al-Sulaiman *et al*. (2011) analysed a trigeneration system powered by solid oxide fuel cells (SOFC), biomass, and solar thermal energy. Their study found that the hybrid system, which utilises biomass and solar thermal energy, achieved the highest trigeneration efficiency, reaching up to 90%.

The maximum operating temperatures of these renewable heat sources vary based on technology and system design. As summarised in Table 2.2, geothermal energy can reach temperatures of up to 350 °C, biomass combustion can reach temperatures of up to 450 °C, and solar thermal systems can reach temperatures of up to 500 °C (Hui-Xing *et al*., 2022; Zhai *et al*., 2016).

These temperature ranges guide the selection of appropriate working fluids and ORC configurations, ensuring optimal performance and energy recovery across diverse renewable applications.

2.4 Turbine/Expander

Turbines, also known as expanders, are mechanical devices that convert the energy in high-pressure fluids into mechanical work. In ORC systems, the turbine/expander plays a crucial role in determining overall system performance. As the working fluid expands through the turbine, mechanical energy is generated and subsequently converted into electricity via a generator coupled to the turbine shaft.

Expanders in ORC systems are broadly categorised into dynamic and volumetric types, as illustrated in Figure 2.11. Dynamic expanders, also known as velocity-type expanders, operate by transforming the momentum of high-velocity fluid into mechanical energy as it passes through a series of blades. During this process, the fluid exits the expander with reduced pressure and enthalpy. These expanders are predominantly used in medium- to large-scale ORC applications due to their superior efficiency and the ability to handle higher mass flow rates. Radial and axial turbines are typical examples of dynamic expanders, with their performance and applicability well-documented in the literature (Alshammari *et al*., 2018b; Rahbar *et al*., 2017).

Volumetric expanders, in contrast, are positive displacement devices that extract power by applying force to a movable mechanical component. In these systems, a chamber is filled with pressurised fluid, and its volume increases as the fluid exerts a net force. Once the chamber reaches its maximum expansion, the low-pressure fluid is discharged through valves that regulate flow and synchronise with the chamber's motion. Volumetric expanders are particularly suited for low-power applications and are often adapted from HVAC compressors for reverse operation. Common types include screw, scroll, rotary vane, and reciprocating piston expanders.

Experimental studies have shown that scroll expanders are the most frequently used in ORC systems, followed closely by radial inflow turbines. Figure 2.11 presents the classification of turbine/expander types, while Table 2.3 provides a detailed overview of empirical investigations involving various expander types, working fluids, operating temperatures, efficiencies, and power outputs. The data indicate that scroll expanders are especially prevalent in small-scale ORC applications due to their compact design and adaptability, whereas radial inflow turbines dominate medium-scale systems where higher efficiency is required.

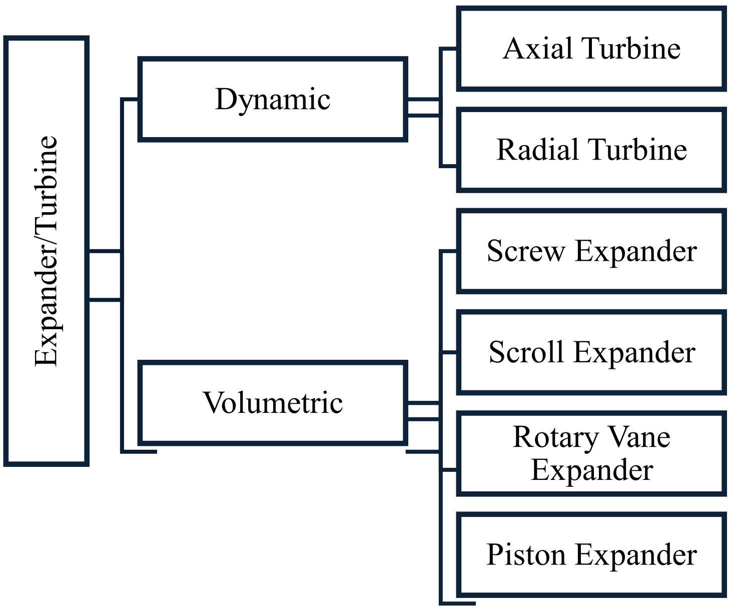

Figure 2.11: Classification of Expander/Turbine Used in ORCs

Source: (Rahbar *et al*., 2017)

Using a temperature range of 58 to 170 °C and working fluids such as R227ea, R245fa, R236fa, R113, R123, R134a, HFE7100, HFE301, HFE7000, CO_2, ammonia, trifluoroethanol (TFE), and n-pentane, both scroll expanders and radial inflow turbines demonstrated high isentropic efficiencies. Scroll expanders using R123 and R245fa achieved isentropic efficiencies of 85.15 and 84.90%, respectively. Similarly, radial inflow turbines using R123, HFE301, and TFE achieved efficiencies of 83.6%, 85%, and 85%, respectively (Rahbar *et al*., 2017; R. Wang *et al*., 2019).

Table 2.3 further shows that axial turbines, screw expanders, reciprocating piston expanders, and rotary vane expanders are less commonly featured in ORC studies, though they still offer viable performance depending on the application. For instance, screw expanders using R245fa achieved efficiencies up to 72.5%, while reciprocating piston expanders using CO_2 reached 62%. Rotary vane expanders, though less efficient, provide operational flexibility in specific low-temperature applications.

These findings emphasise the importance of selecting suitable expander types and working fluids in accordance with the intended application, temperature range, and desired efficiency. The integration of suitable expanders not only enhances the thermodynamic performance of ORC systems but also contributes to their economic and operational viability.

Table 2.3: Overview of Empirical Investigations on ORCs Involving Several Expanders

Expander type	**Working Fluid**	**Evaporator Temperature**	**Maximum efficiency**	**Power Specification**	**Source**
Axial turbine	R227ea	58 °C	η_{exp} = 59 %	10.1 kW	(Klonowicz *et al*., 2014; Klonowicz *et al*., 2014)
Axial turbine	R245fa	108 °C	η_{exp} = 63.7 % $\eta_{cyc,th}$ = 7.94 %	219.5 kW	(Fu *et al*., 2015)

Axial turbine	HFE7100	<100 °C	ηexp = 59.7 % ηcyc,th = 4.01 %	1.03 kW	(Pu *et al.*, 2016)
Axial turbine	R245fa	<100 °C	ηexp = 62 % ηcyc,th = 4.17 %	1.98 kW	(Pu *et al.*, 2016)
Radial inflow turbine	HFE301	70 °C	ηexp = 85 % ηcyc,th = 7.5 %	1.5 kW	(Yagoub *et al.*, 2006)
Radial inflow turbine	R123	75 °C	ηexp = 48 %	0.15 kW	(Yamamoto *et al.*, 2001)
Radial inflow turbine	R123	80 °C	ηexp = 68 % ηcyc,th = 7.4 %	2.4 kW	(Li *et al.*, 2020a)
Radial inflow turbine	R245fa	80 °C	ηexp = 78.7 % ηcyc,th = 5.22 %	32.7 kW	(Kang, 2012)
Radial inflow turbine	R245fa	121 °C	ηexp = 88.6 % ηcyc,th = 9.4 %	300 kW	(Wang *et al.*, 2019)
Radial inflow turbine	Trifluoroethanol (TFE)	77 °C	ηexp = 85 % ηcyc,th = 6.7 %	13.5 kW	(Inoue *et al.*, 2007)
Radial inflow turbine	n-pentane	93 °C	ηexp = 49.8 % ηcyc,th = 4.3%	1.44 kW	(Nguyen *et al.*, 2001)
Radial inflow turbine	R123	105 °C	ηexp = 65 % ηcyc,th = 6.8 %	1 kW	(Pei *et al.*, 2011)

Radial inflow turbine	R245fa	140 °C - 150 °C	ηexp = 72.4 %	201 kW	(Han *et al.*, 2014)
Radial inflow turbine	R245fa	140 °C	ηexp = 68.1 % ηcyc,th = 9.6 %	177 kW	(Sung *et al.*, 2016)
Radial inflow turbine	R123	110–140 °C	ηexp = 83.6 % ηcyc,th = 5.7 %	1.88 kW	(Shao *et al.*, 2017)
Reciprocating piston	CO2		*ηexp* = 62 %		(Zhang *et al.*, 2007)
Reciprocating piston	R245fa	40–90 °C	ηexp = 43.3 % ηcyc,th = 5 %	0.35 kW	(Zheng *et al.*, 2013)
Rotary vane	HFE7000	118 °C	ηexp = 55.45 % ηcyc,th = 3.89 %	0.85 kW	(Qiu *et al.*, 2012)
Rotary vane	R236fa	120 °C	ηcyc,th = 7.6 %	1.47 kW	(Cipollone *et al.*, 2014)
Screw	R113		ηexp = 70 %	20 kW	(Brasz *et al.*, 2000)
Screw	R245fa	80–125 °C	ηexp = 72.5 % ηcyc,th = 10.5 %	50 kW	(Hsu *et al.*, 2014)
Screw	R245fa	85–116 °C	ηcyc,th = 7.57 %	39.9 kW	(Minea, 2014)
Scroll	Ammonia		ηexp = 18.2 %	0.209 kW	(Ingley *et al.*, 2005)
Scroll	R113	136 °C	ηexp = 63 % ηcyc,th = 12	0.45 kW	(Saitoh *et al.*, 2007)

			%		
Scroll	R123	174 °C	ηexp = 49.9 %	0.256 kW	(Peterson *et al.*, 2008)
Scroll	R123		ηexp = 48.3 %	2.9 kW	(Mathias *et al.*, 2009)
Scroll	R123	143 °C	ηexp = 68 %	1.8 kW	(Lemort *et al.*, 2009)
Scroll	R123 R134a	120–150 °C;	ηexp = 68 % ηcyc,th = 13 .67 %	7.32 kW	(Kane *et al.*, 2003)
Scroll	R134a	170 °C	ηexp = 65 %	1–3.5 kW	(Zanelli & Favrat, 1994)
Scroll	R134a		ηexp = 77 %	0.8 kW	(Wang *et al.*, 2009)
Scroll	R134a	70 °C	ηexp = 65 % ηcyc,th = 7. 8 %	2.05 kW	(Manolakos *et al.*, 2007)
Scroll	R245fa	140 °C	ηexp = 68 %	2.2 kW	(Lemort *et al.*, 2012; Manolakos *et al.*, 2007)
Scroll	R123	101–163 °C	ηexp = 68 % ηcyc,th = 7.4 %	1.8 kW	(Quoilin *et al.*, 2010)
Scroll	R245fa	85 °C 110 °C	ηexp = 58 %	3.75 kW	(Ziviani *et al.*, 2018)
Scroll	R245fa/R134a	80–120 °C	ηexp = 65 % ηcyc,th = 6 %	1.2 kW	(Bamorovat Abadi *et al.*, 2015)
Scroll	R245fa	75–95 °C	ηexp = 84.9 % ηcyc,th = 9.28 %	1.2 kW	(Galloni *et al.*, 2015)

Scroll	R123	140 °C	ηexp = 81 % ηcyc,th = 6.39 %	2.35 kW	(Miao *et al*., 2015)
Scroll	R245fa	100–140 °C	ηexp = 77.74 % ηcyc,th = 5.75 %	1.02 kW	(Muhammad *et al*., 2015)
Scroll	R245fa	120 °C	ηexp = 61.4 % ηcyc,th = 7.5 %	3.4 kW	(Yun *et al*., 2015)
Scroll	R123	110–140 °C	ηexp = 85.17 % ηcyc,th = 3.25 %	2.01 kW	(Feng *et al*., 2017)

(Adopted from Rahbar *et al*. (2017) and Wang *et al*. (2019))

2.4.1 Axial Turbine

Axial turbines are suitable for large-scale ORCs that aim for both high efficiency and power output. They are effective at handling high pressures and flow rates, allowing them to convert heat into mechanical power via a working fluid, which in turn promotes the generation of electricity. An axial-flow turbine has a rotor equipped with a series of blades that are driven by high-pressure fluid, as shown in *Figure 2.12*. The blades are arranged to direct the flow in a specific direction, turning the rotor and generating mechanical work (Wang & Peng, 2023). However, axial-flow turbines are sensitive to variations in pressure and flow rate, which can ultimately affect the overall system performance.

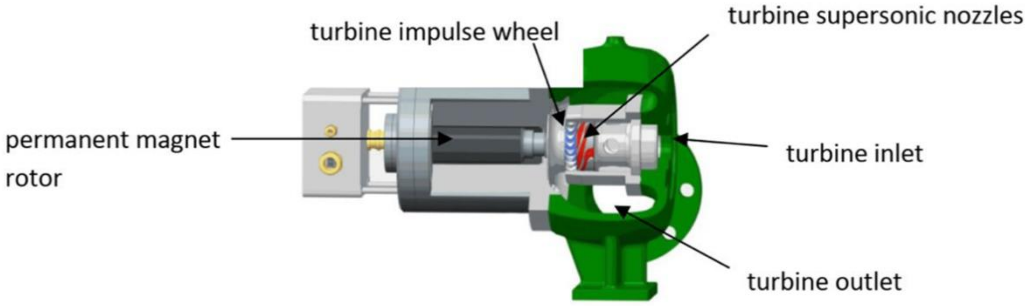

Figure 2.12: The Composition of an Axial Turbine

Source: (Weiß *et al.*, 2020)

2.4.2 Radial Turbines

Radial turbines are suitable for applications with low mass flow rates and high-pressure ratios and exhibit better performance under these conditions because they are less affected by variations in blade profile compared to axial turbines (Rahbar *et al.*, 2017). Radial turbines are commonly of the radial-inflow design; however, recent advancements in turbine technology have also made radial-outflow turbines viable for ORC applications (Alshammari *et al.*, 2018a; Alshammari *et al.*, 2018b; Rahbar *et al.*, 2017).

In a radial inflow turbine shown in Figure 2.13, the high-pressure fluid enters the casing through an inlet and initially flows in an essentially radial direction. This radial flow is then circumferentially transformed to a tangential direction at the inlet to the rotor, where it comprises both radial and tangential components (Alshammari *et al.*, 2018b). The flow direction is changed from radial to axial at the rotor exit, which is generally considered to be the point at which there should be no radial component.

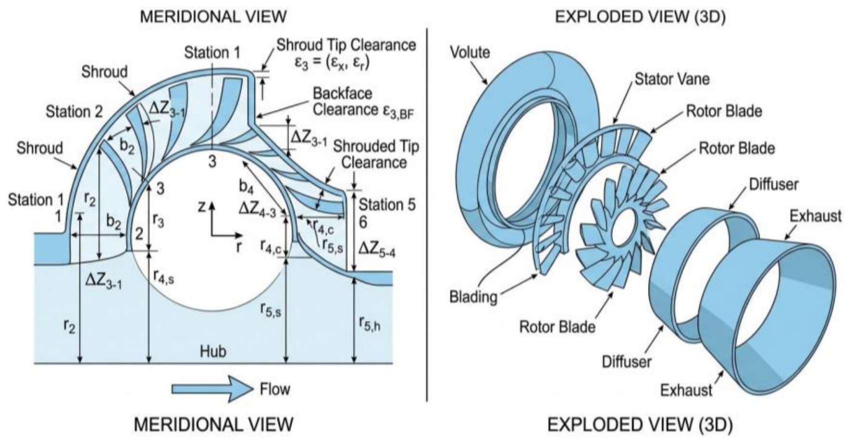

Figure 2.13: Radial Turbine Design (Right) And Meridional View (Left)

Source: (Alshammari *et al.*, 2018b; Rahbar *et al.*, 2017)

The radial outflow turbine (ROT), shown in Figure 2.14, has a flow direction that is the opposite of the flow direction in the radial inflow turbine; fluid enters the ROT in the centre, close to the axis of rotation, and then flows outwards in the radial direction while passing through arrays of rotor and stator blades (Alshammari *et al*., 2018b; Casati *et al*., 2014). This process is repeated until the flow reaches the end of the ROT. The use of ROTs enables the implementation of multi-stator-rotor ring configurations in the radial direction while retaining low peripheral speeds. This results in reduced mechanical strain, lower bearing losses, and simplified connections between the generator and the grid.

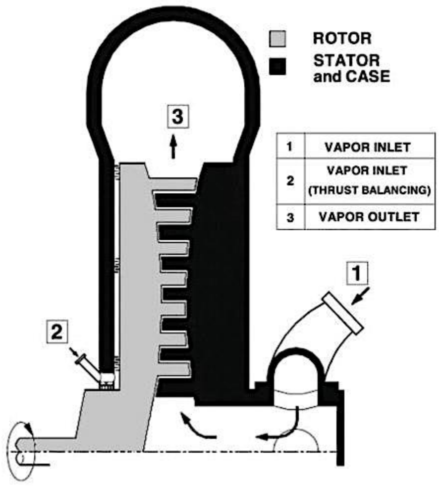

Figure 2.14 Diagram Illustrating the Structure and Operation of a Radial Outflow Turbine

Source: (Alshammari *et al*., 2018b; Rahbar *et al*., 2017)

2.4.3 Screw Expanders

Screw expanders consist of two helical rotors precisely designed with a specific profile to effectively capture the required quantity of working fluid. The coordinated motion of interlocking rotors, as shown in Figure 2.15, produces volume profiles that begin at one end of the rotor and extend to the other, thereby expanding the working fluid within the meshed chamber. Screw expanders are often used as expansion devices in ORC facilities, particularly for geothermal and waste heat applications (Bao & Zhao, 2013).

Figure 2.15: Operation of the Screw Expander

Source: (Rahbar *et al*., 2017)

Wang *et al*. (2011b) conducted experiments on a single screw expander using compressed air to evaluate its performance under varying intake flow rates and rotational speeds. The expander achieved a maximum power output of 4.4 kW and a temperature difference of 45°C between the inlet and outlet. Although single screw expanders offer favourable load characteristics and compact design, their efficiency can vary significantly depending on operating conditions and design parameters.

2.4.4 Scroll Expanders

A scroll expander consists of two spiral wraps, one of which is stationary while the other spins, as shown in Figure 2.16. When the rotational directions of the moving and stationary wraps align, the gap between them narrows, enabling them to function as a compressor. When the direction of rotation is changed, the space between the two layers expands, effectively functioning as an expander (Alshammari *et al*., 2018b; Rahbar *et al*., 2017). They are commonly used because they can be obtained from a scroll compressor, reducing the overall cost of the machine.

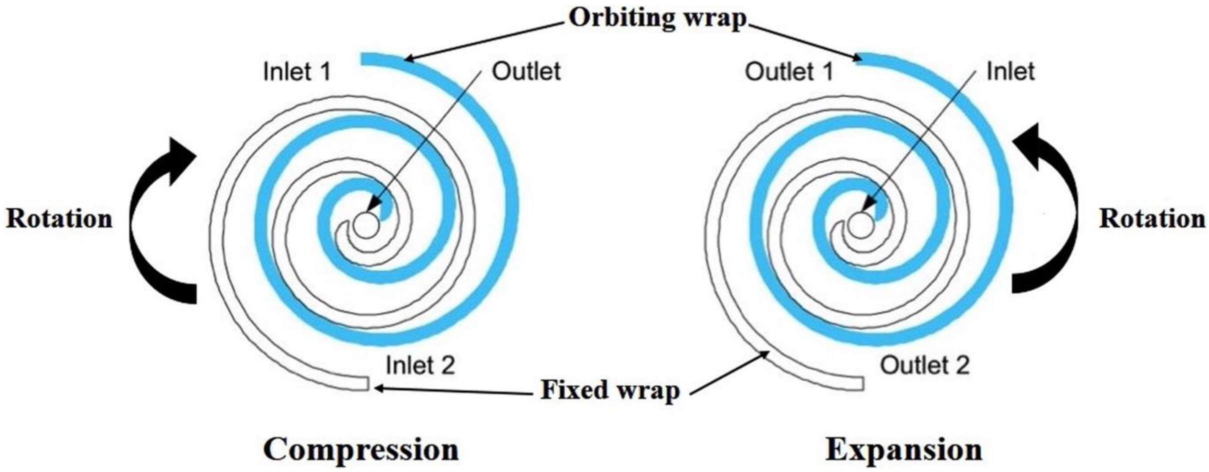

Figure 2.16: Operation of the Scroll Expander

Source: (Rahbar *et al*., 2017)

In a study by Saitoh *et al*. (2007), a low-temperature solar ORC with a scroll expander, using R113 as the working fluid, and a compound parabolic collector (CPC) was experimentally investigated. The results demonstrated that the ORC achieved an efficiency of 12% and the scroll expander achieved an efficiency of 63% when both hot water and actual solar radiation were used as the heating medium.
R134a was used as the working fluid in the dynamic modelling of a scroll expander that was undertaken by Twomey *et al*. (2013) for a small-scale solar ORC. The model's parameters were calibrated using experimental data. When the scroll expander model was validated, it demonstrated a level of consistency within a range of ±10% for shaft power and ±5% for rotational speed. The ORC and scroll expander efficiencies were reported to be 3.47% and 59%, respectively, for a collector area of 50 m², resulting in a total power output of 676 W. Using a solar storage system, they proposed that the generated electricity could be used during times of high load capacity.

2.4.5 Rotary Vane Expanders

The rotary vane expander, shown in Figure 2.17, functions on the Wankel principle. The working fluid enters the expander at a point with a narrow clearance. A rotor equipped with adjustable vanes is connected to another rotor positioned asymmetrically near the casing. The revolution of the rotor facilitates the outward movement of the vanes, effectively capturing the working fluid. As the rotation angle increases, the volume enclosed by successive vanes also increases, leading to expansion of the working fluid.

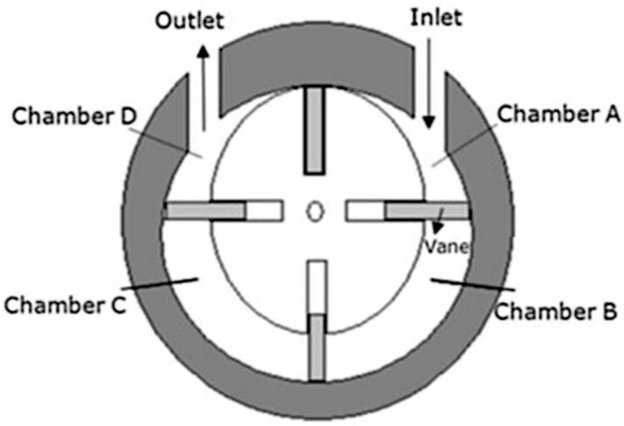

Figure 2.17: Operation of the Rotary Vane Expander

Source: (Alshammari, Usman, *et al*., 2018)

Using a rotary vane expander with HFE7000 and HFE7100 as the working fluids, Qiu *et al*. (2012) conducted an experimental investigation of a biomass-fired ORC system. Under the tested operating conditions, a maximum expander efficiency of 55.45% resulted in a total electrical efficiency of 1.41% and a net power generation of 861 W. In Cipollone *et al*. (2014), the experimental inquiry used R236fa as the working fluid to assess the performance of the rotary vane expander. The examinations yielded a maximum cycle efficiency of 7.6 % and a power output of 1.5 kW. These measurements were obtained during experiments conducted at both the design and off-design operating conditions.

2.4.6 Piston Expanders

Piston expanders, also referred to as reciprocating piston expanders, are shown in Figure 2.18. These systems comprise complex mechanisms that require precise timing of the intake and exhaust valves, resulting in substantial frictional losses from the abundance of moving parts. Nevertheless, wet expansion can be accommodated in this type of expander, making it suitable for ORC heat recovery in most internal combustion engines (ICEs). The working fluid is introduced into the piston expander when the piston is near the top dead centre (TDC), and thereafter, the intake valve is closed. As internal pressure pushes the piston, the fluid expands, transmitting energy to the central crankshaft via the connecting rod. The exit valve opens at the lowest point of the piston's stroke, allowing the enlarged working fluid to leave the chamber. This occurs when the piston advances back towards the top dead centre.

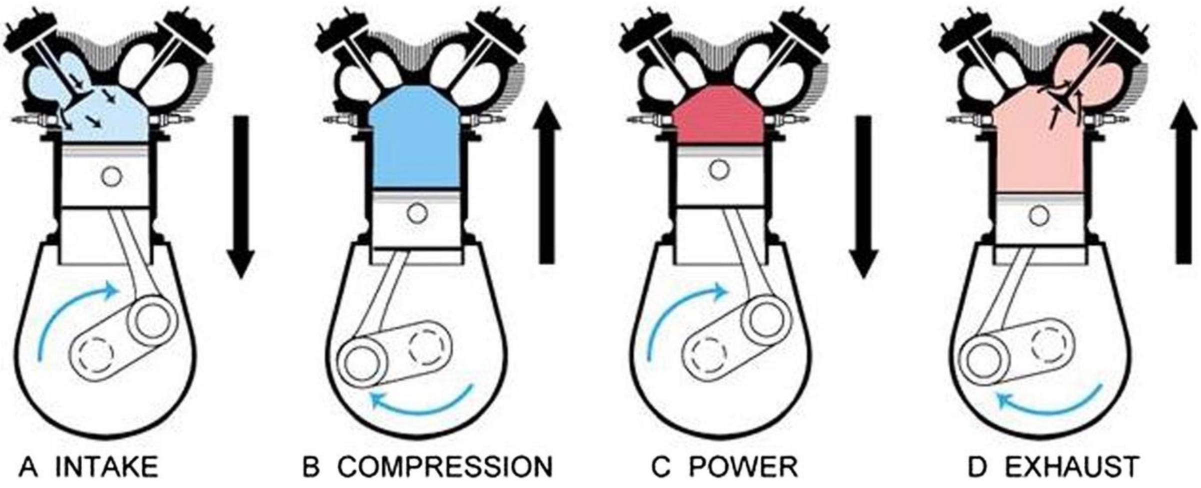

Figure 2.18: Operation of the Rotary Vane Expander

Source: (Rahbar *et al*., 2017)

Glavatskaya *et al*. (2012) presented a stable, empirical model of the reciprocating piston expander that accounted for the effects of ambient and mechanical losses, as well as internal leakage. The model's accuracy was confirmed using manufacturer-provided data, with a maximum deviation of 4.7%. Based on the presented data, the highest expander isentropic efficiency is 70%, and the volumetric efficiency is 60%.

In a study conducted by Clemente *et al*. (2013), a fundamental design for developing a piston expander with an ORC, using R245fa and n-pentane as working fluids, was examined. The study concluded that a low rotational speed is required to achieve a significant displacement, which is why the expander's maximum efficiency does not exceed 65%.

2.5 Working Fluids for ORC

The selection of an appropriate working fluid is a critical determinant of ORC performance. It influences not only the system's thermal and exergy efficiencies but also its environmental impact, operational safety, and economic viability. In addition to fluid selection, other factors, such as heat source temperature, expander configuration, and heat exchanger design, play significant roles in shaping the overall system behaviour.

Numerous studies have demonstrated that increasing the temperature of the heat source can enhance both thermal and exergy efficiencies. Biomass-fired ORCs and solar-driven systems employing parabolic trough collectors, for instance, have shown superior performance compared to those utilising evacuated tube or flat-plate collectors (Gomaa *et al*., 2020; Ismail *et al*., 2016).

Working fluids are categorised as either pure substances or mixtures, with zeotropic mixtures receiving increasing attention due to their non-isothermal phase-change behaviour. This property enables improved thermal matching with variable heat sources, thereby reducing irreversibilities in heat-exchange processes. Fluids may also be classified as wet, dry, or isentropic based on the slope of the saturated vapour line in the temperature-entropy (T–s) diagram, as demonstrated in *Figure 2.19* (Badr *et al*., 1985). Dry and isentropic fluids are typically favoured for their predictable expansion behaviour and reduced risk of liquid droplet formation within the turbine (Babatunde & Sunday, 2018; Tocci *et al*., 2017).

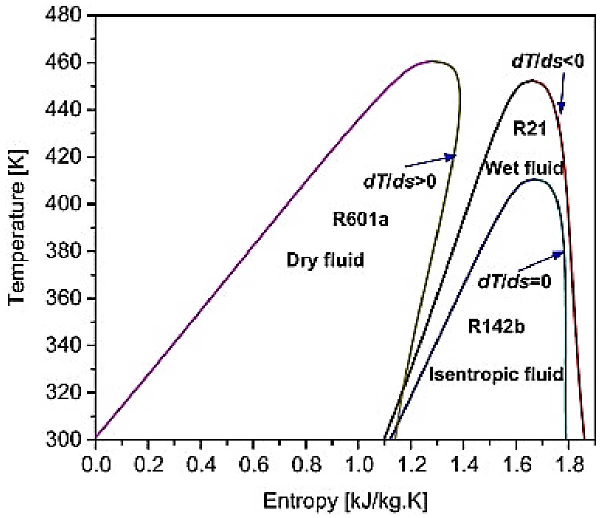

Figure 2.19: Classification of Organic Working Fluids Using the T- s Diagram

Source: (Badr *et al*., 1985; Kruzel *et al*., 2022; Mahmoudi *et al*., 2018; Vicencio & Aedo, 2017)

Environmental considerations have increasingly influenced the selection of fluids. The phase-out of chlorine-based refrigerants under international protocols such as the Kigali Amendment to the Montreal Protocol has accelerated the adoption of low-global warming potential (GWP) alternatives. Hydrofluoroolefins (HFOs) and other advanced organic compounds now offer viable options that balance thermodynamic performance with ecological responsibility (García-Pabón *et al.*, 2021; Minor *et al.*, 2014).

Recent developments in fluid enhancement have introduced nanofluids, base fluids augmented with suspended nanoparticles, as a promising avenue for improving ORC performance. These formulations exhibit superior thermal conductivity, specific heat capacity, and density, which collectively enhance heat transfer and reduce component sizing. Experimental and simulation-based studies have shown that nanoparticle-infused fluids, such as silver-doped pentane, can improve cycle efficiency without increasing pumping power requirements (Mondejar *et al.*, 2017; Saadatfar *et al.*, 2014). Other nanoparticles, including alumina (Al_2O_3), copper oxide (CuO), titanium dioxide (TiO_2), and zinc oxide (ZnO), have also demonstrated potential in various ORC configurations (Loni *et al.*, 2019a; Prajapati & Patel, 2020).

2.5.1 Pure Organic Fluids

The performance of an ORC system depends heavily on the thermophysical properties of its working fluid. While the traditional classification of fluids into wet, dry, and isentropic fluids has guided fluid selection for decades, it has limitations, particularly when predicting condensation behaviour and the risk of droplet formation in the expander. More recent approaches have introduced entropy-based markers and equilibrium-state models to improve accuracy, especially in low-pressure regions (Györke *et al.*, 2018).

A wide range of pure fluids has been studied under different operating conditions. Vidhi *et al.* (2013), for example, assessed supercritical ORC systems using refrigerants such as R23, R32, R125, and R134a with geothermal heat sources ranging from 125°C to 200 °C. Their findings showed that thermal efficiencies could reach up to 21% at higher source temperatures, with moderate efficiencies above 12% at mid-range conditions. Similarly, Siddiqui *et al.* (2023) compared 21 binary mixtures and seven pure fluids in a regenerative ORC setup. They found that pure fluids offered better exergy efficiency, higher specific net power output, and required smaller heat exchanger areas. Among the fluids tested, RE347mcc, neopentane, and isopentane stood out for their strong thermodynamic performance.

The choice of fluid is closely linked to the temperature of the heat source, as shown in *Figure 2.20*. Fluids with lower critical temperatures tend to perform better in low-temperature applications, while those with higher critical points are more suitable for geothermal or solar thermal systems operating above 150 °C (Jiménez-García *et al*., 2023; W. Xu *et al*., 2021). Other properties, such as molecular weight, critical pressure, and specific heat capacity, also play essential roles in aligning fluid behaviour with system-level goals (Linke *et al*., 2015).

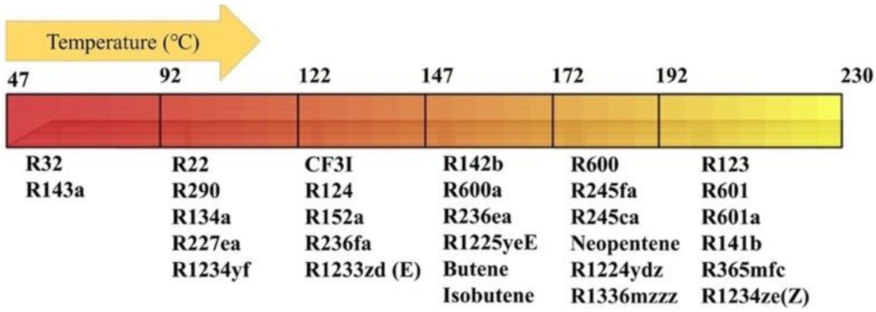

Figure 2.20: Working Fluid Selection as a Function of Heat Source

Source: (Pan *et al*., 2022; Yang *et al*., 2021)

From an environmental standpoint, most pure organic fluids have zero ozone-depletion potential (ODP), making them relatively safe. However, some legacy fluids, such as R123, R22, and R12, have non-zero ODP values and are being phased out under international agreements, including the Montreal Protocol and its Kigali Amendment (Huber *et al*., 2022). The GWP varies widely: while many fluids have GWP values below 20, others, such as R125 and R143a, exceed 3,0 (Domanski *et al*., 2018). Safety is another key concern. Only about 30% of commonly used ORC working fluids are non-flammable, while approximately 8% are considered toxic, highlighting the need to balance thermodynamic performance with operational safety (Babatunde & Sunday, 2018).

Therefore, Table 2.4 summarises the key thermophysical and environmental properties of commonly studied pure fluids in ORC systems. These data provide a comparative basis for evaluating fluid suitability across different temperature ranges, safety profiles, and regulatory constraints.

Table 2.4: Thermophysical and Environmental Properties of Selected ORC Working Fluids

Working Fluid	Molecular Weight (kg/mol)	Critical Temperature (°C)	Critical Pressure (Bar)	GWP	ODP	Flammable?	Toxic?
i-Butane	0.058	134.67	36.29	3	0	Yes	No
n-Pentane	0.072	196.55	33.68	3	0	Yes	No
n-Butane	0.058	151.98	37.96	4	0	Yes	No
i-Pentane	0.072	187.2	33.78	5	0	Yes	No
R290	0.044	96.74	42.51	11	0	Yes	No
i-Butene	0.056	144.94	40.1	20	0	Yes	No
R152a	0.066	113.26	45.17	120	0	Yes	No
R32	0.052	78.11	57.82	650	0	Yes	No
R245ca	0.134	174	39.3	693	0	Yes	No
R227ea	0.17	101.75	29.25	3220	0	Yes	No
R125	0.12	66.02	36.18	3500	0	Yes	No
R143a	0.084	72.7	37.61	4300	0	Yes	No
R1336mzz(Z)	0.164	171.3	26	2	0	No	No
R1234yf	0.114	95	33.81	4	0	No	No
R1234ze	0.114	109.4	36.4	6	0	No	No
R161	0.048	102.2	50.9	12	0	No	No
R245fa	0.134	154.01	36.51	1030	0	No	No
R236ea	0.152	139.29	34.2	1200	0	No	No
R134a	0.102	101.06	40	1300	0	No	No
R123	0.153	183.68	36.72	0	0.02	No	No
Toluene	0.092	318.1	41.26	0	0	Yes	Yes
R22	0.086	96.15	49.9	1700	0.06	Yes	Yes
R113	0.187	214.06	33.92	4800	0.8	Yes	Yes
R12	0.121	111.97	41.36	8500	0.9	Yes	Yes

Source: (Bell *et al*., 2014; Bianchi *et al*., 2021; Saleh *et al*., 2007)

Pure fluids continue to serve as the foundation of ORC technology, offering well-characterised thermodynamic behaviour and broad applicability. However, their selection increasingly demands a careful balance between performance, environmental impact, and safety. As system requirements become more complex and diverse, researchers have turned their attention to alternatives, particularly zeotropic mixtures and nanoparticle-enhanced formulations, which offer greater flexibility in tailoring fluid properties to specific operating conditions and application contexts.

2.5.2 Zeotropic Mixtures

Zeotropic mixtures are gaining traction in ORC systems due to their behaviour during phase change. Unlike pure fluids, which boil and condense at constant temperatures, zeotropic mixtures undergo non-isothermal transitions. This allows them to better match the temperature profile of low-grade heat sources, reducing irreversibilities in the evaporator and condenser and ultimately improving cycle efficiency (Andreasen *et al*., 2014; X. Zhang *et al*., 2020).

One of the key advantages of these mixtures is their ability to narrow the average temperature difference during heat exchange. That means less exergy loss, but it also comes with trade-offs. Minor temperature differences can require larger heat exchanger surfaces, potentially increasing capital costs (Dong *et al*., 2018).

Several studies have explored this balance between performance and cost. Therefore, Heberle and Brüggemann (2016); Oyewunmi and Markides (2016) found that mixtures such as R227ea/R245fa and n-pentane/n-hexane delivered higher thermal efficiencies than their pure counterparts, although they required more substantial investment in heat exchanger infrastructure. Similarly, Heberle *et al*. (2012) and Andreasen *et al*. (2021) reported that i-butane/i-pentane and R32/R134a mixtures improved net power output and lowered specific exergy costs.

Fine-tuning the composition of these mixtures has become a major focus. Yang *et al*. (2017) showed that R1234yf/R32 mixtures could outperform either fluid alone by nearly 5% in thermo-economic terms. Kolahi *et al*. (2016) found that R236ea/c-hexane mixtures offered the highest thermal efficiency across both simple and regenerative ORC setups, while R245fa/c-hexane mixtures minimised investment cost and shortened payback periods. Other researchers, including Imran *et al*. (2015) and Feng *et al*. (2015),have demonstrated that blends such as R245fa/i-pentane can reduce the heat-transfer area and electricity production costs, making them attractive for cost-sensitive applications.

Although zeotropic mixtures often exhibit superior thermodynamic and economic performance compared to their individual pure components, the literature also reports contrasting findings. For example, Le *et al*. (2014) evaluated *n*-pentane, R245fa, and their mixtures in an ORC system and found that, although the mixture yielded favourable results, *n*-pentane alone delivered the highest exergy efficiency and the lowest levelized cost of electricity (LCOE). Similarly, Garg and Orosz (2018) compared pure fluids (R134a, R152a, R161, and R245fa) with their mixtures and reported that the mixtures generally exhibited slightly lower cycle efficiencies, resulting in inferior performance indices. Fang *et al*. (2019) further highlighted the limitations of mixtures in a comparative analysis of *i*-butane, butane, *i*-pentane, pentane, and their blends, showing that *i*-butane achieved the greatest turbine power output and the shortest payback period among the mixtures. Y.-R. Li *et al*. (2014) emphasised that zeotropic mixtures may not universally outperform pure fluids, as their application in certain low-gradient heat exchangers necessitated larger surface areas, thereby increasing capital costs. In addition, Zhang *et al*. (2020), in their screening of 61 zeotropic mixtures for ORC systems using a single screw expander, identified R441A, R436B, and R432A as viable candidates, though they cautioned that mixture selection remains highly context dependent.

The success of zeotropic mixtures depends on the specifics of the system, the heat source temperature, the availability of cooling water, component sizing, and economic constraints. They can be highly effective in high-temperature ORCs, but under low-gradient conditions, their benefits may be offset by increased equipment size and cost.

2.5.3 Nanoparticle-Enhanced Fluids

Nanoparticles have emerged as a promising avenue for enhancing the thermophysical properties of ORC working fluids. When dispersed in a base fluid, they form nanofluids that exhibit higher thermal conductivity, heat capacity, and density compared to conventional fluids. These improvements enhance heat transfer performance, reduce the heat exchanger size, and ultimately improve cycle efficiency.

Most applications of nanoparticles in ORC research have focused on integrating them into heat-transfer fluids for solar collectors, evaporators, and condensers. For instance, Prajapati and Patel (2020) employed CuO-based nanofluids with R245fa as the working fluid, while Loni (2019a) demonstrated that increasing the concentration of Al_2O_3 nanoparticles improved thermal performance and increased power output in a solar dish concentrator system. Their study reported a 19.3% improvement in performance at a nanoparticle concentration of 1.1%. Similar research using CuO/oil, SiO_2/oil, and Al_2O_3/oil mixtures has shown thermal efficiency gains of 2–3%, although SiO_2 typically contributes the least impact.

Carbon nanotubes (CNTs), particularly multi-walled (MWCNTs) and single-walled (SWCNTs), have attracted significant interest due to their exceptional thermal conductivity and heat capacity, surpassing those of conventional nanoparticles such as Al_2O_3 and CuO. Mondejar *et al*. (2017) reported that incorporating 1% CNTs reduced the boiler area by 4% and increased the pressure drop by 18%, while pump power remained largely unaffected. When MWCNTs were used in oil as a heat-transfer fluid with R113 as the working fluid, both system efficiency and the levelized cost of electricity improved.

Despite these encouraging results, the direct use of nanofluids as working fluids in the ORC cycle, rather than solely in external heat exchangers, remains underexplored. Only two studies have explicitly modelled nanoparticle-enhanced working fluids: Saadatfar *et al*. (2014), who tested silver-doped n-pentane and reported significant gains in cycle efficiency alongside reduced condenser and evaporator sizes; and Mondejar *et al*. (2017), who evaluated Al_2O_3, CuO, and ZnO nanoparticles, noting that other particles, such as Ag, SiO_2, TiO_2, Sb_2O_5:SnO_2, and CNTs, appear less frequently in ORC studies.

Recent innovations have introduced metal-organic heat carriers (MOHCs), nanoparticles engineered to absorb and release substances within the fluid. These materials can extract additional heat from the desorption enthalpy, potentially doubling the latent heat of vaporisation. McGrail *et al*. (2013) demonstrated that MOHC/R123 nanofluids improved ORC power output by up to 15%, with no evidence of nanoparticle deposition in capillary tubes under low Reynolds number conditions. Similarly, Cavazzini *et al*. (2019) studied R245fa combined with MIL-101 (a MOHC nanoparticle) and found that the nanofluid improved system efficiency, reduced heat exchanger size, and enhanced overall economic feasibility.

Table 2.5 summarises the thermophysical properties of widely studied nanoparticles, including CuO, Al_2O_3, TiO_2, SiO_2, ZnO, Ag, SWCNT, and MWCNT. While single-fluid nanofluids based on R601, R245fa, and R123 have demonstrated measurable efficiency gains, there is currently no published research on nanofluid-enhanced zeotropic mixtures in ORC applications. Nonetheless, findings from refrigeration systems suggest that combining nanoparticles with zeotropic mixtures could further improve heat transfer, cycle stability, and overall thermodynamic performance, representing an important research frontier.

Table 2.5: Thermophysical Properties of Selected Nanoparticles Used in ORC Systems

Nanoparticle	Heat Capacity, c_p (kJ/kg K)	Thermal Conductivity, k (W/m.K)	Density, ρ (kg/m³)
CuO	0.55	33	6320
Al_2O_3	0.85	25	3960
TiO_2	0.68	8.4	4230
SiO_2	0.93	1.4	2650
ZnO	0.43	13	5610
Ag	0.24	407	10490
SWCNT	2.10	3000	2170
MWCNT	0.733	2586	2100

2.5.4 Hybrid Nanofluid-Zeotropic Systems

Recent research has begun to explore the combination of nanoparticle-enhanced fluids with zeotropic mixtures to further improve ORC performance. The rationale is straightforward: zeotropic mixtures offer better thermal matching with variable heat sources, while nanofluids enhance heat transfer through improved thermophysical properties. Together, they could address both cycle efficiency and component sizing challenges.

Although this concept remains largely theoretical in ORC applications, studies on refrigeration and HVAC systems have demonstrated that nanoparticle-enhanced refrigerant mixtures can enhance heat transfer coefficients and reduce entropy generation during phase change (Loni *et al*., 2019b; Prajapati & Patel, 2019). These findings suggest that similar benefits may be achievable in ORC systems, particularly where heat source variability and compact design are key considerations.

However, integrating nanoparticles into zeotropic mixtures introduces new complexities. Dispersion stability becomes increasingly difficult to maintain, and the interactions between nanoparticles and the behaviour of the multi-component fluid remain poorly understood. Mondejar *et al*. (2017) noted that while Al_2O_3, CuO, and

ZnO nanoparticles are commonly modelled in pure fluids, their behaviour in mixed-fluid environments remains underexplored. Saadatfar *et al*. (2014) demonstrated that silver-doped n-pentane improved cycle efficiency and reduced component size, but similar studies involving zeotropic blends remain scarce.

Emerging work on metal–organic heat carriers (MOHCs) offers a glimpse into what hybrid systems might achieve. Cavazzini *et al*. (2019)demonstrated that MOHC/R123 nanofluids enhanced power output by up to 15% without experiencing fouling or deposition issues. Cavazzini *et al*. (2019) further demonstrated that MIL-101-based MOHC nanoparticles, combined with R245fa, enhanced both thermal and economic performance by reducing the heat exchanger size and improving heat transfer rates.

To date, no studies have documented modelling ORC cycles using nanofluid-enhanced zeotropic mixtures. However, the potential is clear. As summarised in Table 2.5, the thermophysical properties of nanoparticles, such as CuO, Al_2O_3, TiO_2, and CNTs, can complement the temperature glide behaviour of zeotropic blends, offering a new pathway for optimising ORC systems. This represents a promising, yet largely untapped, direction for future research.

2.5.5 Comparative Assessment of Working Fluids

The performance and viability of ORC systems are closely tied to the properties of the working fluid. As explored in previous subsections, pure fluids, zeotropic mixtures, and nanoparticle-enhanced formulations each offer distinct advantages and limitations. This section presents a comparative assessment of these fluid categories, focusing on thermodynamic behaviour, environmental impact, economic feasibility, and practical deployment.

Pure fluids are widely adopted in ORC systems due to their well-characterised phase-change behaviour and compatibility with standard simulation tools. Dry and isentropic fluids support stable expansion and high exergy efficiency (Badr *et al*., 1985; Tocci *et al*., 2017). Zeotropic mixtures introduce non-isothermal phase transitions, which improve thermal matching with low-grade heat sources and reduce irreversibilities in heat exchangers (X. Zhang *et al*., 2020). Nanofluids enhance heat transfer by increasing thermal conductivity and specific heat capacity, often resulting in reduced component sizes and improved cycle efficiency (Prajapati & Patel, 2019; Saadatfar *et al*., 2014).

Environmental regulations have significantly influenced the selection of fluids. Most pure organic fluids have zero ODP, but some, such as R123 and R22, are being phased out due to high GWP and toxicity (Huber *et al*., 2022). Zeotropic mixtures often combine low-GWP components; however, their environmental impact depends on the composition and mass fraction (García-Pabón *et al*., 2021). Nanoparticle-enhanced fluids introduce additional safety concerns, including potential toxicity, long-term stability, and disposal challenges. While metal oxides, such as Al_2O_3 and CuO, are generally considered safe, carbon-based nanoparticles and silver formulations require careful handling and lifecycle assessment (Cavazzini *et al*., 2019; Loni *et al*., 2019a).

Cost remains a central consideration in ORC deployment. Pure fluids are typically low-cost and readily available but may require larger heat exchangers in low-temperature applications. Zeotropic mixtures can improve net power output and reduce exergy losses, but they often require larger heat exchanger surfaces and more complex control systems, thereby increasing capital costs (Andreasen *et al*., 2021; Heberle & Brüggemann, 2016). Nanofluids offer performance gains but introduce material costs and potential maintenance issues related to nanoparticle dispersion and fouling. Hybrid formulations, such as MOHC-enhanced fluids, may offer favourable trade-offs by improving efficiency without significantly increasing system complexity (McGrail *et al*., 2013).

Pure fluids benefit from extensive experimental validation and robust thermodynamic databases (Huber *et al*., 2022). Zeotropic mixtures require more sophisticated modelling due to temperature glide and composition-dependent behaviour. Nanofluids and hybrid systems remain primarily in the research phase, with limited full-cycle modelling and few commercial implementations. Dispersion stability, compatibility with system materials, and long-term reliability are ongoing challenges (Mondejar *et al*., 2017). Table 2.6 summarises the key attributes of each fluid category, along with supporting references.

Table 2.6: Comparative Attributes of Working Fluid Categories in ORC Systems

Attribute	Pure Fluids	Zeotropic Mixtures	Nanoparticle-Enhanced Fluids	Key References

Phase Change Behaviour	Isothermal	Non-isothermal	Variable (depends on base fluid)	(Badr *et al*., 1985; (Zhang *et al*., 2019)
Thermal Efficiency	Moderate to High	High (with thermal matching)	Potentially High (via enhanced conductivity)	(Andreasen *et al*., 2021; Prajapati & Patel, 2020)
Exergy Losses	Moderate	Low	Low to Moderate	(Saadatfar *et al*., 2014; Wu *et al*., 2016)
Environmental Impact	Varies (some high GWP)	Composition-dependent	Depends on nanoparticle type	(Cavazzini *et al*., 2019; García-Pabón *et al*., 2021)
Safety and Toxicity	Well-documented	Varies	Requires careful handling	(Huber *et al*., 2022; Loni *et al*., 2019b)
Heat Exchanger Size	Moderate to Large	Large	Reduced (if stable dispersion)	(Li *et al*., 2020b; Mondejar *et al*., 2017)
Modelling Complexity	Low	Moderate to High	High	(Huber *et al*., 2022; Mondejar *et al*., 2017)
Commercial Availability	High	Moderate	Low	(Cavazzini *et al*., 2019; Tocci *et al*., 2017)

2.6 Modelling of ORC Operations

Although significant advancements have been made in ORC technology, further research is required to facilitate the successful commercialisation of micro- and small-scale systems. System modelling plays a pivotal role in the design, optimisation, and operational control of ORC configurations. A comprehensive understanding of dynamic response characteristics and operating parameters is crucial for accurately evaluating system performance and competitiveness. Inadequate modelling approaches may yield impractical results, particularly at micro and small scales, where systems are subject to pronounced fluctuations that exacerbate challenges related to profitability and reliability.

Numerous studies have contributed to the development of robust ORC models. Jung *et al*. (2015) proposed a numerical model for simulating a standard ORC system and its heat exchangers, serving as a design tool for high-efficiency power plants. Liu *et al*. (2017) developed a practical model tailored for small-scale ORC systems, focusing on fluid charge management and off-design performance analysis. Quoilin *et al*. (2010) integrated computational modelling with empirical data to identify opportunities for performance improvement in scroll expander-based ORC systems. Zhang *et al*. (2012) investigated the dynamic behaviour of ORCs in waste heat recovery applications and introduced a multivariable control strategy to enhance system responsiveness and efficiency. Imran *et al*. (2020) emphasised the critical role of heat exchangers in dynamic modelling and advocated for the use of model predictive controllers to achieve optimal performance.

Simulation tools for ORC systems are broadly categorised into code-based and library-based platforms. The selection of appropriate software depends on the nature of the analysis (steady-state or transient) and the degree of customisation required. Code-based tools offer greater flexibility in defining system equations, whereas library-based tools rely on predefined component models and equations.
Liu *et al*. (2018) provided a comparative overview of popular ORC simulation platforms, summarised in Table 2.7. These tools vary in their capabilities, ranging from thermodynamic analysis and component-level modelling to support for property databases such as REFPROP and COOLProp.

Table 2.7: Overview of Popular Software Capable of Simulating ORC Systems

Software	Type	Summary
Aspen Plus	Library-based Code-based	Supports non-linear algebraic systems, complete fluids, and solids library
AMESim	Library-based	Ready-to-use components, Steady/Unsteady Analyses, REPROP, COOLProp
Cycle-Tempo	Library-based	Thermodynamic analyses, optimisation of energy systems, Fluid prop
DWSIM/DWSIM Pro	Library-based	Ready-to-use components, Steady/Unsteady Analyses, REPROP, COOLProp
Engineering Equation Solver (EES)	Code-based	Supports non-linear algebraic systems, REPROP, COOLProp
FLOWNEX SE	Library-based	Ready-to-use components, Steady/Unsteady Analyses, REPROP, COOLProp
MATLAB/Simulink	Library-based Code-based	S-Functions, Steady/Unsteady Analyses, REPROP, COOLProp
Modelica	Library-based	Object-oriented language, Unsteady analyses, REPROP, COOLProp
Python	Code-based	High-level coding, REPROP, COOLProp

[Adapted from (L. Liu *et al*., 2018)]

2.7 Research Gaps

Despite significant advancements in ORC research, several unresolved issues continue to limit the optimisation, scalability, and practical deployment of ORC systems, particularly those involving advanced working fluids. This section synthesises the key gaps identified in the literature, focusing on zeotropic mixtures, nanoparticle-enhanced fluids, system-level modelling, and real-world implementation challenges.

2.7.1 Limited Comparative Studies on Zeotropic Mixtures

Zeotropic mixtures have garnered attention for their ability to minimise irreversibilities in heat exchangers due to their temperature glide, which enables better thermal matching with heat sources (Chen *et al*., 2010; Saleh *et al*., 2007). However, most studies focus on a limited set of mixtures, often selected based on prior use or commercial availability, rather than through systematic thermodynamic screening.

For example, Yamamoto *et al*. (2001) and Quoilin *et al*. (2013) investigated mixtures such as R245fa/R227ea and n-pentane/n-hexane, demonstrating improved performance over pure fluids. However, these studies rarely compare multiple mixtures under consistent operating conditions, making it difficult to generalise findings or identify optimal combinations for specific applications.

Moreover, environmental and safety considerations, such as flammability, toxicity, and global warming potential, are often overlooked in the selection of mixtures (Heberle & Brüggemann, 2016). There is a need for comprehensive benchmarking that evaluates zeotropic mixtures across thermodynamic, economic, and environmental dimensions, using consistent criteria and simulation frameworks.

2.7.2 Underexplored Role of Nanoparticles in ORC Working Fluids

Nanoparticles have demonstrated remarkable potential in enhancing thermal conductivity and heat transfer rates in various thermal systems (Das & CHOI, 2009; Eastman *et al*., 2001). In conventional applications, such as solar collectors and microchannel heat exchangers, nanofluids have demonstrated efficiency gains of up to 20% (Said *et al*., 2016). However, their integration into ORC working fluids remains underexplored.

Most existing studies on nanofluids concentrate on water or ethylene glycol, but there is notably limited exploration involving organic fluids that are suitable for ORCs (Mahbubul, 2019). Although nanofluid-enhanced heat transfer has been well-studied (including in porous media), the impact of incorporating nanoparticles within zeotropic mixtures remains largely uninvestigated (Kasaeian *et al*., 2017).

The absence of experimental and simulation-based research on hybrid nanofluid–zeotropic systems represents a significant gap. Furthermore, the influence of nanoparticle type, concentration, and surface treatment on full-cycle ORC behaviour, particularly under the low-temperature conditions typical of many ORCs, remains largely unknown.

2.7.3 Dispersion Stability and Practical Deployment Challenges

Simulation studies often assume ideal conditions, including perfect nanoparticle dispersion and stable thermophysical properties. Nanofluids face challenges such as agglomeration, sedimentation, and chemical incompatibility with system materials (Kole & Dey, 2010; Yu & Xie, 2012). These issues can degrade performance over time and complicate maintenance protocols.

Sundar *et al*. (2013) further demonstrated that nanoparticle stability is highly sensitive to fluid chemistry, operating temperature, and flow conditions. These challenges become even more critical in ORC systems, which operate under cyclic thermal loads in closed-loop configurations.

Despite these concerns, limited research addresses long-term stability and proposes practical mitigation strategies, such as surfactants, nanoparticle surface functionalisation, or active mixing techniques (e.g., magnetic stirring). Comprehensive experimental validation and lifecycle assessments are still needed to evaluate the durability, reliability, and maintenance implications of nanoparticle-enhanced working fluids in ORC environments.

2.7.4 Lack of System-Level Performance Evaluation

A significant portion of ORC research focuses on optimising individual components, such as evaporators, condensers, or expanders, without assessing the impact on overall cycle performance (Hung, 2001; Wang *et al*., 2011c). This fragmented approach limits the ability to evaluate trade-offs between subsystems and to optimise the cycle holistically.

For instance, attempts to improve heat transfer in the evaporator can inadvertently increase pumping power due to higher fluid viscosity, ultimately reducing net cycle efficiency. Similarly, deploying high-performance fluids may necessitate more complex control systems, which could affect both reliability and operational costs. Ambriz-Díaz *et al*. (2022) emphasise the importance of integrating thermodynamic, exergy, economic, and environmental metrics when evaluating ORC systems to ensure balanced, system-wide performance analysis.

Robust system-level modelling is essential for capturing these interdependencies and validating the practical viability of proposed ORC configurations. Without such a holistic evaluation, performance improvements derived from optimising isolated components may be misleading or fail to scale in real-world applications.

2.7.5 Gaps in Thermo-Economic and Environmental Evaluation

Most ORC studies prioritise thermodynamic metrics such as efficiency, heat recovery ratio, or exergy destruction, while neglecting economic and environmental considerations (Manente *et al*., 2017; Quoilin *et al*., 2011). However, the selection of working fluid and system configuration has direct implications for capital costs, operating expenses, safety, and sustainability.

To address this, Papadopoulos *et al*. (2010) proposed a multi-criteria decision-making framework that evaluates working fluids and ORC configurations using a combination of economic, environmental (GWP, ODP), safety, and performance indicators. Their case study demonstrated that a fluid with slightly lower thermodynamic efficiency, but better environmental and cost profiles, resulted in a more sustainable and viable system choice.

This holistic assessment approach is especially crucial for decentralised or developing region deployments, where affordability, regulatory compliance, and long-term sustainability are as important as energy performance.

2.8 Summary of Literature Review

This chapter explored the evolving landscape of ORC systems, focusing on how working fluid choices influence thermodynamic performance, environmental impact, and system design. It began by examining pure organic fluids, their strengths and limitations, and why they remain foundational despite growing concerns about their global warming potential and heat source compatibility.

The discussion then shifted to zeotropic mixtures, which offer a unique advantage through their temperature glide. This property enables better thermal matching and reduced irreversibilities, particularly in low-grade heat recovery applications. While promising, the literature shows that only a narrow set of mixtures has been studied, often without consistent benchmarking or consideration of environmental trade-offs. Nanoparticle-enhanced fluids have been introduced as a new frontier. These formulations, ranging from metal oxides to carbon nanotubes, have shown potential to boost heat transfer and reduce component size. However, their use in ORC cycles, particularly in combination with zeotropic blends, remains largely theoretical. Issues such as dispersion stability, long-term reliability, and compatibility with organic fluids remain unresolved.

To clarify these fluid categories, the chapter included a comparative assessment across thermodynamic, economic, and environmental dimensions. Tables summarising fluid properties and nanoparticle characteristics helped visualise the trade-offs engineers face when designing ORC systems.

The final section identified five major research gaps: limited comparative studies on zeotropic mixtures, underexplored nanoparticle integration, challenges with dispersion stability, lack of system-level modelling, and the absence of thermo-economic and environmental trade-off analysis. These gaps highlight the need for a more comprehensive approach, one that prioritises not only efficiency but also considers cost, sustainability, and practical viability in the real world.

Chapter Three

3 Methodology and Simulation Framework

3.1 Introduction

This chapter presents the framework for investigating the thermodynamic performance of advanced working fluids in a hybrid solar–biomass ORC system. The focus is on environmentally friendly zeotropic mixtures enhanced with nanoparticles, tested under dynamic heat input conditions that mimic the behaviour of decentralised renewable energy systems.

The ORC, which is powered by two complementary heat sources, including solar thermal energy and biomass combustion, was integrated through a controlled mixing system with a stratified thermal buffer tank, which helps stabilise the temperature of the heat delivered to the evaporator. This design allows the system to adapt to fluctuations in solar radiation, while the biomass boiler provides steady support to maintain reliable operation.

Two working-fluid sets were considered in this study to assess thermodynamic performance under hybrid solar–biomass conditions. The first set consists of conventional and transitional fluids, R123, R245fa, and R1233zd(E). These are well-known and widely studied, making them useful for benchmarking and comparison. However, their use is limited by environmental concerns, such as ODP, and, in some cases, relatively high GWP.
The second set focuses on advanced zeotropic mixtures for more efficient, environmentally friendly ORC operation. This group includes R1224yd(Z), R1233zd(E), and R1336mzz(Z), whose mixtures were chosen for their favourable temperature glide, high critical temperatures, and ultra-low GWP values. Their zeotropic behaviour also enables better thermal matching in the evaporator, thereby improving cycle efficiency under varying heat-supply conditions.

To further enhance heat transfer, selected nanoparticles, including TiO_2, ZnO, Ag, Al_2O_3, and CuO, were added to the working fluid mixtures in carefully controlled amounts. By increasing thermal conductivity and lowering evaporator thermal resistance, these additives support greater cycle stability, faster response, and higher net power output, even as solar and biomass inputs fluctuate.

The system is modelled in ASPEN Plus using the Peng–Robinson equation of state to capture non-ideal fluid behaviour. Energy balances are applied to each component to evaluate turbine work, cycle efficiency, and evaporator performance. Sensitivity studies were then conducted to investigate the impact of changes in operating temperature, mixture composition, and nanoparticle concentration on the results.

3.2 System Configurations

The hybrid energy system examined in this study combines solar thermal and biomass resources to drive an ORC for small-scale power generation. As shown in Figure 3.1, the solar-biomass hybrid thermal system is configured to handle variable heat inputs, with a stratified buffer tank and a controlled mixing system that ensure steady heat delivery to the ORC evaporator. This arrangement enables flexible prioritisation of energy sources and ensures reliable operation across daily and seasonal fluctuations.

The solar thermal subsystem consists of a collector array, such as parabolic troughs or evacuated tube collectors, which captures radiation and transfers heat to a high-temperature heat transfer fluid (HTF), typically Therminol VP-1. Because solar output varies with irradiance and collector efficiency, dynamic control is required to prevent overheating and maintain a consistent supply. Complementing this is a biomass boiler, which burns agricultural residues or wood pellets to provide dispatchable heat. Its output is controlled by adjusting the fuel feed rate and airflow, enabling rapid ramp-up to offset solar shortfalls or sustain nighttime operation.

A stratified buffer tank provides the thermal interface between the sources and the ORC. Heat from both solar and biomass sources flow into the tank via a control valve, which a controller governs. Four temperature sensors (T1: solar inlet, T2: biomass inlet, T3: buffer outlet, and T4: evaporator inlet) provide feedback, allowing the controller to maintain the buffer outlet temperature at a set point, typically 150–200 °C, depending on the chosen working fluid. The control strategy prioritises solar energy during the day, with biomass supplementing only when the buffer temperature falls below the target. At night or under low irradiance, biomass serves as the primary energy source.

The ORC power block is a closed-loop system comprising a pump, an evaporator, an expander or turbine, a condenser, and a recirculation pump. The working fluid, selected from advanced zeotropic mixtures, is pumped into the evaporator, where it absorbs heat from the buffer. The resulting vapour expands through the turbine to generate shaft power, which can be converted to electricity. To enhance thermal performance, nanoparticle-doped fluids are utilised to improve heat transfer coefficients, reduce thermal resistance, and improve system responsiveness.

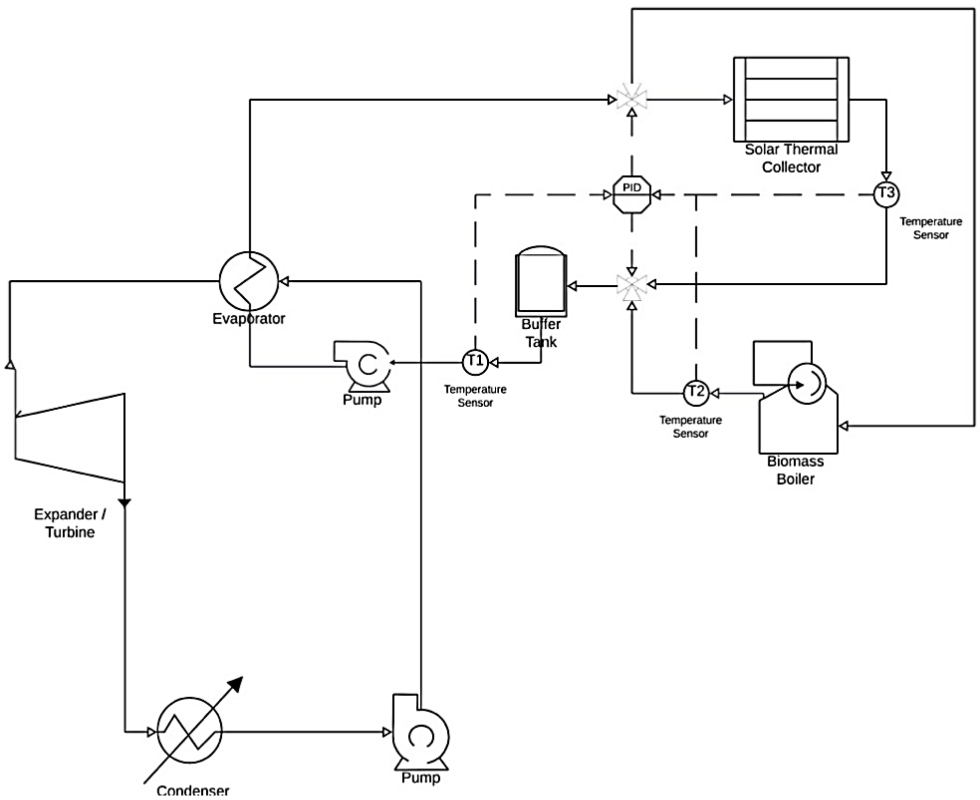

Figure 3.1: Solar-Biomass Hybrid Thermal System

3.3 Working Fluid and Nanoparticle Selection

The selection of working fluids and thermal enhancement additives in this study was guided by thermodynamic suitability, environmental compliance, and compatibility with hybrid solar-biomass heat input conditions. Two distinct sets of working fluids were considered; each paired with specific nanoparticles to evaluate their combined impact on heat transfer performance and cycle efficiency.

3.3.1 Benchmark Fluids and Additives

The first set comprises conventional and transitional fluids, including R123, R245fa, and R1233zd(E), which are used primarily for benchmarking and comparative analysis. These fluids are well-characterised and widely used in ORC systems, offering reliable thermodynamic behaviour and extensive experimental validation. However, their long-term viability is constrained by environmental factors, such as ODP and high GWP.

To enhance the thermal conductivity of these fluids and improve evaporator performance, three nanoparticles were introduced: Ag, Al_2O_3, and CuO. These additives were selected based on their high thermal conductivity, chemical stability, and compatibility with conventional organic fluids. Their inclusion improves heat transfer rates, reduces thermal resistance, and enhances responsiveness under steady-state biomass-dominant conditions.

The thermophysical and environmental properties of the selected working fluids are summarised in

Table 3.*1*.

Table 3.1: Thermophysical and Environmental Properties of Selected Working Fluids

Fluid	Boiling Point (°C)	Critical Temp. (°C)	Critical Pressure (bar)	GWP (AR6, 100-yr)	ODP	Safety Class	Reference
R123	27.6	183.7	36.2	~77	0.01	B1	(Zhou *et*

					2		*al*., 2023)
R245fa	15.3	154.0	36.4	~950	0.00	A1	(Arpagaus & Bertsch, 2021)
R1233zd(E)	18.3	165.5	35.7	~1	0.00	A1	(Fedele *et al*., 2023)
R1224yd(Z)	~14.0	154.6	~32.0	~1.4	0.00	A1	(Arpagaus & Bertsch, 2021)
R1336mzz (Z)	~33.4	171.3	~29.0	~2	0.00	A1	(Fedele *et al*., 2023)

3.3.2 Advanced Zeotropic Mixtures and Additives

The second set focuses on advanced zeotropic mixtures tailored for high-efficiency, low-emission ORC operation. Specifically, the fluids in the mixtures include R1224yd(Z), R1336mzz(Z), and R1233zd(E). These combinations were selected for their favourable temperature glide characteristics, elevated critical temperatures, and ultra-low GWP values. Their zeotropic behaviour enables improved thermal matching between the working fluid and the heat source, reducing irreversibilities in the evaporator and enhancing cycle efficiency under variable operating conditions. To further augment thermal performance, this set was paired with TiO_2, zinc oxide ZnO, and Ag nanoparticles. These additives were chosen for their high thermal conductivity and proven effectiveness in enhancing heat transfer in nanofluid applications. Their integration supports dynamic thermal response, particularly under fluctuating solar input, and improves evaporator effectiveness and net power output.

3.3.3 Nanoparticle Properties and Application Strategy

The thermophysical properties of the selected nanoparticles are presented in Table

3.2. Each nanoparticle was applied to a specific fluid set based on compatibility, dispersion stability, and target operating conditions. Ag was used across both sets due to its exceptional thermal conductivity and versatility.

Table 3.2: Thermophysical Properties of Selected Nanoparticles

Nanoparticle	Density (kg/m³)	Thermal Conductivity (W/m·K)	Specific Heat (J/kg·K)	Particle Size (nm)	Reference
TiO_2	~4200	~8.4	~686	10–50	(Topuz *et al.*, 2021)
ZnO	~5600	23–30	~500	20–50	(Topuz *et al.*, 2021)
Ag	10490	~429	~235	5–50	(Rahman *et al.*, 2024)
Al_2O_3	~3970	~36	~880	20–50	(Said & Saidur, 2017)
CuO	~6500	~76	~540	20–50	(Topuz *et al.*, 2021)

These modified parameters were incorporated into the ASPEN Plus simulation environment to evaluate their impact on evaporator duty, turbine work output, and overall cycle performance. The simulation assumes ideal mixing and single-phase flow, with nanoparticle effects captured through adjusted thermophysical correlations.

3.4 Heat Source Characterisation

The ORC system in this study is driven by a hybrid heat source that combines solar thermal energy with biomass combustion. The principle is straightforward: solar energy is prioritised whenever available, while biomass serves as a reliable backup during periods of low irradiance. This arrangement reflects real-world deployment strategies, particularly in regions such as sub-Saharan Africa, where solar potential is high but subject to daily and seasonal variability.

The solar subsystem is modelled using monthly DNI data to capture seasonal fluctuations in resource availability. Instead of simulating the full year at hourly intervals, representative conditions are defined for three operating modes: solar-dominant, balanced hybrid, and biomass-dominant. A medium-temperature evacuated tube collector was adopted in this study, with an efficiency range of 55-65%, consistent with reported values for evacuated tube collectors operating within the 100-200 °C range. The heat transfer fluid (HTF), Therminol VP-1, circulates through the collector field, transferring energy to a buffer tank. Two HTF flow rates (0.05 kg/s and 0.1 kg/s) are considered to examine the impact of mass flow rate on outlet temperature and subsequent biomass demand.

The biomass subsystem uses agricultural residues or wood pellets as fuel, with a lower heating value (LHV) of 15- 18 MJ/kg. The boiler is assumed to operate at 80-85% efficiency, and its feed rate is dynamically adjusted to maintain the buffer tank outlet temperature. The combustion process is treated as steady and ideal, with transient effects and detailed reaction kinetics excluded from the scope of the present study.

The buffer tank plays a central role in integrating both heat sources. It combines thermal inputs, smooths out short-term fluctuations, and provides a stable temperature to the ORC evaporator. The control strategy prioritises solar energy: biomass is engaged only when the buffer outlet temperature falls below the setpoint by a small deadband (1- 3 °C). This ensures reliable operation while minimising biomass consumption.

For simulation purposes, the buffer outlet temperature is treated as a boundary condition. Four setpoints (140, 160, 180, and 200 °C) are used to represent distinct operating scenarios. These values define the hot-side conditions supplied to the ORC evaporator in ASPEN Plus. By managing the heat source in this manner, the study strikes a balance between realism and computational tractability, enabling consistent comparisons of zeotropic mixtures and nanoparticle-enhanced fluids under hybrid operating conditions.

3.5 Simulation Setup and Modelling Tools

The thermodynamic performance of the hybrid solar-biomass ORC system was evaluated using a steady-state simulation framework developed in ASPEN Plus V14. The simulation replicates the system configuration illustrated in Figure 3.1 and follows a structured design and analysis workflow, as depicted in the flowchart in Figure 3.2. This workflow outlines the iterative process of heat source characterisation, system modelling, baseline simulation, and performance evaluation. Each working fluid–nanoparticle combination was assessed under identical operating conditions to ensure comparability and isolate the effects of fluid composition and thermal enhancement.

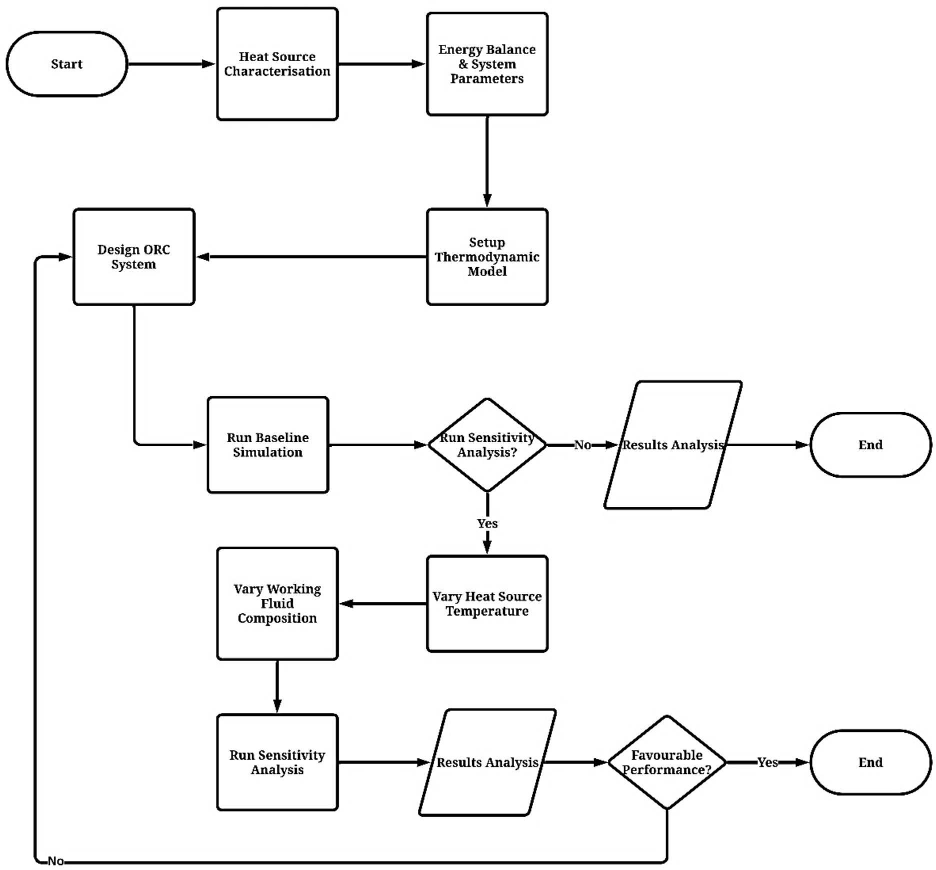

Figure 3.2: Flowchart for ORC System Evaluation

3.5.1 System Boundary and Assumptions

The simulation assumes a closed-loop ORC operating under steady-state conditions. Heat input is supplied from a stratified buffer tank that receives thermal energy from both solar collectors and a biomass boiler. Several simplifying assumptions were made to streamline the modelling process: single-phase flow was assumed for all nanoparticle-enhanced fluids, and pressure drops across heat exchangers were considered negligible. The ambient temperature was maintained at 25 °C for the condenser calculations, and nanoparticle mass fractions were varied from 0.000001 to 0.01 to assess their impact on heat transfer and cycle performance.

3.5.2 Fluid Property Integration

All working fluids and mixtures in this study were modelled in ASPEN Plus V14 using the Peng–Robinson equation of state. This EOS was chosen due to its proven ability to handle the non-ideal behaviour of organic fluids at moderate to high temperatures and pressures. To ensure consistency, the same framework was applied across pure fluids, zeotropic mixtures, and nanoparticle-enhanced formulations.

For nanoparticle-enhanced fluids, the nanofluid was represented as a pseudo-homogeneous mixture. The modified thermophysical properties, density, specific heat, viscosity, and thermal conductivity, were calculated automatically in ASPEN Plus. In this way, PEOS could still perform phase-equilibrium and energy-balance calculations without requiring custom subroutines. The nanoparticles themselves were not modelled as discrete solid phases; rather, their effects were incorporated into the adjusted bulk fluid properties.

This modelling approach provided a uniform thermodynamic framework, enabling direct comparison of base fluids and their nanoparticle-enhanced counterparts. It also ensured that differences in performance could be attributed to fluid properties rather than inconsistencies in the simulation method.

3.5.3 Component Modelling

Each component of the ORC system was modelled in ASPEN Plus V14 using standard unit operation blocks configured to capture realistic thermodynamic behaviour. The evaporator was represented as a counterflow heat exchanger, with the nanoparticle-enhanced working fluid on the tube side and the buffer tank output on the shell side. The temperature gradient and fluid properties drove heat transfer. The expander was implemented using a turbine block, where the enthalpy differences across the expansion process determined the mechanical work output. ASPEN Plus's built-in thermodynamic calculations were used to estimate power output for each fluid configuration.

The condenser was modelled as an air-cooled heat exchanger operating at a fixed ambient temperature of 25 °C. This ensured complete condensation and subcooling of the working fluid before recirculation. The feed pump was defined by pressure rise specifications tailored to each fluid, enabling the accurate estimation of input work and pressurisation.

3.5.4 Simulation Workflow and Analysis

The simulation workflow followed a structured and iterative process, as illustrated in Figure 3.2. It began with the characterisation of the heat source and the definition of key system parameters, after which the thermodynamic model was constructed in ASPEN Plus V14. Baseline simulations were then performed for each working fluid–nanoparticle combination under identical heat source conditions to ensure consistency and comparability across scenarios.

Decision points were built into the workflow to evaluate performance; however, the sensitivity analysis primarily focused on variations in nanoparticle concentration and working fluid composition. Simulation outputs included evaporator duty, turbine work output, thermal efficiency, and condenser load. These performance metrics provided the basis for comparing configurations and identifying the most promising fluid–nanoparticle pairings.

3.6 Governing Thermodynamic Equations

The thermodynamic behaviour of the hybrid ORC system was evaluated using standard energy balance relationships applied to each major component. These equations in Table 3.3 provide the analytical foundation for quantifying energy flows, component efficiencies, and overall cycle performance. Each expression is formulated in terms of measurable parameters such as mass flow rate, enthalpy, pressure, and solar irradiance.

For the pump, the governing relationship estimates the mechanical work required to pressurise the working fluid. The equation assumes incompressible flow and relates the fluid's specific volume to the pressure rise across the pump. This step is important for quantifying parasitic power consumption and, by extension, the net work output of the cycle (Quoilin *et al*., 2013).

In the evaporator, the working fluid absorbs heat until vaporisation occurs. The thermal input is expressed as the enthalpy difference between inlet and outlet states. Depending on the fluid, this may include both sensible heating and latent heat of vaporisation. The effectiveness of this process is strongly influenced by the buffer tank temperature and the selected working fluid (Hung, 2001).

The turbine extracts useful mechanical power during expansion. Its work output is calculated from the enthalpy drop across the turbine, representing the conversion of thermal energy into shaft power. This equation is central to evaluating cycle performance since turbine work directly drives electrical generation.

The condenser is responsible for rejecting residual heat to the surroundings and restoring the fluid to a subcooled liquid state. The enthalpy change across the condenser determines the cooling load. This step not only closes the cycle but also governs the required size and design of the cooling system.

For the solar thermal collector, the available heat is estimated as a function of collector efficiency, aperture area, and incident solar irradiance. This relationship links environmental inputs to the thermal energy supplied to the buffer tank, ensuring that the solar contribution is realistically captured in the model.

When solar energy is insufficient, the biomass boiler provides supplementary heat. Its output is calculated from the fuel mass flow rate and its lower heating value (LHV), assuming complete combustion at steady state. This contribution is essential for simulating hybrid operation, particularly under variable irradiance conditions.

Table 3.3: Governing Thermodynamic Equations for Key ORC Components

Component	Equation	Remarks
Pump	$\dot{W}_{in} = \dot{W}_{pump} = \dot{m} \cdot v \cdot (\Delta P)$	$\dot{m}$= Mass flow rate of the working fluid v= Specific volume of the working fluid ΔP= Pressure rise across the pump
Evaporator	$\dot{Q}_{in} = \dot{Q}_{evap} = \dot{m} \cdot (h_2 - h_1)$	h_1= Enthalpy of the working fluid at the evaporator inlet h_2= Enthalpy of the working fluid at the evaporator outlet
Turbine	$\dot{W}_{out} = \dot{W}_{turb} = \dot{m} \cdot (h_3 - h_4)$	h_3= Enthalpy of the working fluid at the turbine inlet h_4= Enthalpy of the working fluid at the turbine outlet
Condenser	$\dot{Q}_{out} = \dot{Q}_{cond} = \dot{m} \cdot (h_4 - h_1)$	h_1= Enthalpy of the working fluid at the condenser outlet h_4= Enthalpy of the

		working fluid at the condenser inlet
Solar Thermal Collector	$\dot{Q}_{in} = \eta_{collector} \cdot A_{collector} \cdot I$	$\eta_{collector}$= Efficiency of the solar collector $A_{collector}$= Collector surface area I= Solar irradiance
Biomass Boiler	$\dot{Q}_{biomass} = \dot{m}_{fuel} \cdot LHV$	$\dot{m}_{fuel}$= Mass flow rate of the biomass fuel LHV = Lower heating value of the biomass

3.7 Performance Metrics and Evaluation Criteria

The thermodynamic performance of the ORC system was evaluated using a set of core performance metrics designed to capture both overall energy conversion efficiency and component-level effectiveness. These indicators were derived directly from the ASPEN Plus V14 simulation outputs and applied consistently across all working fluid–nanoparticle configurations to ensure comparability.

The primary metric was the thermal efficiency (η), defined as the ratio of the net power output to the total heat input from the buffer tank. This served as the central measure of system performance under hybrid solar–biomass conditions.

To provide further insight into subsystem behaviour, the following component-level metrics were monitored:

i. Evaporator duty ($\dot{Q}evap$): quantifies the heat absorbed by the working fluid during vaporisation.

ii. Turbine work output ($\dot{W}turb$): represents the mechanical energy generated during the expansion process.

iii. Condenser load ($\dot{Q}cond$): measures the heat rejected to the environment, ensuring complete condensation and reliable fluid recirculation.

For comparative analysis, the specific net power output (kJ/kg) was calculated for each working fluid, allowing the results to be normalised to the mass flow rate. In addition, environmental sustainability was evaluated using GWP and ODP values reported in the literature. Finally, safety classifications based on ASHRAE standards were considered to contextualise the thermodynamic results with respect to real-world applicability, encompassing aspects such as flammability and toxicity.

3.8 Validation Strategy and Benchmarking Approach

To ensure the reliability of the simulation outcomes, validation was performed through a combination of literature benchmarking and internal consistency checks. Well-established reference fluids, such as R245fa and R1233zd(E), were chosen for their frequent use in ORC systems and for the availability of published performance data under comparable operating conditions. These fluids were simulated within the hybrid solar–biomass configuration, and key indicators, thermal efficiency, evaporator duty, and turbine work, were compared with ranges reported in peer-reviewed studies.

The benchmarking emphasised trend validation rather than exact numerical replication, confirming that the ASPEN Plus V14 model produced outputs consistent with the expected performance of the reference fluids. Any discrepancies were traced to differences in boundary conditions, component assumptions, or system configuration, and were explicitly documented.

Internal consistency was further ensured by applying uniform heat-source conditions and system parameters across all working-fluid–nanoparticle scenarios. This design controlled for external influences, ensured that performance variations could be attributed solely to fluid properties and nanoparticle effects.

Although experimental validation was beyond the scope of this study, the combination of literature benchmarking and controlled modelling protocols established a robust foundation for assessing the credibility and relevance of the simulation framework.

3.9 Limitations of the Simulation Framework

While the developed simulation framework provides valuable insights into the thermodynamic performance of the hybrid solar–biomass ORC system, several limitations must be acknowledged.

First, the model was restricted to steady-state operation, thereby excluding transient behaviour and dynamic control responses to fluctuating solar input. This simplification was adopted to maintain computational stability and to enable clear comparisons across different fluid configurations.

Second, isentropic efficiencies of the expander and pump were not explicitly varied or calibrated; instead, ASPEN Plus defaults were applied, with work output estimated directly from enthalpy differences. Likewise, pinch-point constraints in the evaporator were not imposed, meaning that heat exchanger performance was determined solely by fluid properties and temperature gradients.

Third, nanoparticle-enhanced fluids were modelled as pseudo-homogeneous mixtures. While the PEOS captured their thermodynamic behaviour, particle-scale effects such as agglomeration, sedimentation, and long-term stability were not included. This limits the framework's ability to replicate real-world transport behaviour under cyclic loading or varying flow regimes.

Finally, the study was confined to thermodynamic analysis. Broader techno-economic, environmental lifecycle, and operational assessments were outside the scope of this study but represent important directions for future research.

Despite these constraints, the modelling framework establishes a consistent and reproducible basis for assessing fluid-side enhancements and provides a useful foundation for subsequent experimental validation and system-level studies.

3.10 Summary of the Methodological Framework

This chapter outlined the methodology adopted to evaluate the thermodynamic performance of a hybrid solar–biomass ORC system using ASPEN Plus V14. The modelling framework began with the detailed configuration of system components and the selection of advanced working fluids, including both conventional refrigerants and nanoparticle-enhanced mixtures. Thermophysical properties were implemented through the PEOS, ensuring consistent treatment of phase behaviour and energy balances across all fluid categories.

System components, including the evaporator, expander, condenser, and pump, were modelled under steady-state conditions using standard ASPEN Plus modules. Although transient dynamics and pinch-point constraints were not explicitly simulated, realistic boundary conditions were applied to reflect both hybrid heat input and working-fluid circulation. The iterative workflow enabled comparative evaluation across multiple fluid–nanoparticle scenarios.

Key performance indicators, including thermal efficiency, evaporator duty, turbine work output, and condenser load, provided a robust basis for analysis. Validation was achieved through benchmarking against the literature and internal consistency checks, lending credibility to the simulation outputs. While the scope was limited to thermodynamic assessment, the framework establishes a reproducible foundation for future extensions into techno-economic and environmental studies, as well as experimental validation.

Chapter Four

4 Results and Discussion

4.1 Introduction

This chapter presents and discusses the results of thermodynamic simulations evaluating the performance of different working-fluid configurations in a hybrid solar–biomass ORC system. The analysis follows the methodological framework outlined in Chapter 3, focusing on how fluid properties, nanoparticle enhancements, and heat source conditions influence overall cycle efficiency and system behaviour.

The results are presented in four main sections. Section 4.2 evaluates system performance under three representative heat-source scenarios, using the buffer outlet temperature as the key control parameter. Section 4.3 compares the behaviour of pure fluids with zeotropic mixtures, highlighting how temperature glide and mixture composition influence energy conversion efficiency. Section 4.4 examines the role of nanoparticles, investigating how particle type and concentration impact heat transfer, cycle efficiency, and potential operational challenges. Section 4.5 consolidates these results by evaluating system-level metrics, including net power output, specific work, and evaporator duty, while also benchmarking the findings against the governing thermodynamic equations introduced in Chapter 3.

Throughout the discussion, performance indicators such as evaporator duty, turbine work, thermal efficiency, and heat rejection are used to assess the viability of each fluid configuration. Where necessary, results are normalised to facilitate fair comparisons across fluids with varying thermophysical properties. The chapter not only evaluates technical performance but also considers practical implications for decentralised renewable energy systems, especially in contexts where reliability and sustainability are as important as efficiency.

4.2 Resource Assessment and Heat Source Behaviour

The viability of a hybrid solar–biomass ORC system depends not only on the presence of renewable energy sources but also on their consistency, thermal quality, and suitability for integration. This section examines the solar irradiance and biomass resources available in the operational region, providing the basis for configuring the system.

The assessment examined both the potential and the limitations of solar and biomass inputs. Regional energy profiles were analysed to understand seasonal variability, resource reliability, and thermal compatibility with ORC requirements. These insights helped shape the design of the hybrid system, ensuring it could realistically operate within the local environment's constraints. While resource availability supports the concept, the findings also highlight the need to carefully balance solar input and biomass supplementation to maintain stable performance throughout the year.

4.2.1 Solar Resource Assessment

To evaluate the compatibility of solar energy with the hybrid solar–biomass ORC system, this study examined the availability and thermal quality of solar irradiance in the operational region, focusing on DNI, which is critical for concentrating solar power applications.

Data from the ESMAP *et al*., (2019), in Figure 4.1, indicate that the average DNI across sub-Saharan Africa is approximately 6.5 kWh/m²/day (El Alani *et al*., 2022; ESMAP *et al*., 2019), confirming the region's strong solar energy potential. This level of irradiance is sufficient to provide meaningful thermal input to the ORC cycle, particularly during the dry season, when solar availability peaks.

The highest solar exposure is observed in Namibia, Botswana, and parts of South Africa, where DNI values exceed 7.0 kWh/m²/day and GHI ranges from 6.6 to 7.0 kWh/m²/day. The Sahel region, including Sudan, Chad, Mali, and Niger, also exhibits elevated DNI levels, making it suitable for solar-thermal applications. In contrast, equatorial and coastal areas, such as West and Central Africa, exhibit more moderate irradiance, with DNI values ranging from 2.0 to 4.0 kWh/m²/day.

Matuszewska (2024) highlights the thermal compatibility between solar collectors and ORC systems, noting that the operating temperatures of typical solar collectors align well with the thermal requirements of ORC processes. This reinforces the feasibility of solar energy as a primary heat source in hybrid configurations, especially when paired with a backup system to mitigate seasonal and diurnal variability.

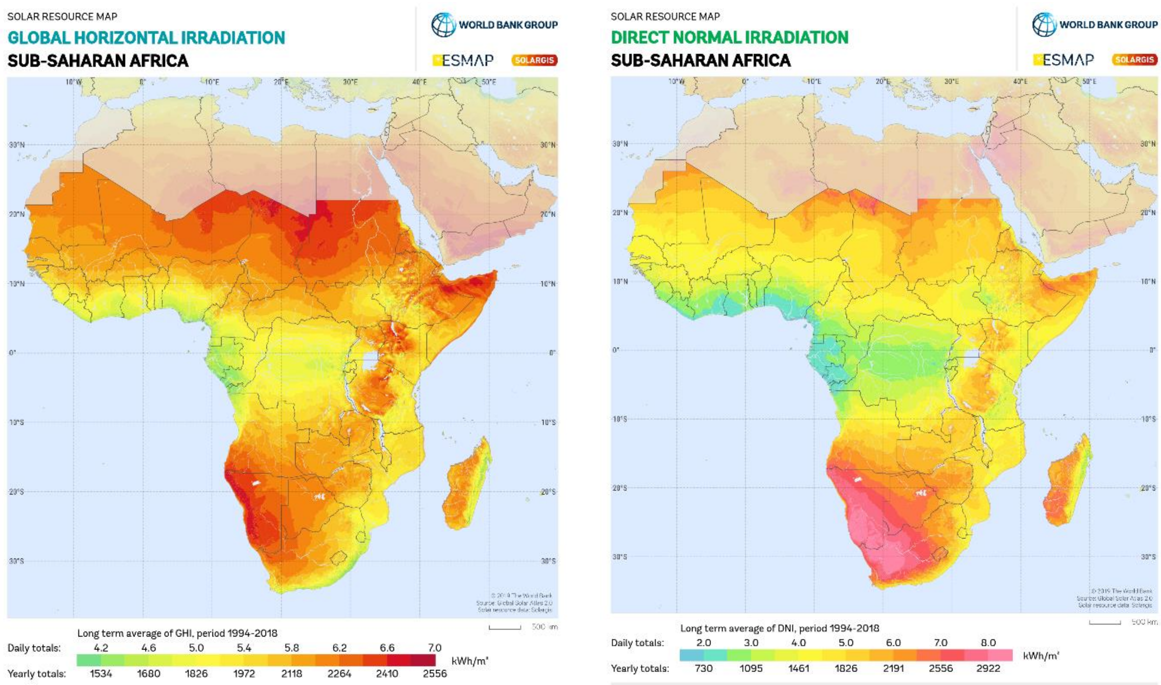

Figure 4.1: GHI and DNI Maps for Sub-Saharan Africa
Source: (ESMAP *et al.*, 2019)

4.2.2 Biomass Resource Assessment

In parallel with the solar evaluation, a biomass resource assessment was conducted to assess its suitability as a stable, dispatchable thermal input for hybrid ORC operation. Sub-Saharan Africa's tropical and subtropical climate supports substantial biomass productivity, with an estimated annual energy potential of 200-400 terajoules (EJ) (International Energy Agency, 2022). However, availability alone does not guarantee usability; factors such as conversion efficiency, supply

consistency, and infrastructure limitations also play a role.
Biomass resources in the region can be broadly categorised into four groups:

i. Agricultural Residues: Maize stalks, rice husks, sugarcane bagasse, cassava waste
ii. Forest Resources: Firewood, charcoal, wood chips
iii. Animal Waste: Cow dung, poultry litter, biogas sludge
iv. Energy Crops: Jatropha, Napier grass, eucalyptus

Each category exhibits distinct energy characteristics, with lower heating values (LHV) ranging from 10 to 22 MJ/kg as shown in Table 4.1. Agricultural residues are widely available in countries such as Nigeria, Ethiopia, and Kenya, while forest-derived fuels remain dominant despite growing concerns over deforestation. Livestock-rich nations, such as Ethiopia, Sudan, and South Africa, generate substantial volumes of organic waste that is suitable for biogas production. Energy crops, particularly Jatropha and Eucalyptus, are recognized for their high LHV and have been increasingly cultivated for biofuel applications. Jatropha has been reported in Ghana, Nigeria, and Tanzania, while Eucalyptus residues are common in South Africa, Kenya, and Ethiopia.

Table 4.1: Estimated LHV of Various Biomass Sources in Sub-Saharan Africa

Biomass Category	Common Examples	Estimated LHV (MJ/kg)
Agricultural Residues	Maize stalks, rice husks, sugarcane bagasse, cassava waste	12 – 18
Forest Resources	Firewood, charcoal, wood chips	15 – 20
Animal Waste	Cow dung, poultry litter, biogas sludge	10 – 16
Energy Crops	Jatropha, Napier grass, eucalyptus	16 – 22

Source:(Basu, 2018; Bishoge *et al*., 2020; Come Zebra *et al*., 2021; IRENA and AfDB, 2022; Röder *et al*., 2022)

Despite its promise, biomass utilisation in the region faces several challenges. Inefficient conversion technologies, limited access to processing infrastructure, and unsustainable harvesting practices, particularly for wood-based fuels, can undermine long-term viability (International Energy Agency, 2022; IRENA and AfDB, 2022). These constraints must be considered when designing systems that rely on biomass as a thermal backbone.

Nonetheless, biomass offers a critical advantage over solar energy: dispatchability. Unlike solar irradiance, which is intermittent and seasonally variable, biomass can provide consistent thermal input, making it a reliable complement in hybrid configurations. Its integration into the ORC system helps stabilise output during low-DNI periods and nighttime operation, ultimately improving system resilience and energy access in off-grid or resource-constrained settings (Alvi *et al*., 2024).

4.2.3 Heat Source Analysis

The thermal energy required to drive the ORC system in this study is supplied by a hybrid configuration consisting of an evacuated tube solar collector (ETC) and a biomass-fired backup boiler. This setup leverages the region's abundant solar resource while ensuring reliability through biomass supplementation during periods of low irradiance or nighttime operation.

The selected site ranks among the highest in West Africa for annual DNI, making it highly suitable for solar thermal applications. Monthly DNI values obtained from ESMAP *et al*. (2019), shown in Figure 4.2, reveal the characteristic seasonal pattern of savannah climates: peak irradiance occurs in December (152.2 kWh/m^2/month pr 4.91 kWh/m^2/day), while the lowest values are recorded in August (89.7 kWh/m^2/month or 2.89 kWh/m^2/day), during the rainy season.

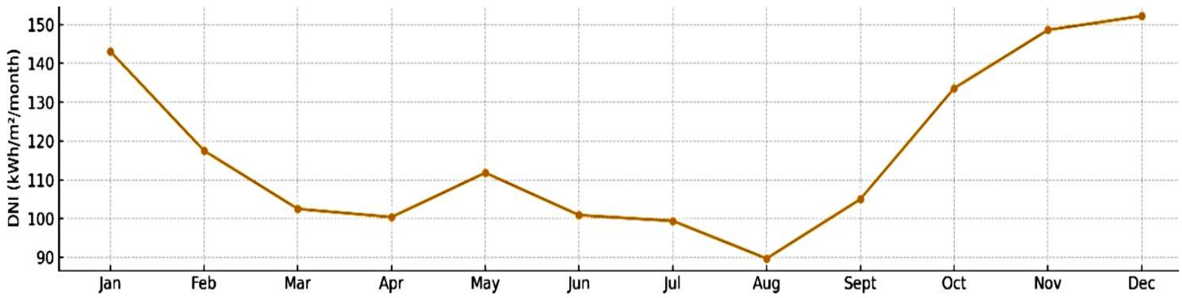

Figure 4.2: Monthly Average DNI

An evacuated tube collector system was chosen for its high efficiency under both direct and diffuse radiation. Therminol VP-1, a synthetic thermal oil, serves as the heat transfer fluid (HTF) due to its stability up to 400 °C, moderate specific heat (approximately 2.3 kJ/kg·K), and density of approximately 1,060 kg/m³.

To examine the effect of mass flow rate on collector performance and biomass demand, two values were assessed: 0.05 and 0.1 kg/s. The collector area was set at 10 m², with an assumed efficiency of 60%, which is typical for commercial ETCs. Solar energy absorption was calculated from monthly DNI values, assuming 12 hours of sunshine per day.

The results in Figure 4.3 show that reducing the flow rate increases outlet temperatures due to longer fluid residence time within the collector. Peak outlet temperatures reached 178.8 °C in December at a flow rate of 0.05 kg/s, compared to 152.1 °C at a flow rate of 0.1 kg/s. However, the lower flow rate limited total heat throughput, thereby increasing the biomass energy required to reach the ORC's operating temperature of 200 °C. The effect of reduced flow rate on heat throughput has been quantified. When the flow rate was decreased by approximately 20%, the total heat throughput was reduced by about 18%. As a result, the biomass energy required to reach the ORC operating temperature of 200 °C increased by nearly 22%.

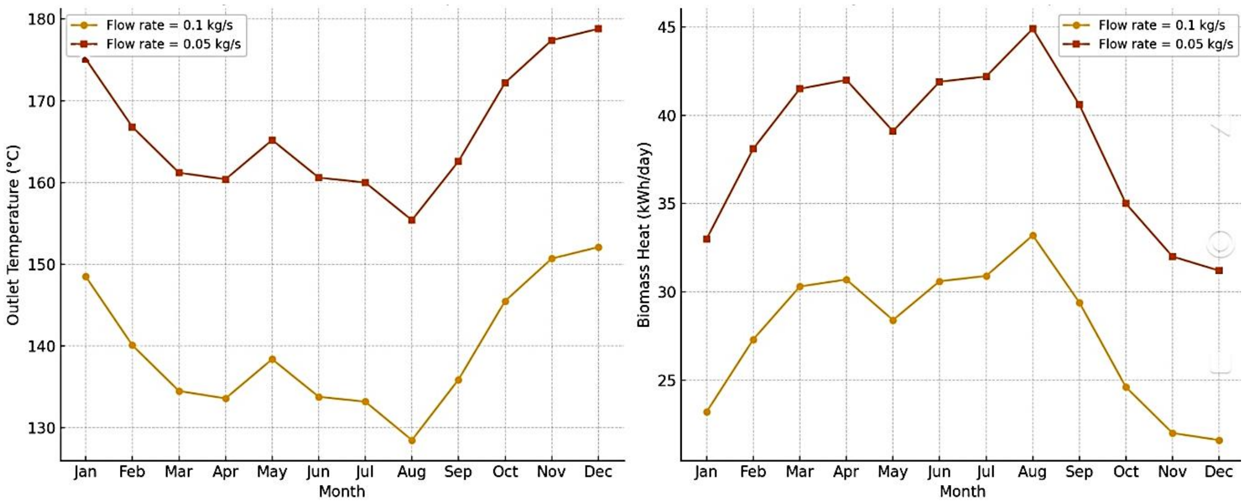

Figure 4.3: Monthly Average Collector Outlet Temperatures at Two Flow Rates

Biomass heat demand was then estimated to compensate for the gap between solar outlet temperature and the ORC setpoint (200 °C).

Figure *4.4* and Table 4.2 summarise the monthly biomass requirement under both flow conditions. As expected, demand is highest during low-DNI months (e.g., August), with lower flow rates amplifying the shortfall.

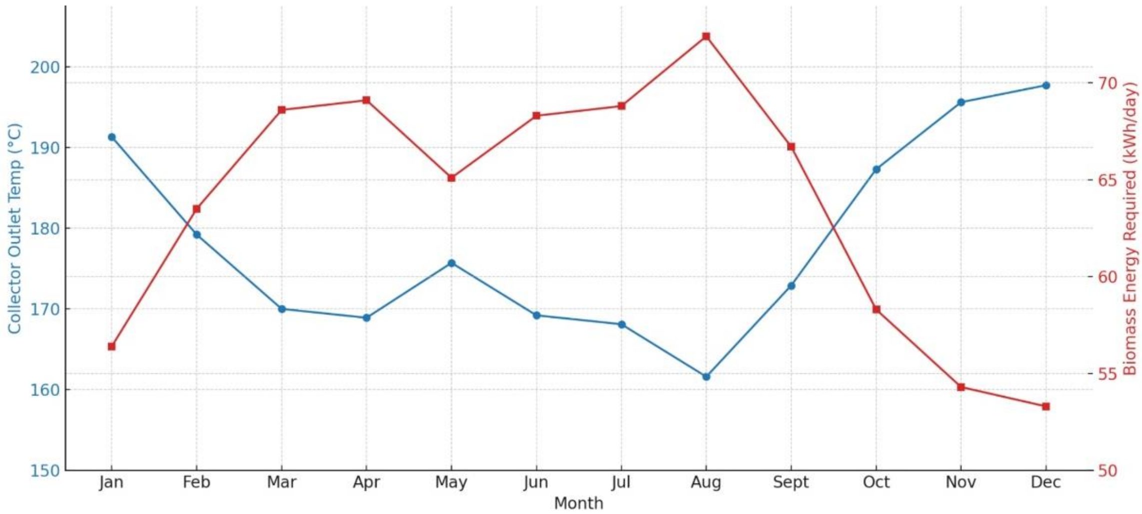

Figure 4.4: Monthly Biomass Heat Requirements

Table 4.2: Monthly Biomass Heat Requirements at Two Flow Rates

Month	DNI (kWh/m^2)	T_{out} @0.1 kg/s (°C)	Biomass Heat @0.1 kg/s (kWh/day)	T_{out} @0.05 kg/s (°C)	Biomass Heat @0.05 kg/s (kWh/day)
Jan	143.1	148.5	23.2	175.1	33.0
Feb	117.5	140.1	27.3	166.8	38.1
Mar	102.5	134.5	30.3	161.2	41.5
Apr	100.4	133.6	30.7	160.4	42.0
May	111.8	138.4	28.4	165.2	39.1
Jun	100.9	133.8	30.6	160.6	41.9
Jul	99.4	133.2	30.9	160.0	42.2
Aug	89.7	128.5	33.2	155.4	44.9
Sept	105.0	135.9	29.4	162.6	40.6
Oct	133.6	145.5	24.6	172.2	35.0
Nov	148.6	150.7	22.0	177.4	32.0
Dec	152.2	152.1	21.6	178.8	31.2

These results highlight a key trade-off in system design: lower flow rates improve collector outlet temperature but also increase biomass fuel demand, particularly in months with low irradiance. Effective system optimisation must therefore balance flow rate, collector sizing, and biomass availability to minimise costs while ensuring thermal reliability.

4.3 Working Fluid Performance Evaluation

This section presents the performance evaluation of the six zeotropic mixtures considered in this study, grouped into two sets based on their critical thermophysical properties. Each mixture was assessed under various operating temperatures, with performance indicators including thermal efficiency (η), net power output ($\dot{W}_{net}$), and heat absorbed ($\dot{Q}in$). Nanoparticle enhancement was subsequently applied to assess how different particle types and concentrations influence cycle behaviour.

4.3.1 Baseline Performance of Zeotropic Mixtures

The baseline performance of the ORC system was evaluated using six zeotropic mixtures grouped into two sets. Simulations were conducted under fixed cycle conditions, with the expander operating at an inlet temperature of 200 °C and a pressure of 800 kPa, while the condenser was maintained at 163 °C and 200 kPa. These conditions provided a consistent reference point for assessing the influence of fluid composition and thermophysical properties on cycle behaviour. The key performance indicators considered were thermal efficiency (η), net work output ($\dot{W}net$), and heat absorbed (Qin).

For the first set of fluids, which involved R245fa/R123, R245fa/R1233zd, and R1233zd/R123 mixtures, and Al_2O_3, CuO, and Ag as nanoparticles, the results showed a clear dependence of performance on the proportion of the more volatile component. As the mass fraction of the lower-boiling fluid (e.g., R1233zd) increased, thermal efficiency rose across all three tested source temperatures (120, 150, and 200 °C), as shown in **Error! Reference source not found.**, 4.6 and 4.7. Among these, the R1233zd/R123 mixture consistently outperformed the others, delivering the highest efficiency and net work output. This trend highlights the advantage of strong temperature glide, which enhances thermal matching in the evaporator and condenser, thereby reducing irreversibility.

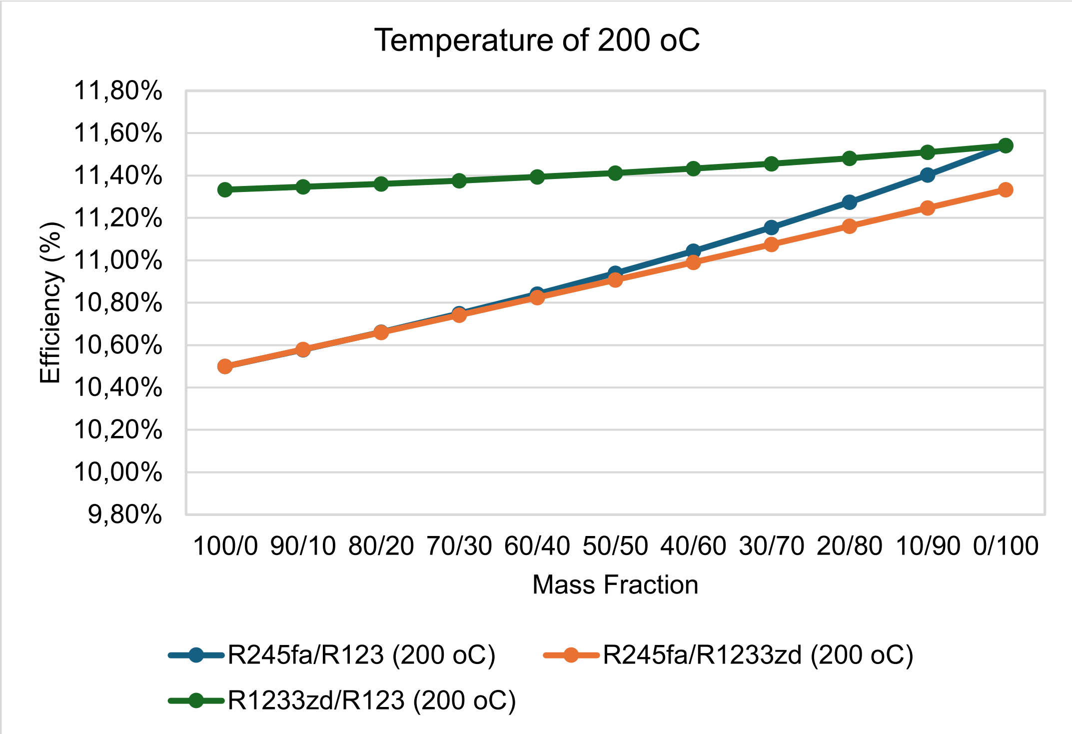

Figure 4.5: Thermal Efficiency Variation with Mass Fraction for Set 1 Mixtures at 200 ^{O}C

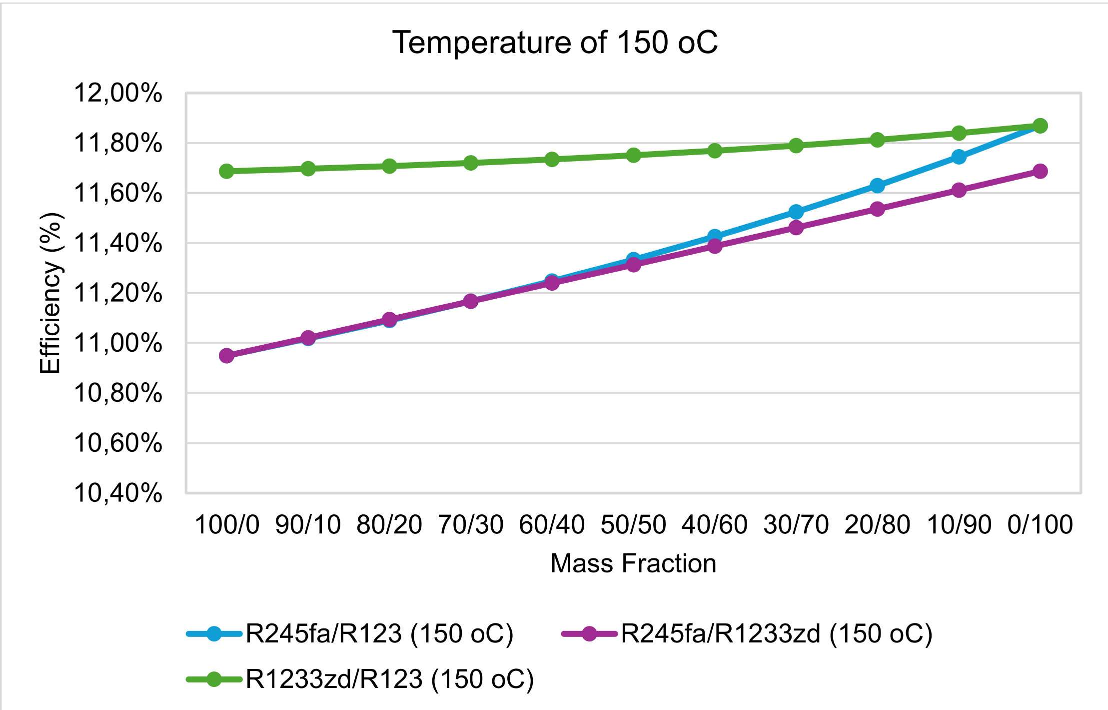

Figure 4.6: Thermal Efficiency Variation with Mass Fraction for Set 1 Mixtures At 150 ^{O}C

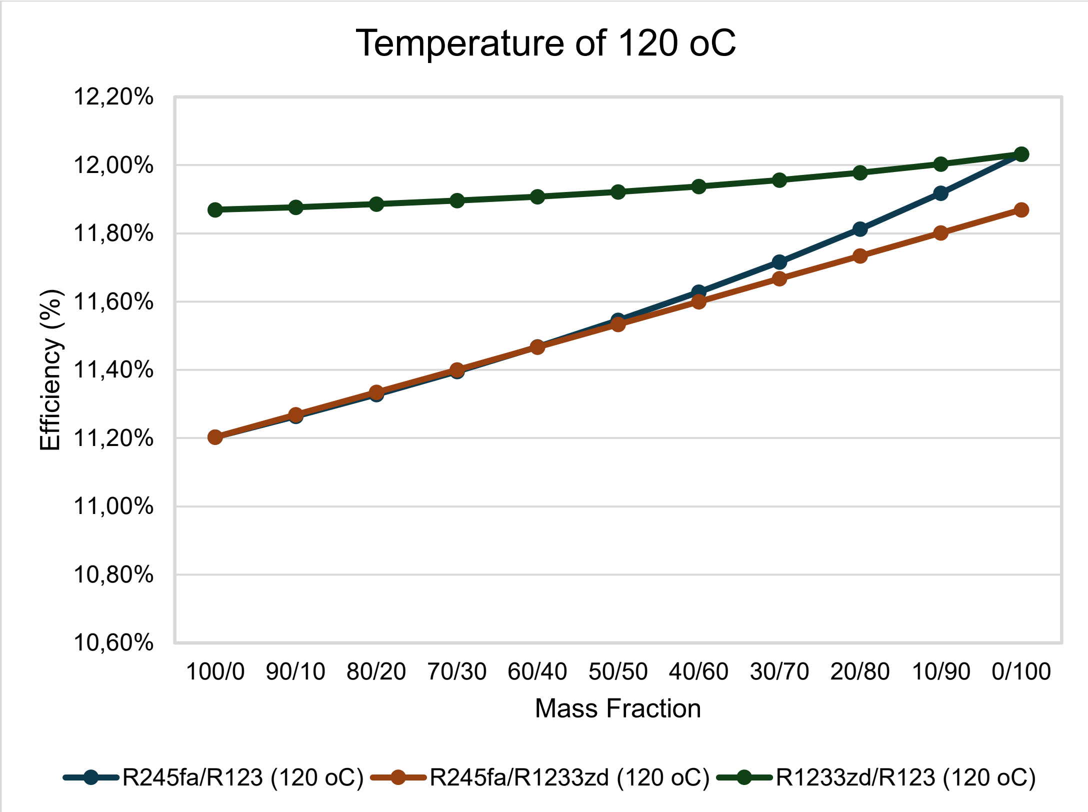

Figure 4.7: Thermal Efficiency Variation with Mass Fraction for Set 1 Mixtures at 120 ^{O}C

Interestingly, higher source temperatures did not always guarantee better performance. At 200 °C, only certain mass fractions showed efficiency gains compared to results at 150 °C or even 120 °C. This suggests that mixture composition is often more critical than an absolute operating temperature. These findings are consistent with earlier reports, such as those by Hamdi *et al*. (2023), which emphasise that improper mixture ratios can lead to pinch-point constraints in heat exchangers.

The second set of fluid mixtures involving R1224yd(Z)/R1233zd(E), R1224yd(Z)/R1336mzz(Z), and R1233zd(E)/R1336mzz(Z) with TiO_2, ZnO, and Ag as nanoparticles, revealed similar composition-driven behaviours, but with some notable differences. The analysis of Set 2 mixtures was conducted at a representative operating temperature of 150 °C, consistent with the mid-range condition applied in Set 1. Since comparable temperature conditions were used, the influence of temperature was not repeated in the graphical presentation, and the trends were interpreted directly from the enthalpy and performance data. Figure 4.8 illustrates the variation in turbine work with mixture composition. For R1224yd(Z)/R1233zd(E), turbine output increased steadily as the share of R1233zd(E) rose, reaching a maximum at 100% R1233zd(E). This confirms the strong thermodynamic potential of R1233zd(E) as a working fluid. By contrast, the R1224yd(Z)/R1336mzz(Z) mixture showed the opposite trend: turbine work decreased as the R1336mzz(Z) proportion increased, with peak performance at 100% R1224yd(Z). Similarly, the R1233zd(E)/R1336mzz(Z) mixture exhibited declining turbine work as R1336mzz(Z) was added, again highlighting the limitations of this fluid for high-performance ORC systems.

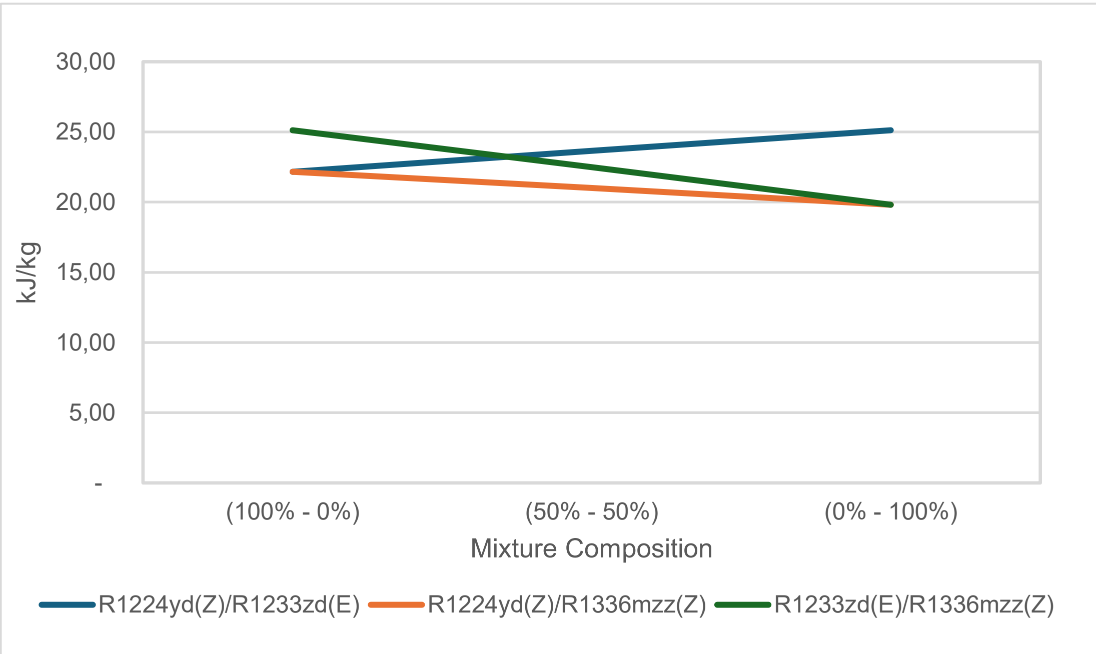

Figure 4.8: Turbine Work Variation for Set 2 Mixtures

The role of critical properties is especially important in explaining these results. Figure 4.9 illustrates that the R1224yd(Z)/R1233zd(E) mixture achieved the highest net work output (23.2 kJ/kg) and thermal efficiency (8.5%). This is largely due to the favourable balance between their critical temperatures (153.7 °C for R1224yd(Z) and 165.6 °C for R1233zd(E)) and critical pressures (approximately 3.6 MPa), which enabled effective energy absorption and expansion. In contrast, R1224yd(Z)/R1336mzz(Z) delivered the weakest performance (20.5 kJ/kg and 8.0% efficiency). Although R1336mzz(Z) has a relatively high critical temperature (171.3 °C), its lower critical pressure (2.90 MPa) limits its expansion potential, resulting in poorer cycle efficiency. The R1233zd(E)/R1336mzz(Z) blend yielded intermediate results, with a net work output of approximately 22.20 kJ/kg and a corresponding efficiency of 8.2%, consistent with the thermodynamic definition of cycle efficiency as the ratio of net work to heat input. This suggests that although R1336mzz(Z) tends to reduce performance, its impact is less pronounced when paired with R1233zd(E).

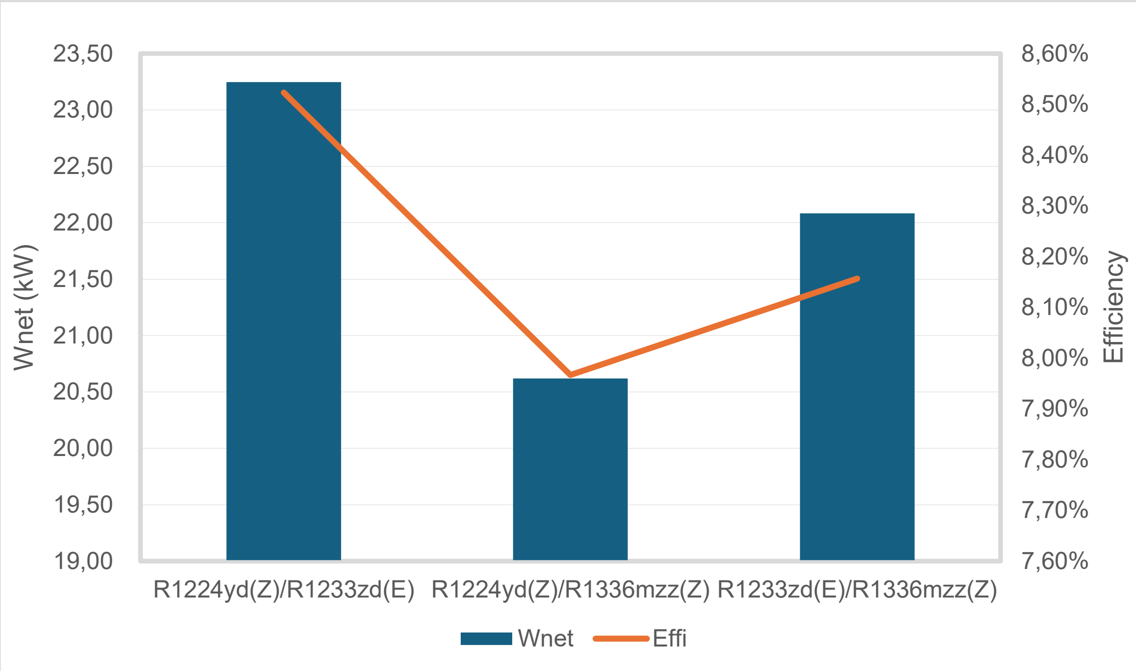

Figure 4.9: Net Work Output and Efficiency Comparison for Set 2 Mixtures

Overall, these baseline results confirm that fluid composition exerts a stronger influence on ORC performance than source temperatures alone. Mixtures containing R1233zd(E) consistently demonstrated superior efficiency and work output, making them more promising candidates for hybrid solar-biomass ORC systems. By contrast, fluids with a higher proportion of R1336mzz(Z) exhibit less favourable thermodynamic behaviour and are, therefore, less suitable for small-scale power applications.

4.3.2 Net Power Output and Heat Absorption

The net power output of the Set 1 mixtures was strongly influenced by both composition and source temperature. As shown in **Error! Reference source not found.** – 4.8, the R1233zd/R123 mixture consistently produced the highest $\dot{W}_{net}$ across all operating conditions. This superior performance stems from the high volatility of R1233zd, which enhances evaporation and expansion processes.

By contrast, the R245fa/R123 mixture showed a steady decline in net power output as the R123 fraction increased. The reduced volatility of R123 compromised turbine inlet conditions, resulting in reduced work output. The R245fa/R1233zd blend delivered intermediate results but showed greater sensitivity at higher temperatures, especially at 200 °C, where phase-change mismatches limited output.

Heat absorption behaviour followed similar trends. **Error! Reference source not found.** 4.12 shows that R1233zd/R123 exhibited relatively high heat input requirements, particularly at elevated temperatures, but did not consistently require the greatest $\dot{Q}_{in}$ across all mass fractions and operating conditions. The mixture nevertheless demonstrated efficient conversion of absorbed heat into turbine work, providing a thermodynamic advantage over the R245fa-based mixtures.

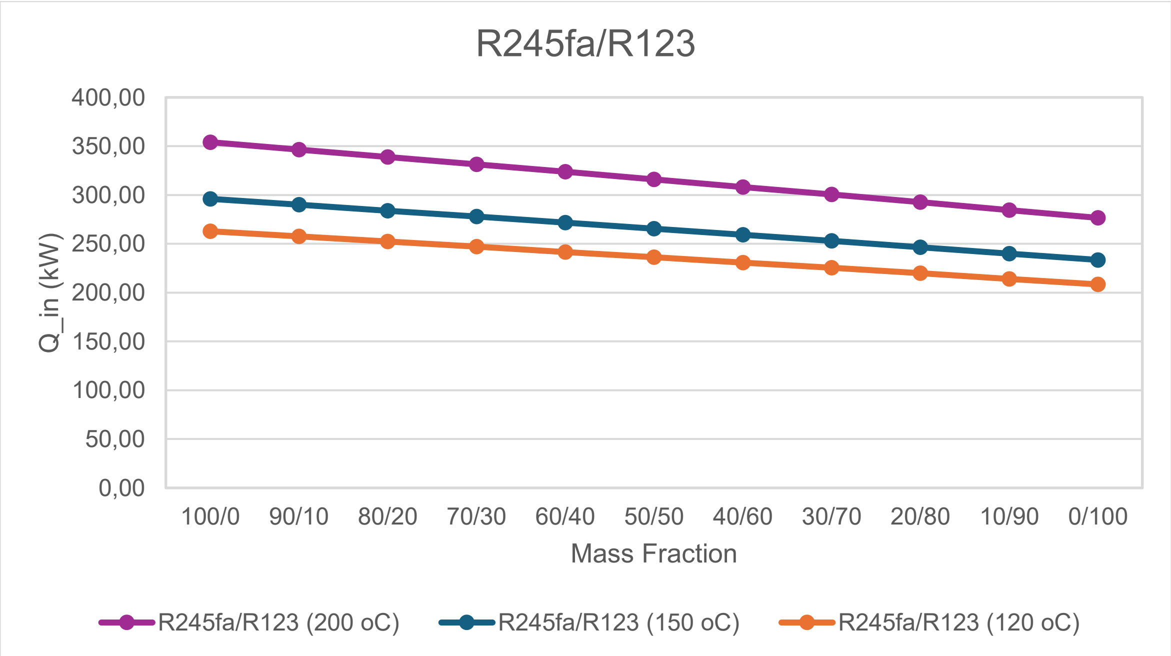

Figure 4.10: Heat Input for Set 1 Mixture R245fa/R123

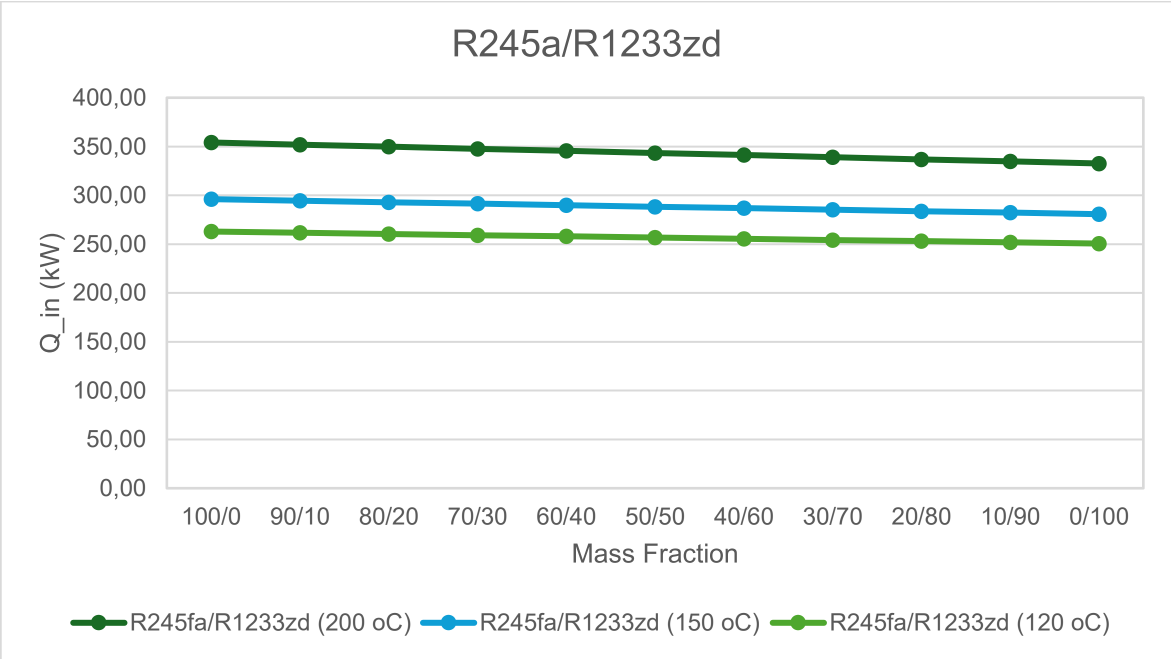

Figure 4.11: Heat Input for Set 1 Mixture R245fa/R1233zd

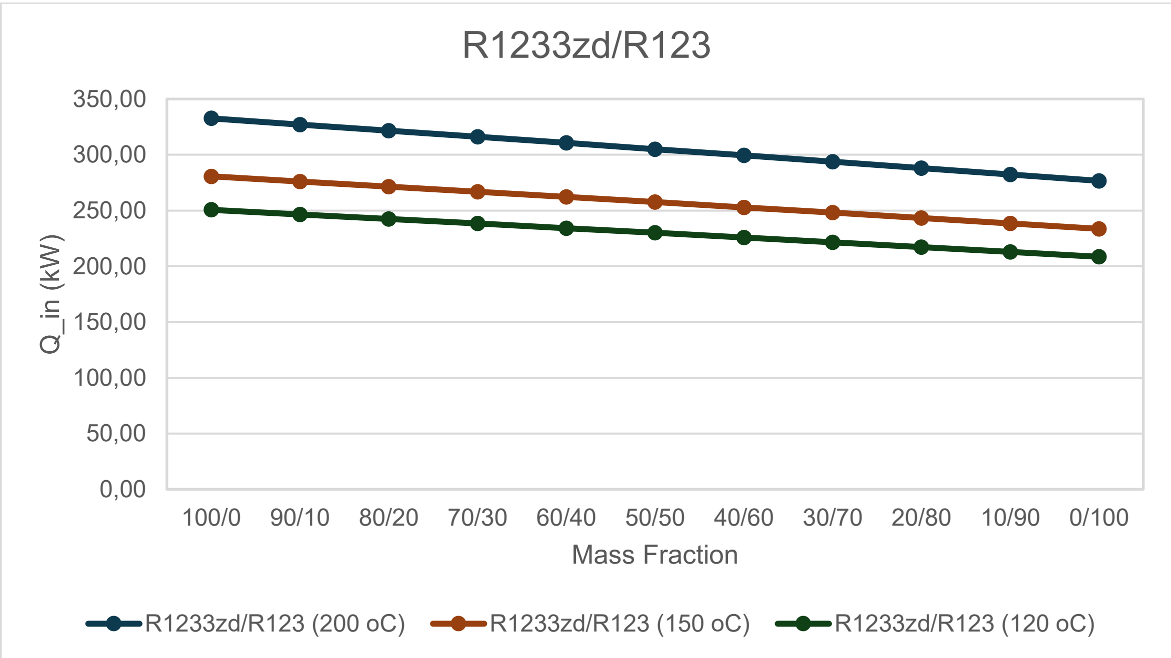

Figure 4.12: Heat Input for Set 1 Mixture R1233zd/R123

4.3.3 Nanoparticle Effects

This section examines how nanoparticle type and concentration affect the performance of the two sets of zeotropic mixtures. The analysis focuses on three key indicators: thermal efficiency, net power output, and heat absorption, all of which are evaluated under varying operating conditions.

4.3.3.1 Mixture Set 1: R245fa/R1233zd(E), R245fa/R123, and R1233zd(E)/R123

This set comprises transitional refrigerants that are frequently studied in ORC research. A fixed base ratio of 20/80 was applied, and three nanoparticles, Ag, Al_2O_3, and CuO, were dispersed at concentrations ranging from 0.000001 to 0.01 by mass.

As shown in **Error! Reference source not found.** – 4.15, Ag nanoparticles consistently outperformed the oxide-based particles. Efficiency gains reached as high as 16% at a concentration of 0.01, a direct result of silver's superior thermal conductivity (429 W/m·K). By contrast, both Al_2O_3 and CuO produced negligible improvements at low concentrations and even reduced efficiency at higher ones. At a mass fraction of 0.01, efficiency declined by 2% for Al_2O_3 and by 1% for CuO, most likely due to increased viscosity and associated flow resistance. For Ag, the decline in generator efficiency observed as the mass fraction increased from 0.01 to 0.1 has been attributed to compositional effects that alter vaporization characteristics and increase irreversibility in the generator. The mismatch between heat input and effective vapor generation becomes more pronounced at higher mass fractions, leading to reduced efficiency.

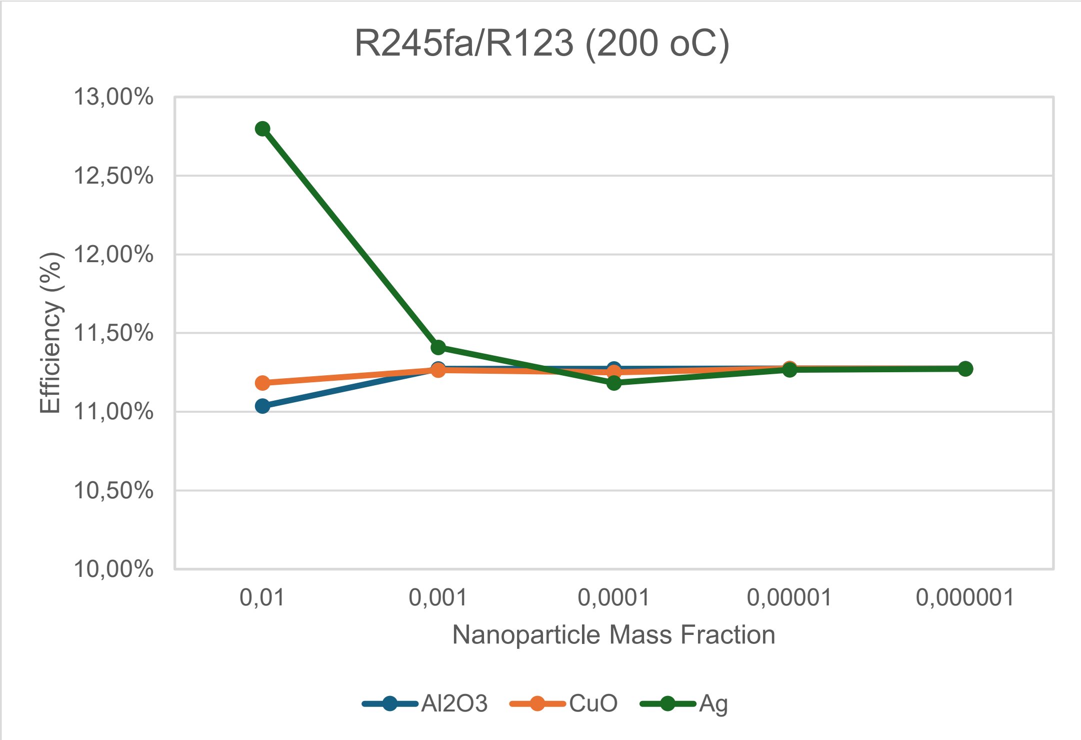

Figure 4.13: Thermal Efficiency vs. Nanoparticle Mass Fraction for R245fa/R123

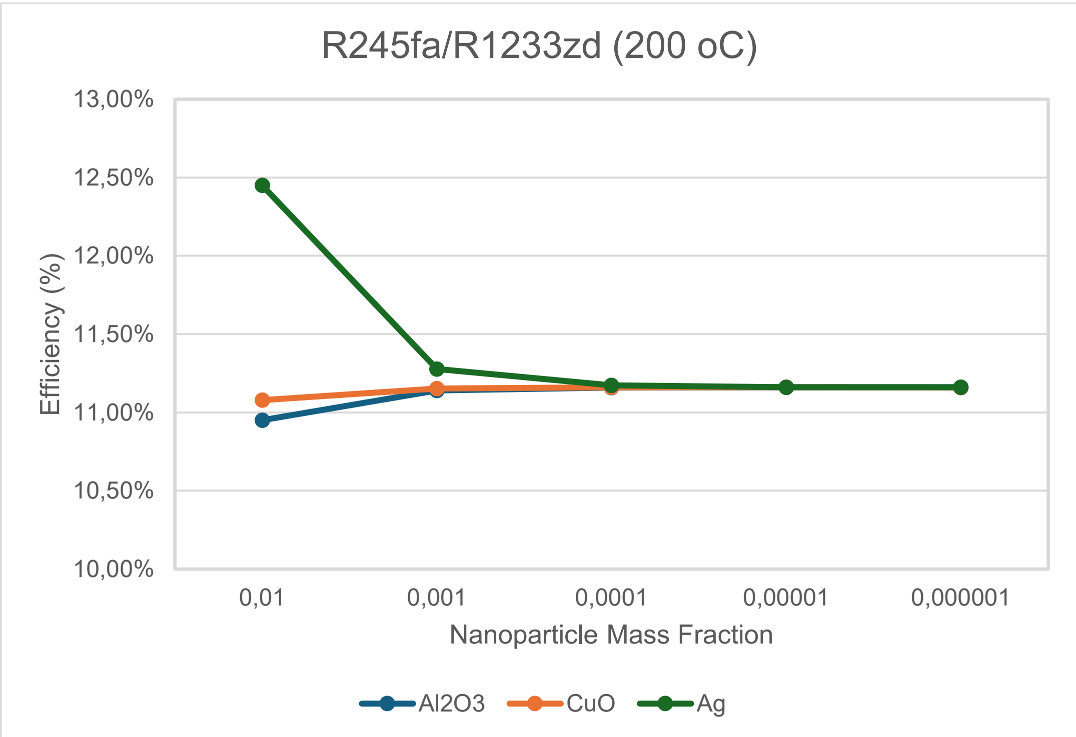

Figure 4.14: Thermal Efficiency vs. Nanoparticle Mass Fraction for R245fa/R1233zd

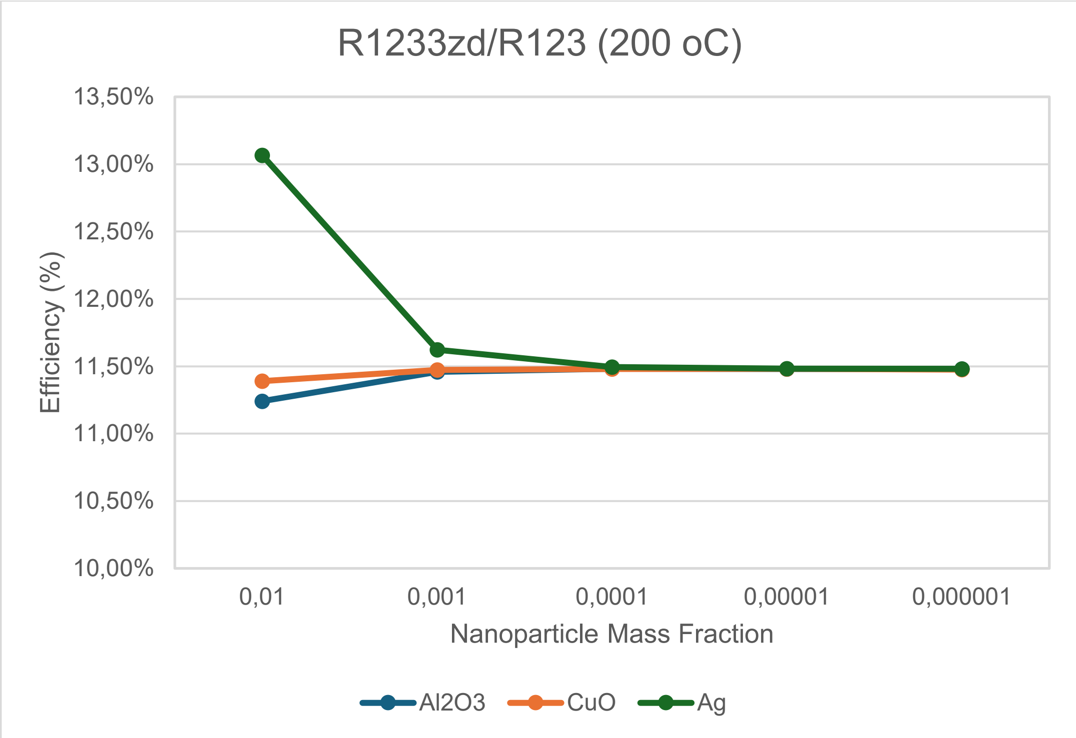

Figure 4.15: Thermal Efficiency vs. Nanoparticle Mass Fraction R1233zd/R123

Trends in net work, shown in **Error! Reference source not found.** – 4.18, mirrored the efficiency results. Ag nanoparticles delivered higher output in all three mixtures, with the effect strongest in R245fa/R1233zd(E) and R1233zd(E)/R123. CuO and Al_2O_3 slightly improved the net work up to a mass fraction of 0.001 but plateaued or declined at higher concentrations. Ag showed some variability in the R245fa/R123 mixture but still outperformed oxide nanoparticles overall.

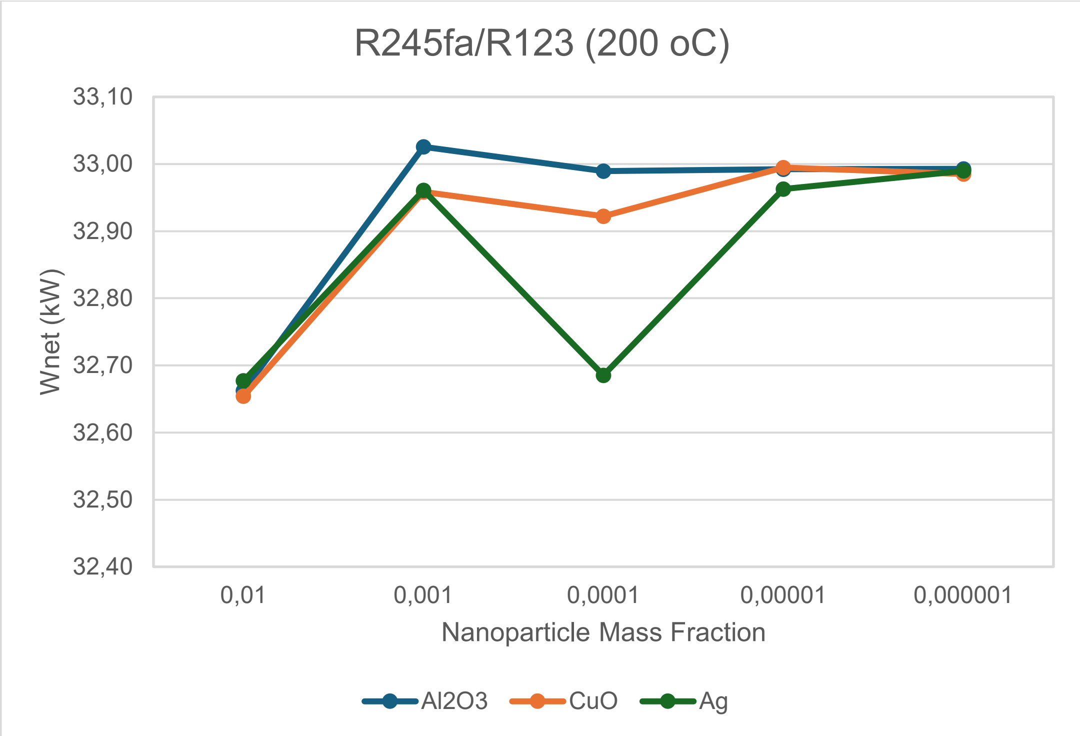

Figure 4.16: Net Power Output vs. Nanoparticle Mass Fraction for R245fa/R123

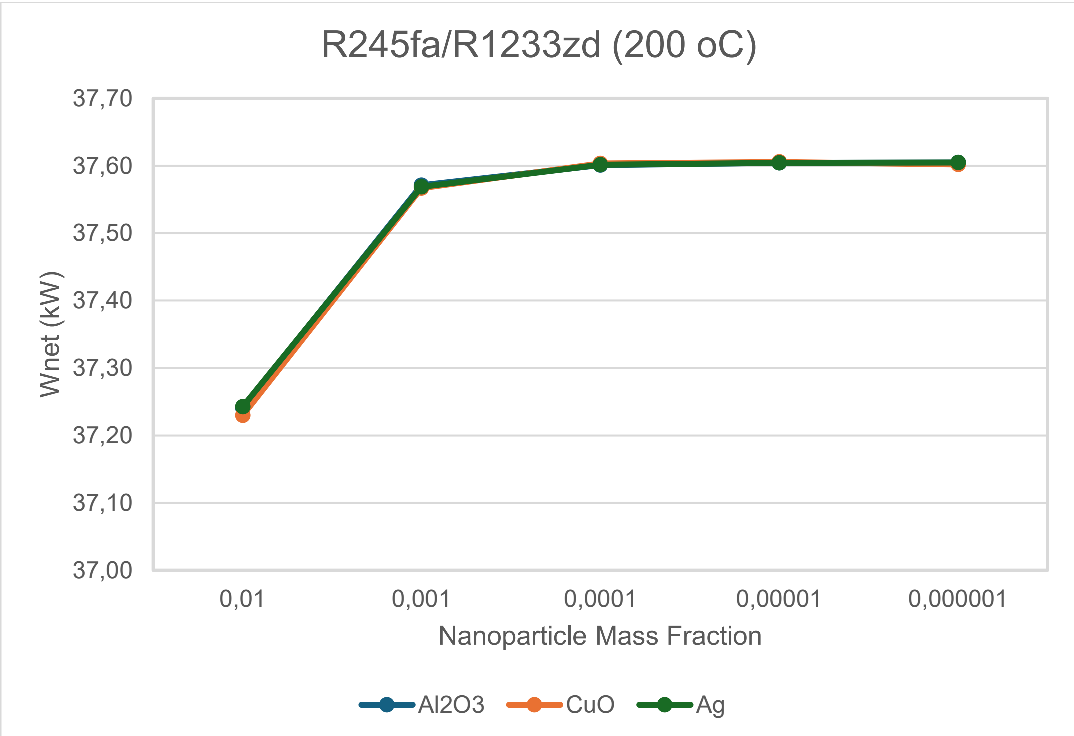

Figure 4.17: Net Power Output vs. Nanoparticle Mass Fraction for R245fa/R1233zd

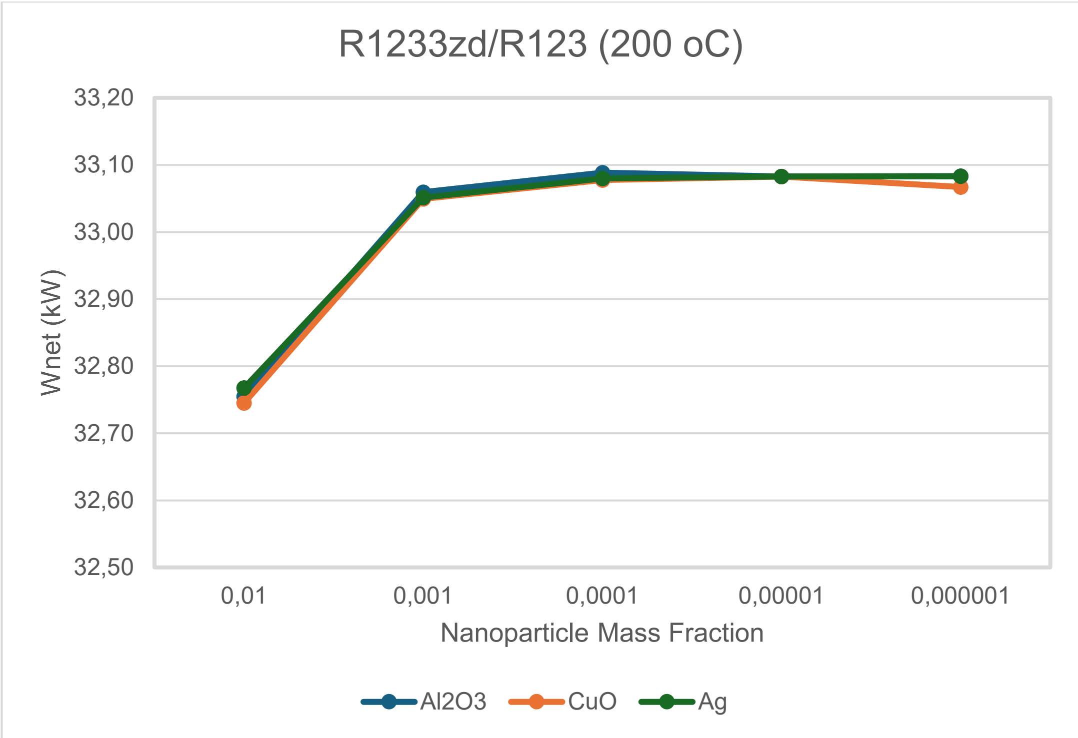

Figure 4.18: Net Power Output vs. Nanoparticle Mass Fraction for R1233zd/R123

Heat input behaviour demonstrated in **Error! Reference source not found.** – 4.21 highlighted silver's advantage at low concentrations, particularly in the R245fa/R123 blend. However, this benefit diminished as concentration increased, again because higher viscosity reduced flow and heat transfer efficiency. Al_2O_3 and CuO supported stable heat absorption, with small peaks around 0.001 mass fraction, after which further increases yielded diminishing returns.

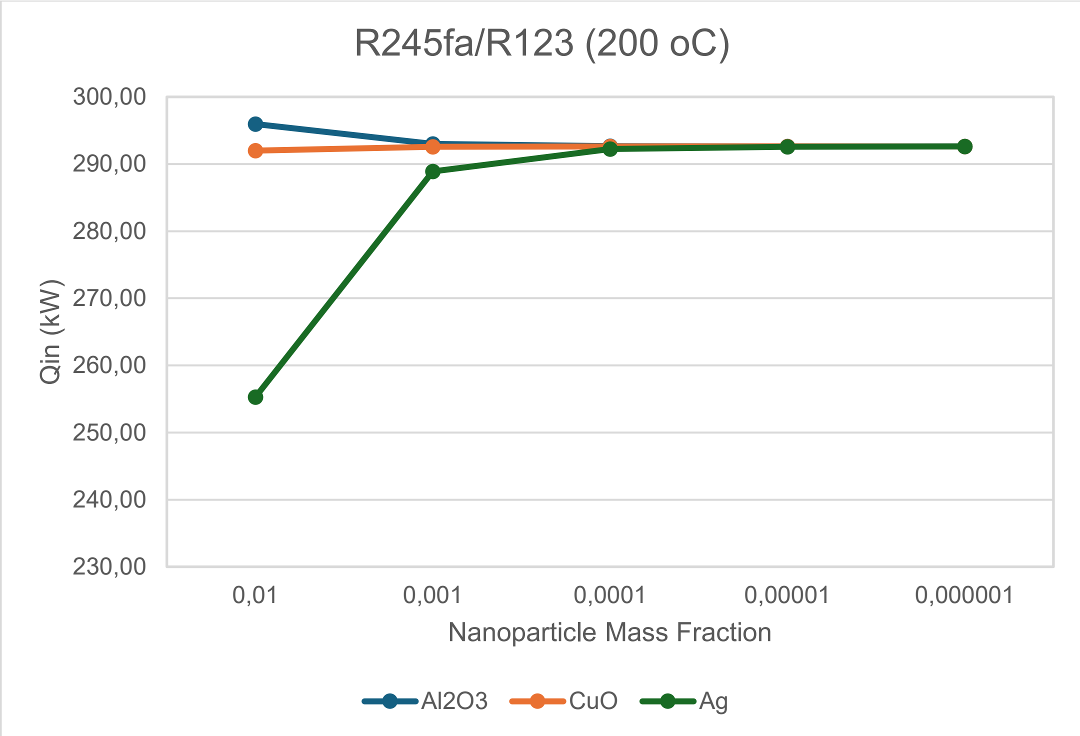

Figure 4.19: Heat Absorbed vs. Nanoparticle Mass Fraction for R245fa/R123

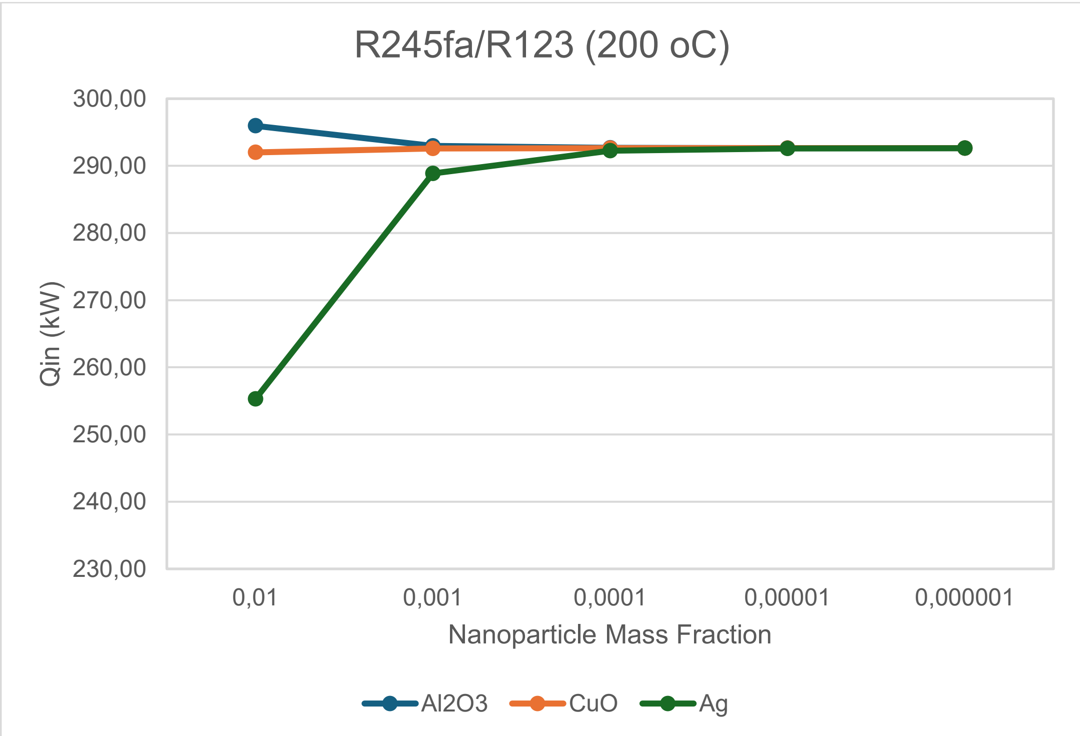

Figure 4.20: Heat Absorbed vs. Nanoparticle Mass Fraction for R245fa/R1233zd

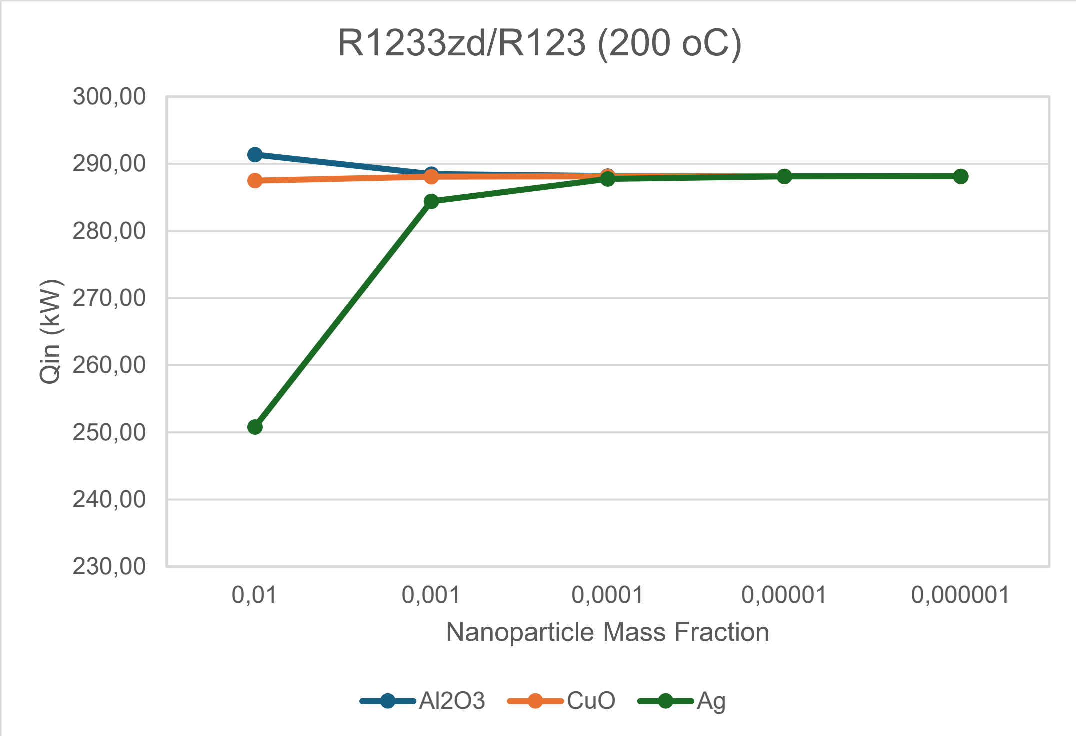

Figure 4.21: Heat Absorbed vs. Nanoparticle Mass Fraction for R1233zd/R123

For Set 1, silver nanoparticles offered the greatest improvements in efficiency, net work, and heat absorption, but only when the concentration was optimised. Overdosing undermined performance by raising viscosity and hydraulic losses. The oxide nanoparticles provided greater thermal stability but lacked the conductivity advantage needed to significantly boost performance.

4.3.3.2 Mixture Set 2: R1224yd(Z)/R1233zd(E), R1224yd(Z)/R1336mzz(Z), and R1233zd(E)/R1336mzz(Z)

This mixture set features newer low-GWP fluids, designed for higher-temperature ORC systems. Nanoparticles assessed Ag, TiO_2, and ZnO at mass fractions of 0.0001, 0.001, 0.01, and 0.1.

Silver once again produced the largest efficiency improvements, peaking at 10.68% for R1224yd(Z)/R1336mzz(Z) and 10.77% for R1224yd(Z)/R1233zd(E) at a 0.1 mass fraction, as shown in **Error! Reference source not found.** – 4.24. TiO_2 and ZnO maintained a steady efficiency of 8.3% at lower fractions but exhibited slight declines at 0.1 because higher viscosity reduced turbine effectiveness.

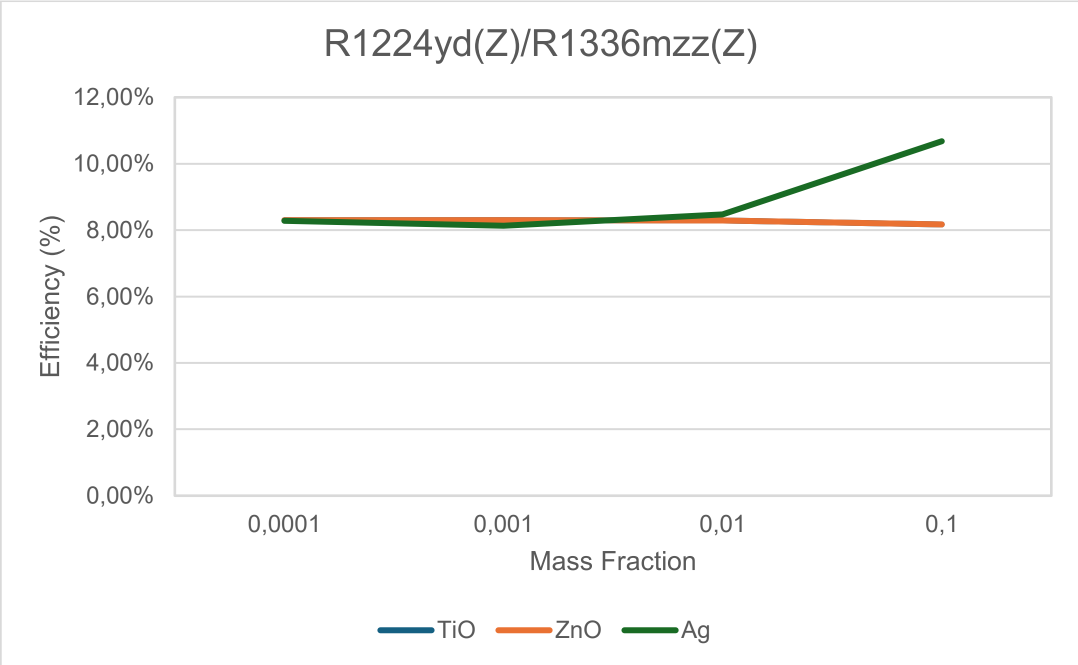

Figure 4.22: Variation of Thermal Efficiency with Nanoparticle Mass Fraction for R1224yd(Z)/R1336mzz(Z)

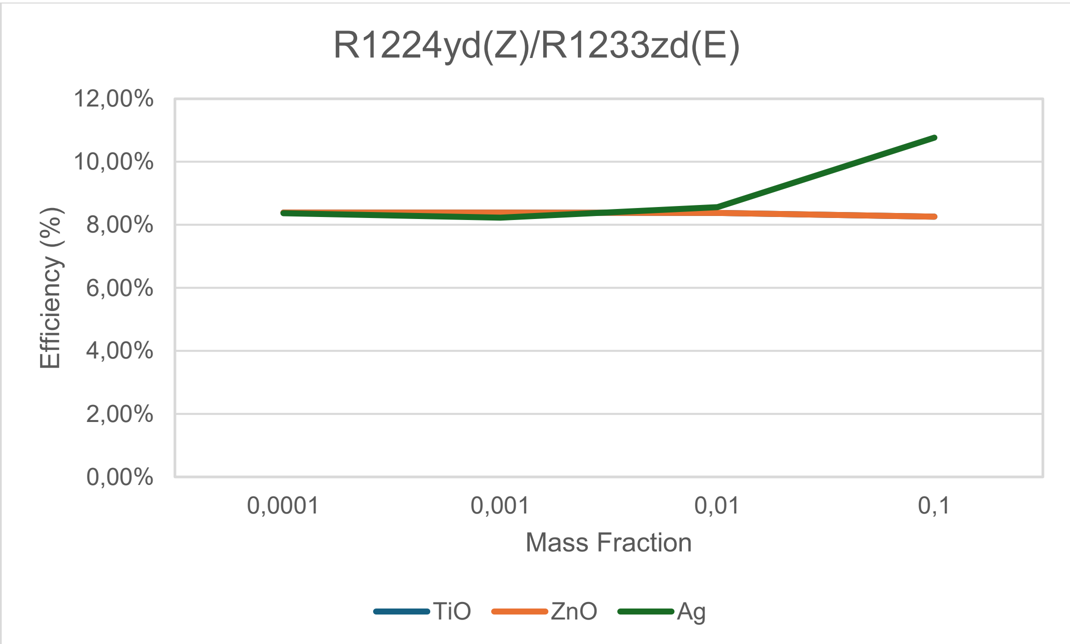

Figure 4.23: Variation of Thermal Efficiency with Nanoparticle Mass Fraction for R1224yd(Z)/R1233zd(E)

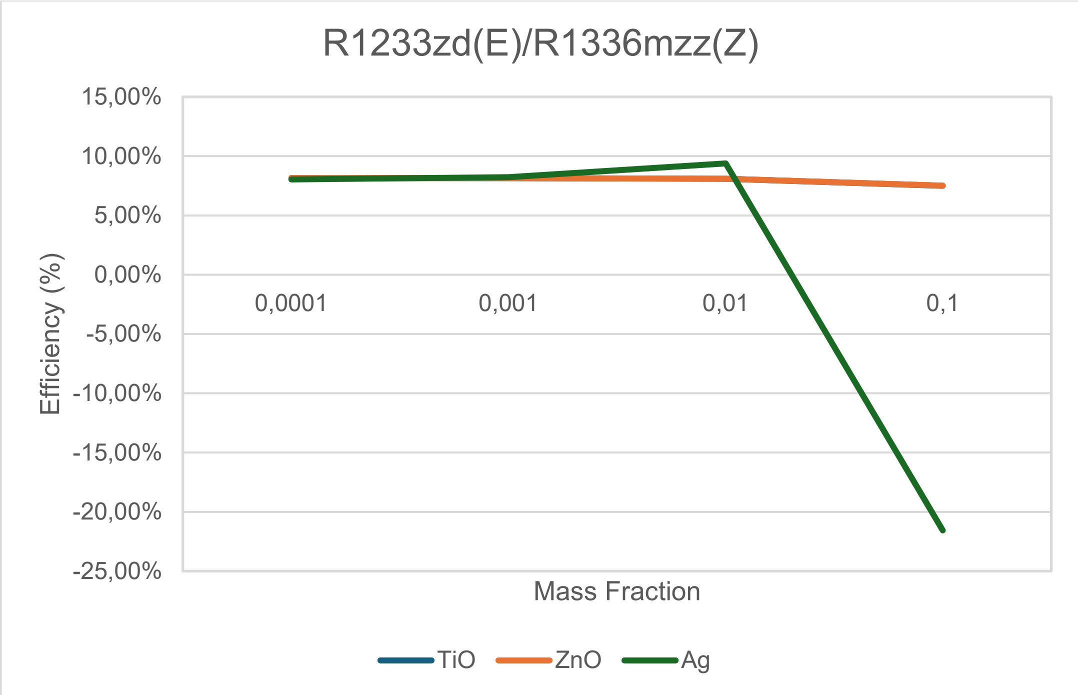

Figure 4.24: Variation of thermal efficiency with nanoparticle mass fraction for R1233zd(E)/R1336mzz(Z)

Among the three mixtures, R1224yd(Z)/R1233zd(E) produced the highest net work values across all nanoparticle cases, as shown in Figure 4.25 - 4.27. At low concentrations, TiO_2 and ZnO exceeded 147 kJ/kg, while Ag peaked at 132.4 kJ/kg at 0.1 mass fraction. By contrast, R1233zd(E)/R1336mzz(Z) delivered the lowest overall net work, ranging from 21.8 to 22.3 kJ/kg. At high Ag fractions (0.1), negative turbine work was observed in some cases, suggesting phase instability or phase incompatibility.

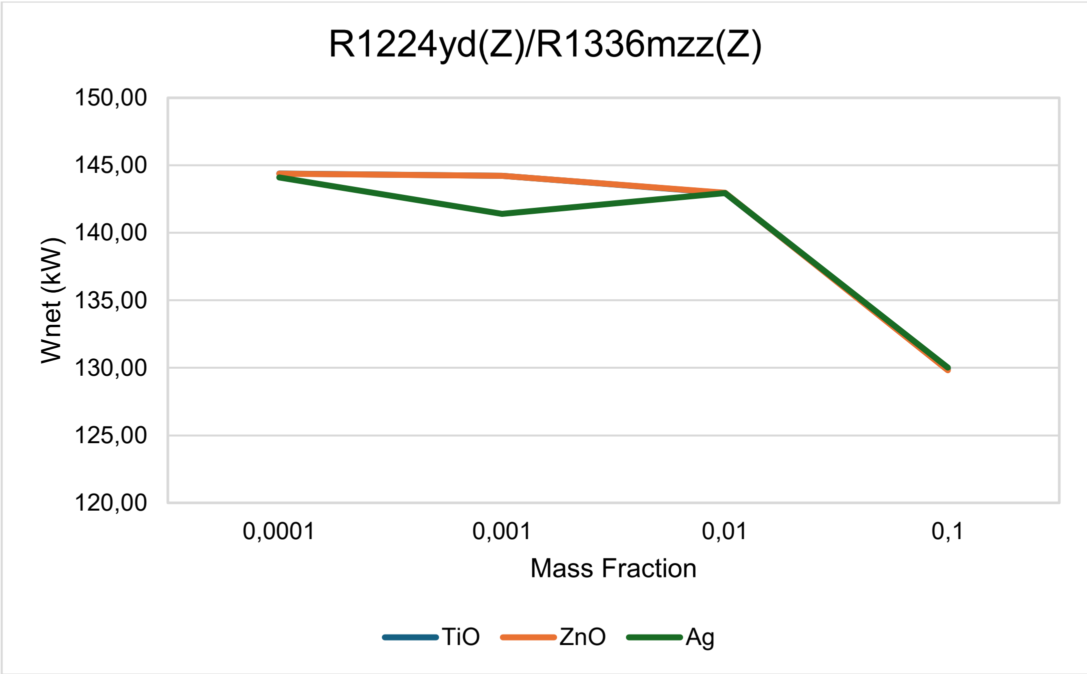

Figure 4.25: Net Power Output Variation with Nanoparticle Mass Fraction for R1224yd(Z)/R1336mzz(Z)

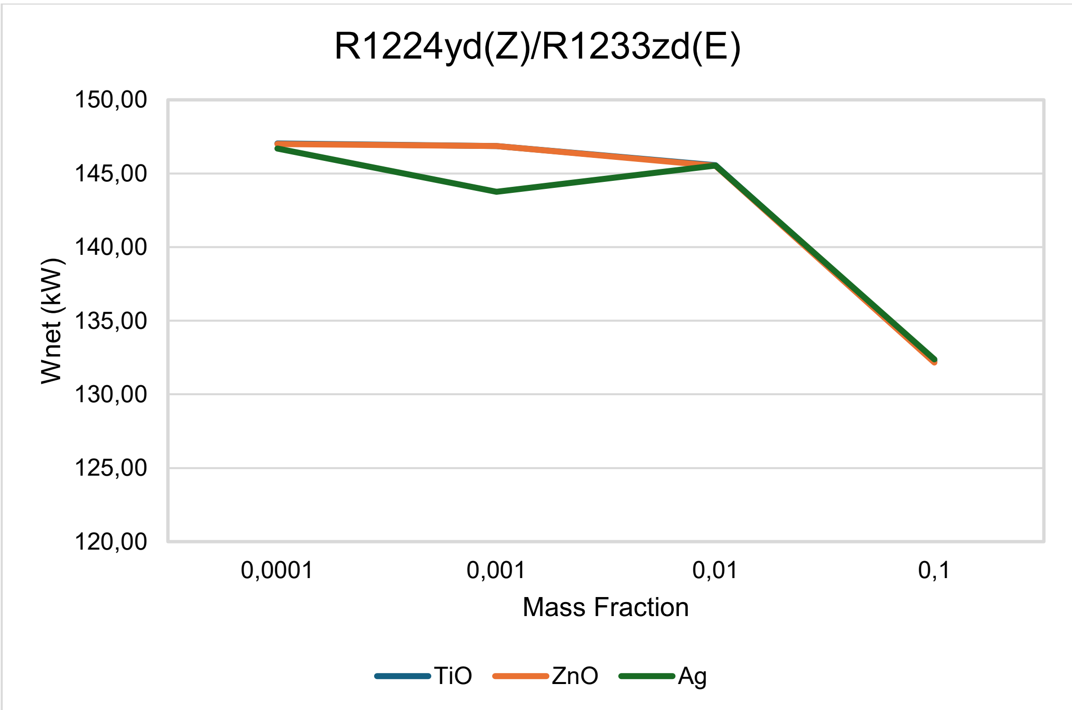

Figure 4.26: Net Power Output Variation with Nanoparticle Mass Fraction for R1224yd(Z)/R1233zd(E)

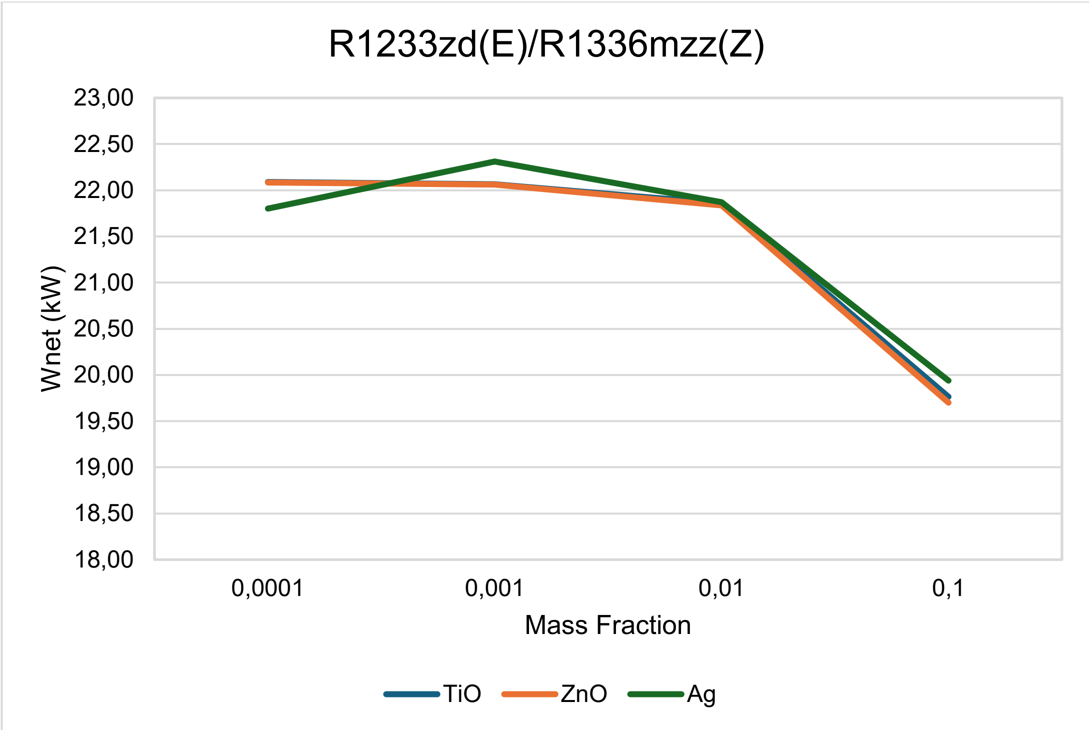

Figure 4.27: Net Power Output Variation with Nanoparticle Mass Fraction for R1233zd(E)/R1336mzz(Z)

While silver offers the strongest thermophysical advantages, high concentrations or extended cycling may lead to agglomeration, sedimentation, or chemical reactivity with metals such as stainless steel or copper. TiO_2 and ZnO, though less conductive, are more stable and less prone to dispersion issues.

Nanoparticles do not alter the vapour–liquid equilibrium of zeotropic mixtures. The base fluids retain their characteristic temperature glide, with nanoparticles only modifying transport properties. This is consistent with previous findings (Mondejar & Thern, 2017; Saadatfar *et al.*, 2014).

Mixture Set 2 confirms that silver can significantly enhance efficiency and net power output, particularly in R1224yd(Z)/R1233zd(E), but its benefits are highly concentration-dependent. TiO_2 and ZnO provide smaller but more stable improvements, making them preferable where operational stability is prioritised over peak efficiency.

4.4 Comparative Analysis with Existing ORC Systems

The comparison of the two zeotropic mixture sets reveals distinct thermodynamic performance profiles that align with trends reported in recent ORC literature. At a heat source temperature of 200 °C, Mixture Set 2, comprising newer low-GWP fluids, consistently delivered higher specific work and comparable or slightly higher thermal efficiency than Mixture Set 1. These outcomes reflect the benefits of temperature glide and critical property matching, which underpin improved thermal integration and reduced irreversibility. Similar conclusions have been drawn by Siddiqui *et al*. (2023) and Saadatfar *et al*. (2014), who emphasise that well-designed mixtures enhance exergy utilisation even when specific power may be constrained by pinch point behaviour or component sizing.

4.4.1 Mixture Sets in the Context of Literature Benchmarks

The best-performing blend in Set 1, R1233zd(E)/R123, achieved the highest thermal efficiency and net power output within the group. However, its performance remains moderate when compared to newer mixtures. This trend is consistent with experimental findings by Wang *et al*. (2023), who reported thermal efficiencies of 5–6% and exergy efficiencies up to 23.2% for R245fa/R141b mixtures in scroll-based ORC systems. These legacy blends benefit from temperature glide but are often limited in specific power due to pinch point constraints at elevated source temperatures.

The simulated results show higher thermal efficiency than those reported in small-scale experimental setups, as expected given the idealised modelling assumptions and optimised heat-source coupling. Nonetheless, the directional trade-offs, in which mixture glide improves exergy efficiency, but pure fluids may yield higher specific power, are consistent with the comparative analyses of Siddiqui *et al*. (2023) and Zhao *et al*. (2020b).

Among the Set 2 mixtures, R1224yd(Z)/R1233zd(E) demonstrated superior performance, achieving approximately 23 kJ/kg in net work output and thermal efficiencies of 8.3–8.5%. This reflects strong thermodynamic compatibility between the pair, driven by favourable critical properties and robust temperature glide. In contrast, R1224yd(Z)/R1336mzz(Z) lagged on both metrics, while R1233zd(E)/R1336mzz(Z) delivered intermediate results.

These findings align with the work of Saadatfar *et al*. (2014) and Mondejar & Thern (2017), who showed that low-GWP fluids with well-matched critical properties and non-ideal phase behaviour can reduce entropy generation and improve thermal matching. Gains in exergy efficiency often coincide with modest penalties in specific power when mixtures are not perfectly aligned with heat exchanger pinch points or when one component (e.g., R1336mzz(Z)) limits expansion potential.

Mixture Set 2 outperformed Set 1 in both specific work and thermal efficiency at 200 °C. This advantage is attributed to stronger property matching and more effective glide behaviour. The observed trade-off, higher thermal efficiency from mixtures versus potentially higher power density from pure fluids, is consistent with the findings of Siddiqui *et al*. (2023) and Blondel *et al*. (2023), who note that pursuing higher specific power with pure fluids often demands larger heat exchanger areas and tighter control of pinch conditions.

4.4.2 Implications Relative to Reported Trade-Offs

Although exergy efficiency was not explicitly calculated in this chapter, the observed trends, such as reduced irreversibility in Set 2 mixtures and improved thermal matching, suggest superior exergy behaviour compared to Set 1. This inference is supported by Saadatfar *et al*. (2014) and Mondejar & Thern (2017), who demonstrated that zeotropic mixtures with strong temperature glide reduce entropy generation and improve exergy utilisation. Siddiqui *et al*. (2023) further noted that pure fluids may yield slightly higher specific net power at 200 °C, but mixtures offer more stable efficiency under variable heat-source profiles.

Findings from Siddiqui *et al*. (2023) and Blondel *et al*. (2023) confirm that pure fluids require larger heat exchanger areas to achieve higher specific power. The results show that Set 2’s leading pair (R1224yd(Z)/R1233zd(E)) mitigates this risk by improving critical property alignment and glide behaviour, enabling a more compact and efficient system design.

Experimental scroll-based systems typically report lower absolute thermal efficiencies than simulations (Budianto *et al*., 2024; Liang & Yu, 2021). The higher thermal efficiency values observed in this chapter at 200 °C are consistent with idealised modelling and improved resource coupling. The alignment with experimental trends strengthens confidence in the comparative insights, even when absolute magnitudes differ.

4.5 System-Level Performance

The interplay between working fluid properties, heat source behaviour, component-level dynamics, and enhancement strategies such as nanoparticle doping, shapes system-level performance in ORC applications. This section consolidates the findings from previous analyses to evaluate how these factors collectively influence key performance metrics, including thermal efficiency, net power output, and evaporator duty.

4.5.1 Thermodynamic Integration and Temperature Glide

Zeotropic mixtures demonstrated a clear advantage over pure fluids in terms of temperature glide, enabling improved thermal matching in both the evaporator and the condenser. This alignment reduced irreversibility and exergy destruction, particularly under variable-heat-source conditions. Mixtures such as R1224yd(Z)/R1233zd(E) demonstrated strong compatibility with the hybrid solar–biomass input profile, maintaining stable performance across seasonal DNI fluctuations and biomass-supplementation cycles.

These findings are consistent with the work of Saadatfar *et al*. (2014), who emphasised that zeotropic mixtures with well-matched critical properties reduce entropy generation and improve exergy utilisation in hybrid ORC systems. Mondejar & Thern (2017) further demonstrated that temperature glide enhances heat-source coupling and reduces pinch-point constraints, allowing smoother heat exchange and better utilisation of available thermal energy.

4.5.2 Nanoparticle Enhancement and Hydraulic Trade-offs

Silver nanoparticles consistently improve heat transfer performance due to their high thermal conductivity (429 W/m·K). At optimal concentrations (typically ≤ 0.01 mass fraction), Ag-enhanced mixtures achieved thermal efficiency gains of up to 16% and notable increases in net power output. However, higher concentrations introduced instabilities in the system.

Ali *et al*. (2018) reported similar trends, noting that while metallic nanoparticles such as Ag offer superior thermal conductivity, they also pose challenges related to dispersion stability and hydraulic losses. Oxide-based nanoparticles (Al_2O_3, CuO, TiO_2, ZnO) offered more stable but modest improvements. Their lower conductivity limited heat transfer enhancement, but they maintained dispersion stability and avoided the agglomeration risks associated with metallic nanoparticles. These trade-offs underscore the need for careful dosage control and compatibility assessment when integrating nanofluids into ORC systems.

4.5.3 Component-Level Interactions and Cycle Behaviour

The performance of individual components, particularly the evaporator and expander, was sensitive to both fluid composition and nanoparticle concentration. Mixtures with strong temperature glide reduced thermal mismatches and improved evaporator duty, while high-conductivity nanofluids accelerated heat absorption. However, turbine performance was constrained when fluid viscosity exceeded optimal thresholds, especially at high nanoparticle loadings.

The condenser performance remained stable across most configurations, but mixtures with poor critical property alignment (e.g., R1224yd(Z)/R1336mzz(Z)) exhibited reduced expansion potential and lower net work output. These observations reinforce the findings of Siddiqui *et al*. (2021), who showed that fluid compatibility and phase behaviour significantly influence component-level efficiency and cycle stability.

4.5.4 System Optimisation and Design Implications

Achieving optimal system-level performance requires an integrated design approach. Isolated enhancements, such as selecting a high-efficiency fluid or adding nanoparticles, are insufficient unless they align with the broader thermodynamic and hydraulic context. The most promising configurations in this study, which balanced fluid composition, nanoparticle concentration, and heat source variability, delivered consistent performance.

For decentralised energy systems, especially in off-grid or resource-variable settings, this balance is critical. Mixtures such as R1224yd(Z)/R1233zd(E) with Ag doping at controlled concentrations offer a viable pathway to high-efficiency, low-GWP power generation. However, long-term stability, material compatibility, and lifecycle impacts must be addressed through experimental validation and robust control strategies, as emphasised by Ali *et al*. (2018) and Mondejar and Thern (2017).

4.6 Summary of Results and Discussions

This chapter presented a comprehensive thermodynamic evaluation of a hybrid solar–biomass ORC system that integrates zeotropic mixtures and nanoparticle-enhanced working fluids. The key findings are summarised below:

i. The selected West African site demonstrated strong solar potential, with peak DNI exceeding 150 kWh/m² during the dry season. Biomass resources, including agricultural residues, forest products, and animal waste, provided a stable thermal baseline, ensuring year-round operability. The hybrid configuration effectively balanced seasonal variability, leveraging solar input when available and supplementing it with biomass during periods of DNI.
ii. Lower mass flow rates (e.g., 0.05 kg/s) improved collector outlet temperatures due to increased residence time, reaching up to 178.8°C in December. However, this came at the cost of reduced throughput and increased biomass demand. Optimal flow rate selection must strike a balance among heat recovery, fuel cost, and system efficiency.
iii. Zeotropic mixtures outperformed pure fluids in terms of thermal matching and

temperature glide. Mixture Set 2, particularly R1224yd(Z)/R1233zd(E), achieved the highest net work output (~23 kJ/kg) and thermal efficiency (~8.3–8.5%), benefiting from favourable critical property alignment and robust glide behaviour. These results align with findings by Saadatfar *et al*. (2014) and Mondejar and Thern (2017), who emphasised the exergy advantages of well-matched mixtures.

iv. Silver nanoparticles delivered the most significant thermal gains, with optimal concentrations (≤ 0.01 mass fraction) yielding up to a 16% improvement in thermal efficiency. However, higher loadings introduced viscosity penalties and dispersion instability. Oxide-based nanoparticles (Al_2O_3, CuO, TiO_2, ZnO) offered more stable but modest enhancements. These trends are consistent with the work of Ali *et al*. (2018), who highlighted the trade-offs between conductivity and hydraulic performance.

v. The most effective configurations balanced the fluid composition, nanoparticle concentration, and heat-source variability. Mixtures with strong temperature glide reduced irreversibility and improved evaporator duty, while Ag-enhanced fluids accelerated heat absorption. However, turbine performance was sensitive to viscosity increases, particularly at high nanoparticle loadings. These findings underscore the importance of integrating design strategies that account for thermodynamic, hydraulic, and operational constraints.

vi. Mixture Set 2 consistently outperformed Set 1 in both net work and thermal efficiency, confirming literature trends that favour low-GWP, high-stability fluids with synergistic phase behaviour. The trade-offs between exergy efficiency and power density observed in this study mirror those reported by Siddiqui *et al*. (2023), underscoring the importance of fluid-property matching and pinch point control.

Chapter Five

5 Conclusions and Recommendations

5.1 Summary of Major Findings and Contributions

This chapter concludes the thesis by synthesising its principal findings and highlighting original contributions to the field of thermodynamic system optimisation. The research focused on enhancing the performance of hybrid ORC systems powered by solar and biomass heat sources, using HFO-based zeotropic mixtures and nanoparticle-enhanced working fluids. Through rigorous simulation and comparative analysis, the study addressed key challenges in low-grade heat utilisation, fluid selection, and hybrid energy integration, with particular relevance to energy-constrained regions such as Sub-Saharan Africa.

The investigation yielded several notable insights:

i. Among the fluid sets explored, R1224yd(Z)/R1233zd(E) emerged as the most thermodynamically favourable. Its strong temperature glide and well-aligned critical properties enabled improved heat source matching and reduced entropy generation during phase transitions.
ii. Silver nanoparticles, when applied at optimal mass fractions (NPF $\leq$ 0.01), significantly enhanced thermal conductivity and system efficiency. Peak thermal efficiencies reached up to 10.77%, outperforming oxide-based alternatives such as TiO_2 and ZnO. However, the study also emphasised the importance of dosage control and dispersion stability to mitigate hydraulic losses.
iii. The combination of solar and biomass inputs within a parallel configuration improved operational reliability and ensured continuity of thermal supply under variable environmental conditions. This dual-source strategy effectively addressed the intermittence challenges associated with solar energy alone.

iv. A modular simulation environment was constructed in ASPEN Plus to model ORC behaviour under varying fluid compositions, nanoparticle concentrations, and heat-source conditions. This framework enabled sensitivity analysis and performance benchmarking across multiple design scenarios.
v. Drawing on simulation insights and the literature, the study proposes a modular, scalable ORC system architecture tailored for decentralised energy deployment. The design prioritises adaptability, ease of integration, and compatibility with locally available renewable resources.

The research questions outlined in Section 1.4 were systematically addressed throughout the study. Research Question (i) was resolved in Section 4.1 and reinforced in Section 5.1.iii, where the dual-source solar–biomass configuration improved reliability. Research Question (ii) was examined in Section 4.2 and concluded in Section 5.2, with R1224yd(Z)/R1233zd(E) identified as the most favourable mixture. Research Question (iii) was addressed in Section 4.3 and summarised in Section 5.2, where silver nanoparticles at NPF ≤ 0.01 enhanced conductivity and efficiency. Finally, Research Question (iv) was explored in Sections 4.2–4.3 and synthesised in Section 5.1.iv, confirming that composition often outweighs absolute temperature in determining performance.

5.2 Thermophysical Insights and Fluid-Selection Guidance

This research provided detailed thermophysical insights that guided the selection and optimisation of working fluids for ORC applications. The findings highlight how fluid behaviour, environmental compatibility, and nanoparticle integration collectively influence system performance.

Zeotropic mixtures, particularly those based on hydrofluoroolefins, demonstrated significant advantages over pure fluids. Their non-isothermal phase transitions enabled the gradual absorption and rejection of heat, creating a temperature glide that improved thermal matching with the heat source. This behaviour reduced entropy generation and enhanced exergy efficiency, especially at medium temperatures.

HFO-based fluids emerged as environmentally responsible alternatives to legacy refrigerants. With low GWP, zero ODP, and favourable thermodynamic properties, these fluids are well-suited for sustainable deployment in decentralised energy systems.

Among the nanoparticle types investigated, silver exhibited exceptional thermal conductivity and maintained stable dispersion at low mass fractions. When paired with the R1224yd(Z)/R1233zd(E) mixture, Ag nanoparticles enhanced heat transfer and reduced thermodynamic irreversibilities. However, the study also underscored the importance of dosage control. While low nanoparticle mass fractions (NPF ≤ 0.01) improved performance, excessive doping (NPF = 0.1) increased viscosity, pumping work, and net power output.

Based on these insights, the R1224yd(Z)/R1233zd(E) mixture doped with Ag at NPF = 0.01 is recommended as the optimal working fluid for hybrid ORC systems operating within the 100-200 °C temperature range. This pairing strikes a balance between thermal enhancement and fluid stability, offering a promising pathway for efficient and environmentally conscious energy conversion.

5.3 System Design Recommendations

Building on the thermophysical insights and simulation results, this section presents practical system design recommendations for hybrid ORC configurations operating within the 100-200 °C temperature range. These recommendations aim to guide future implementation, improve operational reliability, and support scalable deployment in decentralised energy contexts.

i. The R1224yd(Z)/R1233zd(E) zeotropic mixture, doped with silver nanoparticles at a mass fraction of NPF = 0.01, is recommended as the optimal working fluid. This pairing offers strong temperature glide, enhanced thermal conductivity, and low global warming potential, making it suitable for medium-grade heat recovery and environmentally conscious design.

ii. A hybrid configuration that combines solar collectors and biomass boilers is recommended to ensure thermal continuity. Solar energy should be prioritised during high-DNI periods, while biomass serves as a reliable auxiliary source during low insolation or nighttime operation. This dual-source strategy mitigates intermittency and supports stable power generation.

iii. Parallel heat exchanger arrangements are recommended to allow independent or simultaneous engagement of solar and biomass inputs. This configuration improves thermal control, simplifies flow management, and enhances system flexibility. Careful sizing based on fluid properties and expected operating conditions is essential to minimise pinch point losses.

iv. To maintain nanoparticle stability and prevent agglomeration, low-concentration doping (NPF ≤ 0.01) should be used. Advanced dispersion techniques, such as ultrasonic agitation or surfactant stabilisation, may be considered in experimental setups. Real-time monitoring of viscosity and flow behaviour is critical to ensure consistent performance.

v. Thermostatic and flow-based control systems should be implemented to regulate the engagement of the heat source and maintain fluid stability. Sensor networks for temperature, pressure, and nanoparticle dispersion can support adaptive operation and fault detection, especially in off-grid or remote installations.

vi. The proposed ORC architecture should adopt modular design principles to support scalability, ease of maintenance, and integration with locally available resources. Modular components, including pumps, turbines, and heat exchangers, allow for flexible system expansion and tailored deployment across diverse geographic and economic settings.

5.4 Limitations and Future Experimental Directions

While the study provided valuable modelling insights into hybrid ORC systems, several limitations were acknowledged, warranting further investigation and experimental validation.

First, the simulations were conducted under steady-state conditions and assumed ideal component behaviour. In practice, ORC systems exhibit dynamic responses, transient effects, and nonlinear interactions that the current framework does not capture. These real-world complexities may influence system stability, control strategies, and overall performance.

Second, nanoparticle dispersion stability was modelled using empirical correlations. The study did not experimentally validate agglomeration, sedimentation, or long-term fluid compatibility, all of which are critical factors for sustained thermal enhancement and reliable operation. Without laboratory verification, the practical viability of nanofluid integration remains uncertain.

Third, the economic feasibility of the proposed system was not assessed. Key financial metrics such as capital investment, operational costs, payback period, and lifecycle emissions were beyond the scope of this thesis. However, these considerations are essential for commercialisation and policy adoption, particularly in resource-constrained regions.

Fourth, the environmental impact of nanoparticle disposal and fluid degradation was not evaluated. The long-term ecological implications of nanofluid use, including potential toxicity, recyclability, and waste management, require careful research to ensure safe and sustainable deployment.

To address these limitations, future research should focus on the following areas:

i. Experimental validation of nanoparticle-enhanced zeotropic mixtures under controlled laboratory conditions, including thermal cycling, flow stability, and material compatibility assessments.

ii. Development of advanced dispersion techniques, including ultrasonic agitation, surfactant stabilisation, and magnetic alignment, to enhance nanoparticle distribution and prevent agglomeration.

iii. Techno-economic modelling to evaluate the cost-effectiveness, scalability, and financial viability of hybrid ORC systems across diverse geographic and socio-economic contexts.

iv. Integration of intelligent control algorithms and sensor networks to enable adaptive operation, fault detection, and real-time performance optimisation, especially in decentralised or off-grid environments.

These directions will help bridge the gap between simulation and deployment, ensuring that future ORC systems are not only thermodynamically optimised but also economically viable, environmentally responsible, and operationally robust.

5.5 Contribution to Knowledge

The contributions presented in this study have been derived from a rigorous thermodynamic optimisation and modelling framework. Although real-time experimental validation was not conducted, the reliability of the findings has been supported through benchmarking against established reference fluids and systematic energy-exergy analysis across hybrid solar-biomass scenarios. The absence of experimental validation defines the scope of the work as computational optimisation and highlights the need for subsequent empirical studies. In this way, the contributions are positioned as credible within the modelling domain, while also providing a clear foundation for future experimental verification and practical deployment.

Key contributions include:

i. The identification and thermodynamic characterisation of the R1224yd(Z)/R1233zd(E) zeotropic mixture, especially when doped with silver nanoparticles at low mass fractions, offers a novel working fluid configuration that balances thermal efficiency, environmental responsibility, and fluid stability. This pairing has not been extensively explored in prior literature and demonstrates strong potential for medium-grade heat applications.

ii. The proposed dual-source configuration, combining solar and biomass heat sources, provides a resilient, context-sensitive solution to the intermittency challenges of renewable energy. This framework supports continuous thermal input and is particularly relevant for decentralised energy systems in Sub-Saharan Africa and other regions with energy constraints.

iii. The development of a modular ASPEN Plus simulation environment enables detailed performance benchmarking across fluid compositions, nanoparticle concentrations, and heat source conditions. This framework supports reproducibility, comparative analysis, and future adaptation to emerging fluids and technologies.

iv. The study introduces a modular and scalable ORC architecture tailored for off-grid deployment. By emphasising adaptability, ease of integration, and compatibility with locally available resources, the design contributes to the practical advancement of sustainable power generation technologies.

v. The research deepens an understanding of how temperature glide, critical property alignment, and nanoparticle doping influence exergy efficiency and system behaviour. These insights inform fluid selection strategies and highlight the trade-offs between thermal enhancement and hydraulic performance.

References

Ali, N., Teixeira, J. A., & Addali, A. (2018). A Review on Nanofluids: Fabrication, Stability, and Thermophysical Properties. Journal of Nanomaterials, 2018, 1–33. https://doi.org/10.1155/2018/6978130

Allison, T. C., Wygant, K., Wilkes, J. C., & Pelton, R. (2022). Technoeconomic Comparison of sCO2 and ORC Systems for Waste Heat Recovery. Proceedings of the ASME Turbo Expo, 9. https://doi.org/10.1115/GT2022-83434

Almehmadi, F. A., Elattar, H. F., Fouda, A., Alqaed, S., Mustafa, J., Alharthi, M. A., & Refaey, H. A. (2022). Energy Performance Assessment of a Novel Solar Poly-Generation System Using Various ORC Working Fluids in Residential Buildings. Energies, 15(21). https://doi.org/10.3390/EN15218286

Alshammari, F., Karvountzis-Kontakiotis, A., Pesyridis, A., & Usman, M. (2018a). Expander technologies for automotive engine organic rankine cycle applications. In Energies (Vol. 11, Number 7). https://doi.org/10.3390/en11071905

Alshammari, F., Usman, M., & Pesyridis, A. (2018b). Expanders for Organic Rankine Cycle Technology. In Organic Rankine Cycle Technology for Heat Recovery. https://doi.org/10.5772/intechopen.78720

Al-Sulaiman, F. A., Hamdullahpur, F., & Dincer I, I. (2011). Performance comparison of three trigeneration systems using organic rankine cycles. Energy, 36(9). https://doi.org/10.1016/j.energy.2011.06.003

Alvi, J. Z., Guan, Z., & Imran, M. (2024). Thermoeconomic Evaluation and Sustainability Insights of Hybrid Solar–Biomass Powered Organic Rankine Cycle Systems: A Comprehensive Review. Biomass 2024, Vol. 4, Pages 1092-1121, 4(4), 1092–1121. https://doi.org/10.3390/BIOMASS4040061

Ambriz-Díaz, V. M., Rosas, I. Y., Chávez, O., & Rubio-Maya, C. (2022). 4E Assessment of an Organic Rankine Cycle (ORC) Activated with Waste Heat of a Flash–Binary Geothermal Power Plant. Entropy, 24(12). https://doi.org/10.3390/E24121832

Ancona, M. A., Bianchi, M., Branchini, L., De Pascale, A., Melino, F., Peretto, A., &

Torricelli, N. (2021). Systematic Comparison of ORC and s-CO2 Combined Heat and Power Plants for Energy Harvesting in Industrial Gas Turbines. Energies, 14(12), 3402. https://doi.org/10.3390/en14123402

Andreasen, J. G., Baldasso, E., Kærn, M. R., Weith, T., Heberle, F., Brüggemann, D., & Haglind, F. (2021). Techno-economic feasibility analysis of zeotropic mixtures and pure fluids for organic Rankine cycle systems. Applied Thermal Engineering, 192, 116791. https://doi.org/10.1016/j.applthermaleng.2021.116791

Andreasen, J. G., Larsen, U., Knudsen, T., Pierobon, L., & Haglind, F. (2014). Selection and optimization of pure and mixed working fluids for low grade heat utilization using organic Rankine cycles. Energy, 73, 204–213. https://doi.org/10.1016/j.energy.2014.06.012

Arpagaus, C., & Bertsch, S. (2021). Experimental Comparison of HCFO and HFO R1224yd(Z), R1233zd(E), R1336mzz(Z), and HFC R245fa in a High Temperature Heat Pump up to 150 °C Supply Temperature. 18th International Refrigeration and Air Conditioning Conference. https://docs.lib.purdue.edu/iracc

Babatunde, A. F., & Sunday, O. O. (2018). A Review of Working Fluids for Organic Rankine Cycle (ORC) Applications. IOP Conference Series: Materials Science and Engineering, 413, 012019. https://doi.org/10.1088/1757-899X/413/1/012019

Badr, O., Probert, S. D., & O'Callaghan, P. W. (1985). Selecting a working fluid for a Rankine-cycle engine. Applied Energy, 21(1), 1–42. https://doi.org/10.1016/0306-2619(85)90072-8

Bamorovat Abadi, G., Yun, E., & Kim, K. C. (2015). Experimental study of a 1 kw organic Rankine cycle with a zeotropic mixture of R245fa/R134a. Energy, 93, 2363–2373. https://doi.org/10.1016/J.ENERGY.2015.10.092

Bao, J., Zhang, R., Lin, Y., Zhang, N., Zhang, X., & He, G. (2018). Simultaneous optimization of system structure and working fluid for the three-stage condensation Rankine cycle utilizing LNG cold energy. Applied Thermal Engineering, 140, 120–130. https://doi.org/10.1016/j.applthermaleng.2018.05.049

Bao, J., & Zhao, L. (2013). A review of working fluid and expander selections for organic Rankine cycle. Renewable and Sustainable Energy Reviews, 24, 325–342. https://doi.org/10.1016/j.rser.2013.03.040

Basu, P. (2018). Biomass Gasification, Pyrolysis and Torrefaction. In Biomass Gasification, Pyrolysis and Torrefaction: Practical Design and Theory. Elsevier. https://doi.org/10.1016/C2016-0-04056-1

Bederna, B. G., Barta, R. B., & Hesse, U. (2021). COMPOSITION OPTIMIZATION OF ZEOTROPIC MIXTURES FOR ORC SYSTEMS CONSIDERING CONSTRAINTS. International Seminar on ORC Power Systems.

Bell, I. H., Wronski, J., Quoilin, S., & Lemort, V. (2014). Pure and Pseudo-pure Fluid Thermophysical Property Evaluation and the Open-Source Thermophysical Property Library CoolProp. Industrial & Engineering Chemistry Research, 53(6), 2498–2508. https://doi.org/10.1021/ie4033999

Bellos, E., & Tzivanidis, C. (2017). Parametric analysis and optimization of an Organic Rankine Cycle with nanofluid based solar parabolic trough collectors. Renewable Energy. https://doi.org/10.1016/j.renene.2017.06.055

Benato, A., & Macor, A. (2017). Biogas Engine Waste Heat Recovery Using Organic Rankine Cycle. Energies, 10(3), 327. https://doi.org/10.3390/en10030327

Bianchi, M., Branchini, L., De Pascale, A., Melino, F., Ottaviano, S., Peretto, A., & Torricelli, N. (2021). Performance modelling and greenhouse impact assessment of a micro-ORC energy system working with HFCs, low GWP fluids and mixtures. E3S Web of Conferences, 238, 10002. https://doi.org/10.1051/e3sconf/202123810002

Bishoge, O. K., Kombe, G. G., & Mvile, B. N. (2020). Renewable energy for sustainable development in sub-Saharan African countries: Challenges and way forward. Journal of Renewable and Sustainable Energy, 12(5). https://doi.org/10.1063/5.0009297/1017497

Blondel, Q., Tauveron, N., Lhermet, G., & Caney, N. (2023). Zeotropic mixtures study in plate heat exchangers and ORC systems. Applied Thermal Engineering, 219, 119418. https://doi.org/10.1016/j.applthermaleng.2022.119418

Braimakis, K., & Karellas, S. (2018). Energetic optimization of regenerative Organic Rankine Cycle (ORC) configurations. Energy Conversion and Management, 159, 353–370. https://doi.org/10.1016/j.enconman.2017.12.093

Branchini, L., De Pascale, A., & Peretto, A. (2013). Systematic comparison of ORC configurations by means of comprehensive performance indexes. Applied Thermal Engineering, 61(2), 129–140. https://doi.org/10.1016/J.APPLTHERMALENG.2013.07.039

Brasz, J. J., Smith, I. K., & Stosic, N. (2000). Development of a Twin Screw Expressor as a Throttle Valve Replacement for Water-Cooled Chillers. International Compressor Engineering Conference. Paper 1488. https://docs.lib.purdue.edu/icec/1488

Canada, S., Cohen, G., Cable, R., Brosseau, D., & Price, H. (2005). Parabolic Trough Organic Rankine Cycle Power Plant. 2004 DOE Solar Energy Technologies Program Review Meeting. https://www.osti.gov/biblio/860827-parabolic-trough-organic-rankine-cycle-power-plant

Cao, Y., Taghvaie Nakhjiri, A., Sarkar, S. M., & Ghadiri, M. (2023). Integration of ANN and NSGA-II for Optimization of Nusselt Number and Pressure Drop in a Coiled Heat Exchanger via Water-Based Nanofluid Containing Alumina and Ag Nanoparticles. Arabian Journal for Science and Engineering, 48(7), 8861–8869. https://doi.org/10.1007/S13369-022-07480-3/METRICS

Casati, E., Vitale, S., Pini, M., Persico, G., & Colonna, P. (2014). Centrifugal turbines for mini-organic rankine cycle power systems. Journal of Engineering for Gas Turbines and Power, 136(12). https://doi.org/10.1115/1.4027904/373784

Cavazzini, G., Bari, S., McGrail, P., Benedetti, V., Pavesi, G., & Ardizzon, G. (2019). Contribution of Metal-Organic-Heat Carrier nanoparticles in a R245fa low-grade heat recovery Organic Rankine Cycle. Energy Conversion and Management, 199, 111960. https://doi.org/10.1016/j.enconman.2019.111960

Chen, H., Goswami, D. Y., & Stefanakos, E. K. (2010). A review of thermodynamic cycles and working fluids for the conversion of low-grade heat. Renewable and Sustainable Energy Reviews, 14(9), 3059–3067. https://doi.org/10.1016/j.rser.2010.07.006

Cheng, Z., Tan, Z., Guo, Z., Yang, J., & Wang, Q. (2020). Technologies and fundamentals of waste heat recovery from high-temperature solid granular materials. Applied Thermal Engineering, 179, 115703.

https://doi.org/10.1016/J.APPLTHERMALENG.2020.115703

Chys, M., van den Broek, M., Vanslambrouck, B., & De Paepe, M. (2012). Potential of zeotropic mixtures as working fluids in organic Rankine cycles. Energy, 44(1). https://doi.org/10.1016/j.energy.2012.05.030

Cipollone, R., Bianchi, G., Di Battista, D., Contaldi, G., & Murgia, S. (2014). Mechanical Energy Recovery from Low Grade Thermal Energy Sources. Energy Procedia, 45, 121–130. https://doi.org/10.1016/J.EGYPRO.2014.01.014

Civgin, M. G., & Deniz, C. (2021). Analyzing the dual-loop organic rankine cycle for waste heat recovery of container vessel. Applied Thermal Engineering, 199, 117512. https://doi.org/10.1016/j.applthermaleng.2021.117512

Clemente, S., Micheli, D., Reini, M., & Taccani, R. (2013). Bottoming organic Rankine cycle for a small scale gas turbine: A comparison of different solutions. Applied Energy, 106, 355–364. https://doi.org/10.1016/J.APENERGY.2013.02.004

Collings, P. (2018). Theoretical and experimental analysis of an Organic Rankine Cycle [University of Glasgow]. http://theses.gla.ac.uk/30642/1/2018CollingsPhD.pdf

Come Zebra, E. I., van der Windt, H. J., Nhumaio, G., & Faaij, A. P. C. (2021). A review of hybrid renewable energy systems in mini-grids for off-grid electrification in developing countries. Renewable and Sustainable Energy Reviews, 144, 111036. https://doi.org/10.1016/j.rser.2021.111036

Dai, Y., Wang, J., & Gao, L. (2009). Parametric optimization and comparative study of organic Rankine cycle (ORC) for low grade waste heat recovery. Energy Conversion and Management, 50(3), 576–582. https://doi.org/10.1016/j.enconman.2008.10.018

Daniarta, S., & Kolasiński, P. (2022). A Comparative Study of Cooling Sources in Organic Rankine Cycle for Low-Temperature Geothermal Heat Sources. IOP Conference Series: Earth and Environmental Science, 1014(1), 012008. https://doi.org/10.1088/1755-1315/1014/1/012008

Das, S. K., & CHOI, S. U. S. (2009). A Review of Heat Transfer in Nanofluids. In Advances in Heat Transfer (Vol. 41, pp. 81–197). Elsevier. https://doi.org/10.1016/S0065-2717(08)41002-X

Deniz, C. (2015). Thermodynamic and Environmental Analysis of Low-Grade Waste Heat Recovery System for a Ship Power Plant. International Journal of Energy Science, 1(1), 23–34. https://doi.org/10.12783/ijes.2015.0501.04

Desideri, A., Gusev, S., van den Broek, M., Lemort, V., & Quoilin, S. (2016). Experimental comparison of organic fluids for low temperature ORC (organic Rankine cycle) systems for waste heat recovery applications. Energy, 97, 460–469. https://doi.org/10.1016/j.energy.2015.12.012

Domanski, P. A., Brignoli, R., Brown, J. S., Kazakov, A. F., & Mclinden, M. O. (2018). Low-GWP Refrigerants; Options and Issues. https://doi.org/10.1038/ncomms14476

Dong, B., Xu, G., Li, T., Quan, Y., & Wen, J. (2018). Thermodynamic and economic analysis of zeotropic mixtures as working fluids in low temperature organic Rankine cycles. Applied Thermal Engineering, 132, 545–553. https://doi.org/10.1016/J.APPLTHERMALENG.2017.12.083

Doninelli, M., & Di Marcoberardino, G. (2024). On the Design of Recuperator for Transcritical Cycle Adopting CO2-Based Mixture as Working Fluid: A Focus on Transport Properties Prediction. Energy Technology, 12(1), 2300677. https://doi.org/10.1002/ENTE.202300677

Eastman, J. A., Choi, S. U. S., Li, S., Yu, W., & Thompson, L. J. (2001). Anomalously increased effective thermal conductivities of ethylene glycol-based nanofluids containing copper nanoparticles. Applied Physics Letters, 78(6), 718–720. https://doi.org/10.1063/1.1341218

El Alani, O., Ghennioui, H., Abraim, M., Ghennioui, A., Blanc, P., Saint-Drenan, Y.-M., & Naimi, Z. (2022). Solar Energy Resource Assessment Using GHI and DNI Satellite Data for Moroccan Climate. In Lecture Notes on Data Engineering and Communications Technologies (Vol. 110, pp. 275–285). Springer, Cham. https://doi.org/10.1007/978-3-030-94188-8_26

ESMAP, SOLARGIS, WB, & IFC. (2019). Global Solar Atlas. In Global Solar Atlas.

Faghih, S., & Pourshaghaghy, A. (2022). Selecting working fluids in organic Rankine cycle (ORC) for waste heat applications and optimal cycle parameters for different hot source temperatures. Journal of Thermal Analysis and Calorimetry, 147(23), 13737–13755. https://doi.org/10.1007/S10973-022-11502-5/METRICS

Fang, Y., Yang, F., & Zhang, H. (2019). Comparative analysis and multi-objective optimization of organic Rankine cycle (ORC) using pure working fluids and their zeotropic mixtures for diesel engine waste heat recovery. Applied Thermal Engineering, 157, 113704. https://doi.org/10.1016/j.applthermaleng.2019.04.114

Fedele, L., Lombardo, G., Greselin, I., Menegazzo, D., & Bobbo, S. (2023). Thermophysical Properties of Low GWP Refrigerants: An Update. International Journal of Thermophysics, 44(5), 80. https://doi.org/10.1007/s10765-023-03191-5

Feng, Y., Hung, T. C., Greg, K., Zhang, Y., Li, B., & Yang, J. (2015). Thermoeconomic comparison between pure and mixture working fluids of organic Rankine cycles (ORCs) for low temperature waste heat recovery. Energy Conversion and Management, 106. https://doi.org/10.1016/j.enconman.2015.09.042

Feng, Y.-Q., Hung, T.-C., Wu, S.-L., Lin, C.-H., Li, B.-X., Huang, K.-C., & Qin, J. (2017). Operation characteristic of a R123-based organic Rankine cycle depending on working fluid mass flow rates and heat source temperatures. Energy Conversion and Management, 131, 55–68. https://doi.org/10.1016/j.enconman.2016.11.004

Fergani, Z., Morosuk, T., & Touil, D. (2021). Exergy-Based Multi-Objective Optimization of an Organic Rankine Cycle with a Zeotropic Mixture. Entropy, 23(8), 954. https://doi.org/10.3390/e23080954

Freeman, J., Guarracino, I., Kalogirou, S. A., & Markides, C. N. (2017). A small-scale solar organic Rankine cycle combined heat and power system with integrated thermal energy storage. Applied Thermal Engineering, 127, 1543–1554. https://doi.org/10.1016/j.applthermaleng.2017.07.163

Freeman, J., Hellgardt, K., & Markides, C. N. (2015). An assessment of solar-powered organic Rankine cycle systems for combined heating and power in UK domestic applications. Applied Energy, 138, 605–620. https://doi.org/https://doi.org/10.1016/j.apenergy.2014.10.035

Fu, B. R., Lee, Y. R., & Hsieh, J. C. (2015). Design, construction, and preliminary results of a 250-kW organic Rankine cycle system. Applied Thermal Engineering, 80. https://doi.org/10.1016/j.applthermaleng.2015.01.077

Galloni, E., Fontana, G., & Staccone, S. (2015). Design and experimental analysis of a mini ORC (organic Rankine cycle) power plant based on R245fa working fluid. Energy, 90, 768–775. https://doi.org/10.1016/j.energy.2015.07.104

García-Pabón, J. J., Méndez-Méndez, D., Belman-Flores, J. M., Barroso-Maldonado, J. M., & Khosravi, A. (2021). A Review of Recent Research on the Use of R1234yf as an Environmentally Friendly Fluid in the Organic Rankine Cycle. Sustainability, 13(11), 5864. https://doi.org/10.3390/su13115864

Garg, P., & Orosz, M. S. (2018). Economic optimization of Organic Rankine cycle with pure fluids and mixtures for waste heat and solar applications using particle swarm optimization method. Energy Conversion and Management, 165, 649–668. https://doi.org/10.1016/j.enconman.2018.03.086

Glavatskaya, Y., Podevin, P., Lemort, V., Shonda, O., & Descombes, G. (2012). Reciprocating expander for an exhaust heat recovery rankine cycle for a passenger car application. Energies, 5(6). https://doi.org/10.3390/en5061751

Gomaa, M. R., Mustafa, R. J., Al-Dhaifallah, M., & Rezk, H. (2020). A low-grade heat Organic Rankine Cycle driven by hybrid solar collectors and a waste heat recovery system. Energy Reports, 6, 3425–3445. https://doi.org/10.1016/J.EGYR.2020.12.011

Györke, G., Deiters, U. K., Groniewsky, A., Lassu, I., & Imre, A. R. (2018). Novel classification of pure working fluids for Organic Rankine Cycle. Energy, 145, 288–300. https://doi.org/10.1016/j.energy.2017.12.135

Hamdi, B., Kheiri, A., Mabrouk, M. T., & Kairouani, L. (2023). Organic Rankine Cycle Systems with Mixture of Pure Fluids: On Infeasible Fluid's Fractions Due to the Interaction between the Mixture Glide and the hexs pinchs. Journal of Thermal Engineering, 125–156. https://doi.org/10.18186/thermal.1268844

Han, S., Seo, J. B., & Choi, B. S. (2014). Development of a 200 kW ORC radial turbine for waste heat recovery. Journal of Mechanical Science and Technology, 28(12). https://doi.org/10.1007/s12206-014-1147-6

Heberle, F., & Brüggemann, D. (2016). Thermo-Economic Analysis of Zeotropic Mixtures and Pure Working Fluids in Organic Rankine Cycles for Waste Heat Recovery. Energies, 9(4), 226. https://doi.org/10.3390/en9040226

Heberle, F., Preißinger, M., & Brüggemann, D. (2012). Zeotropic mixtures as working fluids in Organic Rankine Cycles for low-enthalpy geothermal resources. Renewable Energy, 37(1), 364–370. https://doi.org/10.1016/j.renene.2011.06.044

Herath, H. M. D. P., Wijewardane, M. A., Ranasinghe, R. A. C. P., & Jayasekera, J. G. A. S. (2020). Working fluid selection of Organic Rankine Cycles. Energy Reports, 6, 680–686. https://doi.org/10.1016/j.egyr.2020.11.150

Howard, S. S. (2022). Study of Concentrated Solar Power Collectors with Organic Rankine Cycle and Magnetized Nanofluids . American Journal of Engineering and Applied Sciences, 15(1). https://doi.org/10.3844/ajeassp.2022.101.117

Hsu, S. W., Chiang, H. W. D., & Yen, C. W. (2014). Experimental investigation of the performance of a hermetic screw-expander organic rankine cycle. Energies, 7(9). https://doi.org/10.3390/en7096172

Huber, M. L., Lemmon, E. W., Bell, I. H., & McLinden, M. O. (2022). The NIST REFPROP Database for Highly Accurate Properties of Industrially Important Fluids. Industrial & Engineering Chemistry Research, 61(42), 15449–15472. https://doi.org/10.1021/acs.iecr.2c01427

Hui-Xing, Z., Wei, D., Lin, S., Qing-Song, A., Sui-Lin, W., & Bao-Lin, A. (2022). Theoretical selection criteria of organic Rankine cycle form for different heat sources. Energy, 238. https://doi.org/10.1016/j.energy.2021.122039

Hung, T.-C. (2001). Waste heat recovery of organic Rankine cycle using dry fluids. Energy Conversion and Management, 42(5), 539–553. https://doi.org/10.1016/S0196-8904(00)00081-9

IEA (2020), Tracking SDG7: The Energy Progress Report, 2020, IEA, Paris https://www.iea.org/reports/tracking-sdg7-the-energy-progress-report-2020

Imran, M., Park, B. S., Kim, H. J., Lee, D. H., Usman, M., & Heo, M. (2014). Thermo-economic optimization of Regenerative Organic Rankine Cycle for waste heat recovery applications. Energy Conversion and Management, 87. https://doi.org/10.1016/j.enconman.2014.06.091

Imran, M., Pili, R., Usman, M., & Haglind, F. (2020). Dynamic modeling and control strategies of organic Rankine cycle systems: Methods and challenges. Applied Energy, 276. https://doi.org/10.1016/j.apenergy.2020.115537

Imran, M., Usman, M., Lee, D.-H., & Park, B.-S. (2015). Thermoeconomic analysis of organic Rankine cycle using zeotropic mixtures. 3rd International Seminar on ORC Power Systems, 161.

Ingley, H. A., Reed, R., & Goswami, D. Y. (2005). Optimization of a scroll expander applied to an ammonia/water combined cycle system for hydrogen production. Proceedings of the Solar World Congress 2005: Bringing Water to the World, Including Proceedings of 34th ASES Annual Conference and Proceedings of 30th National Passive Solar Conference, 3.

Inoue, N., Kaneko, A., Watanabe, H., Uchimura, T., & Irie, K. (2007). Development of electric power generation unit driven by waste heat (study on working fluids and expansion turbines). Proceedings of the ASME Turbo Expo, 3. https://doi.org/10.1115/gt2007-27749

International Energy Agency. (2022). World Energy Outlook Special Report Africa Energy Outlook 2022. www.iea.org/t&c/

IRENA and AfDB. (2022). Renewable Energy Market Analysis: Africa and Its Regions. International Renewable Energy Agency and African Development Bank. www.afdb.org

Ismail, H., Aziz, A. A., Rasih, R. A., Jenal, N., Michael, Z., & Roslan, A. (2016). Performance of Organic Rankine Cycle Using Biomass as Source of Fuel. Journal of Advanced Research in Applied Sciences and Engineering Technology, 4(1), 29–46.

Jafarmadar, S., & Habibzadeh, A. (2017). Study of a Combined Power and Ejector Refrigeration Cycle with Low-temperature Heat Sources by Applying Various Working Fluids. IOP Conference Series: Earth and Environmental Science, 83(1), 012008. https://doi.org/10.1088/1755-1315/83/1/012008

Jiménez-García, J. C., Ruiz, A., Pacheco-Reyes, A., & Rivera, W. (2023). A Comprehensive Review of Organic Rankine Cycles. Processes, 11(7), 1982. https://doi.org/10.3390/pr11071982

Jung, H.-C., Taylor, L., & Krumdieck, S. (2015). An experimental and modelling study of a 1 kW organic Rankine cycle unit with mixture working fluid. Energy, 81, 601–614. https://doi.org/10.1016/j.energy.2015.01.003

Kane, M., Larrain, D., Favrat, D., & Allani, Y. (2003). Small hybrid solar power system. Energy, 28(14). https://doi.org/10.1016/S0360-5442(03)00127-0

Kang, S. H. (2012). Design and experimental study of ORC (organic Rankine cycle) and radial turbine using R245fa working fluid. Energy, 41(1), 514–524. https://doi.org/10.1016/J.ENERGY.2012.02.035

Kasaeian, A., Daneshazarian, R., Mahian, O., Kolsi, L., Chamkha, A. J., Wongwises, S., & Pop, I. (2017). Nanofluid flow and heat transfer in porous media: A review of the latest developments. International Journal of Heat and Mass Transfer, 107, 778–791. https://doi.org/10.1016/j.ijheatmasstransfer.2016.11.074

Kılıç B (2020), Analysis of ORC for waste heat recovery from marine engines using plate heat exchangers. *Emerging Materials Research*, Vol. 9 No. 4 pp. 1274–1282, doi: https://doi.org/10.1680/jemmr.20.00266

Kindra, V., Komarov, I., Osipov, S., Zlyvko, O., & Maksimov, I. (2022). Feasibility Study of the CO2 Regenerator Parameters for Oxy-Fuel Combustion Power Cycle. Inventions, 7(3). https://doi.org/10.3390/INVENTIONS7030066

Klonowicz, P., Borsukiewicz-Gozdur, A., Hanausek, P., Kryłłowicz, W., & Brüggemann, D. (2014). Design and performance measurements of an organic vapour turbine. Applied Thermal Engineering, 63(1). https://doi.org/10.1016/j.applthermaleng.2013.11.018

Klonowicz, P., Heberle, F., Preißinger, M., & Brüggemann, D. (2014). Significance of loss correlations in performance prediction of small scale, highly loaded turbine stages working in Organic Rankine Cycles. Energy, 72. https://doi.org/10.1016/j.energy.2014.05.040

Kolahi, M., Yari, M., Mahmoudi, S. M. S., & Mohammadkhani, F. (2016). Thermodynamic and economic performance improvement of ORCs through using zeotropic mixtures: Case of waste heat recovery in an offshore platform. Case Studies in Thermal Engineering, 8, 51–70. https://doi.org/10.1016/j.csite.2016.05.001

Kole, M., & Dey, T. K. (2010). Thermal conductivity and viscosity of Al2O3 nanofluid based on car engine coolant. Journal of Physics D: Applied Physics, 43(31), 315501. https://doi.org/10.1088/0022-3727/43/31/315501

Kruzel, M., Bohdal, T., Dutkowski, K., Kuczyński, W., & Chliszcz, K. (2022). Current Research Trends in the Process of Condensation of Cooling Zeotropic Mixtures in Compact Condensers. Energies, 15(6), 2241. https://doi.org/10.3390/en15062241

Kumar, R., Memon, A. G., Tariq, A. Bin, & Yousfani, F. M. (2021). Energy Analysis and Working Fluid Selection of Combined ORC-VCC Refrigeration System Operated by Low-Grade Thermal Energy Sources. International Conference on Electrical and Control Engineering. https://doi.org/10.1109/ICECE51984.2021.9406304

Larsen, U., Pierobon, L., Haglind, F., & Gabrielii, C. (2013). Design and optimisation of organic Rankine cycles for waste heat recovery in marine applications using the principles of natural selection. Energy, 55. https://doi.org/10.1016/j.energy.2013.03.021

Le, V. L., Kheiri, A., Feidt, M., & Pelloux-Prayer, S. (2014). Thermodynamic and economic optimizations of a waste heat to power plant driven by a subcritical ORC (Organic Rankine Cycle) using pure or zeotropic working fluid. Energy, 78, 622–638. https://doi.org/10.1016/j.energy.2014.10.051

Lecompte, S., Huisseune, H., van den Broek, M., Vanslambrouck, B., & De Paepe, M. (2015). Review of organic Rankine cycle (ORC) architectures for waste heat recovery. Renewable and Sustainable Energy Reviews, 47, 448–461. https://doi.org/10.1016/j.rser.2015.03.089

Lemmens, S. (2016). Cost engineering techniques & their applicability for cost estimation of organic rankine cycle systems. Energies, 9(7). https://doi.org/10.3390/en9070485

Lemort, V., Declaye, S., & Quoilin, S. (2012). Experimental characterization of a hermeti scroll expander for use in a micro-scale Rankine cycle. Proceedings of the Institution of Mechanical Engineers, Part A: Journal of Power and Energy, 226(1). https://doi.org/10.1177/0957650911413840

Lemort, V., Quoilin, S., Cuevas, C., & Lebrun, J. (2009). Testing and modeling a scroll expander integrated into an Organic Rankine Cycle. Applied Thermal Engineering, 29(14–15). https://doi.org/10.1016/j.applthermaleng.2009.04.013

Li, G. (2016). Organic Rankine cycle performance evaluation and thermoeconomic assessment with various applications part I: Energy and exergy performance evaluation. Renewable and Sustainable Energy Reviews, 53, 477–499. https://doi.org/10.1016/j.rser.2015.08.066

Li, J. F., Guo, H., Lei, B., Wu, Y. T., Ye, F., & Ma, C. F. (2021). An overview on subcritical organic rankine cycle configurations with pure organic fluids. International Journal of Energy Research, 45(9), 12536–12563. https://doi.org/10.1002/er.6653

Li, L., Tao, L. R., & Liu, Q. Q. (2020a). Experimental analysis of organic Rankine cycle power generation system with radial inflow turbine and R245fa. Advances in Mechanical Engineering, 12(5). https://doi.org/10.1177/1687814020921663

Li, M., Wang, J., He, W., Gao, L., Wang, B., Ma, S., & Dai, Y. (2013). Construction and preliminary test of a low-temperature regenerative Organic Rankine Cycle (ORC) using R123. Renewable Energy, 57. https://doi.org/10.1016/j.renene.2013.01.042

Li, Q., Cai, S., & Liu, C. (2020b). Molecular simulation of energy storage of R1234yf, R1234ze(z), R32, and their mixtures in Co-MOF-74 materials. Chinese Science Bulletin, 65(7), 633–640. https://doi.org/10.1360/TB-2019-0435

Li, X., Zhao, C., & Hu, X. (2012). Thermodynamic analysis of Organic Rankine Cycle with Ejector. Energy, 42(1). https://doi.org/10.1016/j.energy.2012.03.047

Li, Y.-R., Du, M.-T., Wu, C.-M., Wu, S.-Y., & Liu, C. (2014). Potential of organic Rankine cycle using zeotropic mixtures as working fluids for waste heat recovery. Energy, 77, 509–519. https://doi.org/10.1016/j.energy.2014.09.035

Liang, Y., & Yu, Z. (2021). Experimental investigation of an Organic Rankine cycle system using an oil-free scroll expander for low grade heat recovery. International Journal of Green Energy, 18(8), 812–821. https://doi.org/10.1080/15435075.2021.1880915

Linke, P., Papadopoulos, A. I., & Seferlis, P. (2015). Systematic methods for working fluid selection and the design, integration and control of organic Rankine cycles - A review. In Energies (Vol. 8, Number 6). https://doi.org/10.3390/en8064755

Liu, L., Zhu, T., Gao, N., & Gan, Z. (2018). A Review of Modeling Approaches and Tools for the Off-design Simulation of Organic Rankine Cycle. In Journal of Thermal Science (Vol. 27, Number 4). https://doi.org/10.1007/s11630-018-1023-2

Liu, L., Zhu, T., & Ma, J. (2017). Working fluid charge oriented off-design modeling of a small scale Organic Rankine Cycle system. Energy Conversion and

Management, 148, 944–953. https://doi.org/10.1016/j.enconman.2017.06.009

Liu, Z., Yang, X., Yang, X., Zhai, H., & Duan, Z. (2022). Performance Evaluation on the In-Cylinder Heat Transfer of a Reciprocating Compressor using CO2 as a Working Fluid. Journal of Thermal Science, 31(5), 1518–1530. https://doi.org/10.1007/S11630-022-1456-5/METRICS

Loni, R., Askari Asli-Ardeh, E., Ghobadian, B., Najafi, G., & Bellos, E. (2019a). Effects of size and volume fraction of alumina nanoparticles on the performance of a solar organic Rankine cycle. Energy Conversion and Management, 182, 398–411. https://doi.org/10.1016/j.enconman.2018.12.079

Loni, R., Najafi, G., Asli-Ardeh, E. A., Ghobadian, B., G. Le Roux, W., & Yusaf, T. (2019b). Performance Investigation of Solar ORC Using Different Nanofluids. Applied Sciences, 9(15), 3048. https://doi.org/10.3390/app9153048

Lopes, T., Fasquelle, T., & Silva, H. G. (2021). Pressure drops, heat transfer coefficient, costs and power block design for direct storage parabolic trough power plants running molten salts. Renewable Energy, 163, 530–543. https://doi.org/10.1016/j.renene.2020.07.110

Ma, Q., Huang, J., Gao, Z., Lu, H., Luo, H., Li, J., Wu, Z., & Feng, X. (2023). Performance Improvement of OTEC-ORC and Turbine Based on Binary Zeotropic Working Fluid. International Journal of Chemical Engineering, 2023, 1–13. https://doi.org/10.1155/2023/8892450

Mago, P. J., Srinivasan, K. K., Chamra, L. M., & Somayaji, C. (2008). An examination of exergy destruction in organic Rankine cycles. International Journal of Energy Research, 32(10), 926–938. https://doi.org/10.1002/er.1406

Mahbubul, I. M. (2019). Thermophysical Properties of Nanofluids. In Preparation, Characterization, Properties and Application of Nanofluid (pp. 113–196). Elsevier. https://doi.org/10.1016/B978-0-12-813245-6.00004-6

Mahmoudi, A., Fazli, M., & Morad, M. R. (2018). A recent review of waste heat recovery by Organic Rankine Cycle. Applied Thermal Engineering, 143, 660–675. https://doi.org/10.1016/j.applthermaleng.2018.07.136

Mana, A. A., Kaitouni, S. I., Kousksou, T., & Jamil, A. (2023). Enhancing sustainable energy conversion: Comparative study of superheated and recuperative ORC systems for waste heat recovery and geothermal applications, with focus on 4E performance. Energy, 284, 128654. https://doi.org/10.1016/J.ENERGY.2023.128654

Manente, G., Lazzaretto, A., & Bonamico, E. (2017). Design guidelines for the choice between single and dual pressure layouts in organic Rankine cycle (ORC) systems. Energy, 123. https://doi.org/10.1016/j.energy.2017.01.151

Manolakos, D., Kosmadakis, G., Kyritsis, S., & Papadakis, G. (2009). On site experimental evaluation of a low-temperature solar organic Rankine cycle system for RO desalination. Solar Energy, 83(5), 646–656. https://doi.org/10.1016/j.solener.2008.10.014

Manolakos, D., Papadakis, G., Kyritsis, S., & Bouzianas, K. (2007). Experimental evaluation of an autonomous low-temperature solar Rankine cycle system for reverse osmosis desalination. Desalination, 203(1–3). https://doi.org/10.1016/j.desal.2006.04.018

Mariani, A., Morrone, B., Laiso, D., Prati, M. V., & Unich, A. (2022). Waste Heat Recovery in a Compression Ignition Engine for Marine Application Using a Rankine Cycle Operating with an Innovative Organic Working Fluid. Energies, 15(21). https://doi.org/10.3390/en15217912

Matuszewska, D. (2024). Solar Organic Rankine Cycle (ORC) Systems: A Review of Technologies, Parameters, and Applications. Energies, 17(20), 5106. https://doi.org/10.3390/en17205106

Mazzi, N., Rech, S., & Lazzaretto, A. (2015). Off-design dynamic model of a real Organic Rankine Cycle system fuelled by exhaust gases from industrial processes. Energy, 90. https://doi.org/10.1016/j.energy.2015.07.083

McGrail, B. P., Thallapally, P. K., Blanchard, J., Nune, S. K., Jenks, J. J., & Dang, L. X. (2013). Metal-organic heat carrier nanofluids. Nano Energy, 2(5), 845–855. https://doi.org/10.1016/j.nanoen.2013.02.007

Meinel, D., Wieland, C., & Spliethoff, H. (2014). Effect and comparison of different working fluids on a two-stage organic rankine cycle (ORC) concept. Applied Thermal Engineering, 63(1). https://doi.org/10.1016/j.applthermaleng.2013.11.016

Miao, Z., Xu, J., Yang, X., & Zou, J. (2015). Operation and performance of a low temperature organic Rankine cycle. Applied Thermal Engineering, 75, 1065–1075. https://doi.org/10.1016/J.APPLTHERMALENG.2014.10.065

Minea, V. (2014). Power generation with ORC machines using low-grade waste heat or renewable energy. Applied Thermal Engineering, 69(1–2). https://doi.org/10.1016/j.applthermaleng.2014.04.054

Minor, B., Kontomaris, K. (Kostas), & Hydutsky, B. (2014). Nonflammable Low GWP Working Fluid for Organic Rankine Cycles. Volume 3B: Oil and Gas Applications; Organic Rankine Cycle Power Systems; Supercritical CO2 Power Cycles; Wind Energy, 3B. https://doi.org/10.1115/GT2014-26855

Mondejar, M. E., Andreasen, J. G., Regidor, M., Riva, S., Kontogeorgis, G., Persico, G., & Haglind, F. (2017). Prospects of the use of nanofluids as working fluids for organic Rankine cycle power systems. Energy Procedia, 129, 160–167. https://doi.org/10.1016/j.egypro.2017.09.098

Mondejar, M. E., & Thern, M. (2017). Analysis of isentropic mixtures for their use as working fluids in organic Rankine cycles. Environmental Progress & Sustainable Energy, 36(3), 921–935. https://doi.org/10.1002/ep.12520

Muhammad, U., Imran, M., Lee, D. H., & Park, B. S. (2015). Design and experimental investigation of a 1 kW organic Rankine cycle system using R245fa as working fluid for low-grade waste heat recovery from steam. Energy Conversion and Management, 103, 1089–1100. https://doi.org/10.1016/J.ENCONMAN.2015.07.045

Muratori, M., Ledna, C., McJeon, H., Kyle, P., Patel, P., Kim, S. H., Wise, M., Kheshgi, H. S., Clarke, L. E., & Edmonds, J. (2017). Cost of power or power of cost: A U.S. modeling perspective. Renewable and Sustainable Energy Reviews, 77, 861–874. https://doi.org/10.1016/j.rser.2017.04.055

Nguyen, V. M., Doherty, P. S., & Riffat, S. B. (2001). Development of a prototype low-temperature Rankine cycle electricity generation system. Applied Thermal Engineering, 21(2). https://doi.org/10.1016/S1359-4311(00)00052-1

Nondy, J., & Gogoi, T. K. (2021). Exergoeconomic investigation and multi-objective optimization of different ORC configurations for waste heat recovery: A comparative study. Energy Conversion and Management, 245, 114593. https://doi.org/10.1016/J.ENCONMAN.2021.114593

Omosehin, O. S., Adelaja, A. O., Olakoyejo, O. T., & Oyekeye, M. O. (2022). Numerical study of the thermal performance and pressure drops of water-based Al2O3 - Cu hybrid nanofluids of different compositions in a microchannel heat sink. Microfluidics and Nanofluidics, 26(7), 1–13. https://doi.org/10.1007/S10404-022-02550-2/METRICS

Oyewunmi, O., & Markides, C. (2016). Thermo-Economic and Heat Transfer Optimization of Working-Fluid Mixtures in a Low-Temperature Organic Rankine Cycle System. Energies, 9(6), 448. https://doi.org/10.3390/en9060448

Pambudi, N. A., Wibowo, S., Ranto, & Saw, L. H. (2021). Experimental Investigation of Organic Rankine Cycle (ORC) for Low Temperature Geothermal Fluid: Effect of Pump Rotation and R-134 Working Fluid in Scroll-Expander. Energy Engineering, 118(5), 1565–1576. https://doi.org/10.32604/EE.2021.016642

Papadopoulos, A. I., Stijepovic, M., & Linke, P. (2010). On the systematic design and selection of optimal working fluids for Organic Rankine Cycles. Applied Thermal Engineering, 30(6–7), 760–769. https://doi.org/10.1016/j.applthermaleng.2009.12.006

Pei, G., Li, J., & Ji, J. (2010). Analysis of low temperature solar thermal electric generation using regenerative Organic Rankine Cycle. Applied Thermal Engineering, 30(8–9). https://doi.org/10.1016/j.applthermaleng.2010.01.011

Pei, G., Li, J., Li, Y., Wang, D., & Ji, J. (2011). Construction and dynamic test of a small-scale organic rankine cycle. Energy, 36(5). https://doi.org/10.1016/j.energy.2011.03.010

Peris, B., Navarro-Esbrí, J., & Molés, F. (2013). Bottoming organic Rankine cycle configurations to increase Internal Combustion Engines power output from cooling water waste heat recovery. Applied Thermal Engineering, 61(2). https://doi.org/10.1016/j.applthermaleng.2013.08.016

Peterson, R. B., Wang, H., & Herron, T. (2008). Performance of a small-scale regenerative Rankine power cycle employing a scroll expander. Proceedings of the Institution of Mechanical Engineers, Part A: Journal of Power and Energy, 222(3). https://doi.org/10.1243/09576509JPE546

Pikra, G., Rohmah, N., Pramana, R. I., & Purwanto, A. J. (2020). Open feed organic heater pressure analysis on single-stage regenerative organic Rankine cycle performance. Journal of Mechatronics, Electrical Power, and Vehicular Technology, 11(1), 30–37. https://doi.org/10.14203/J.MEV.2020.V11.30-37

Pourahmad, S., Pesteei, S. M., & Mehrabi, M. (2018). The effect of geometrical characteristics of wavy strip turbulator and thermodynamic properties of fluid on exergy loss and heat transfer in a tube in tube heat exchanger. Experimental Heat Transfer, 32(4), 393–409. https://doi.org/10.1080/08916152.2018.1526229

Prajapati, P. P., & Patel, V. K. (2019). Comparative analysis of nanofluid-based Organic Rankine Cycle through thermoeconomic optimization. Heat Transfer—Asian Research, 48(7), 3013–3038. https://doi.org/10.1002/HTJ.21528

Prajapati, P. P., & Patel, V. K. (2020). Thermo-economic optimization of a nanofluid based organic Rankine cycle: A multi-objective study and analysis. Thermal Science and Engineering Progress, 17, 100381. https://doi.org/10.1016/j.tsep.2019.100381

Pu, W., Yue, C., Han, D., He, W., Liu, X., Zhang, Q., & Chen, Y. (2016). Experimental study on Organic Rankine cycle for low grade thermal energy recovery. Applied Thermal Engineering, 94, 221–227. https://doi.org/10.1016/j.applthermaleng.2015.09.120

Qiu, G., Shao, Y., Li, J., Liu, H., & Riffat, S. . B. (2012). Experimental investigation of a biomass-fired ORC-based micro-CHP for domestic applications. Fuel, 96, 374–382. https://doi.org/10.1016/j.fuel.2012.01.028

Quaschning, V. (2014). Understanding Renewable Energy Systems. In Understanding Renewable Energy Systems. Routledge. https://doi.org/10.4324/9781315800493

Quoilin, S., Broek, M. Van Den, Declaye, S., Dewallef, P., & Lemort, V. (2013). Techno-economic survey of organic rankine cycle (ORC) systems. In Renewable and Sustainable Energy Reviews. https://doi.org/10.1016/j.rser.2013.01.028

Quoilin, S., Lemort, V., & Lebrun, J. (2010). Experimental study and modeling of an Organic Rankine Cycle using scroll expander. Applied Energy, 87(4), 1260–1268. https://doi.org/10.1016/j.apenergy.2009.06.026

Quoilin, S., Orosz, M., Hemond, H., & Lemort, V. (2011). Performance and design optimization of a low-cost solar organic Rankine cycle for remote power generation. Solar Energy. https://doi.org/10.1016/j.solener.2011.02.010

Rahbar, K., Mahmoud, S., Al-Dadah, R. K., Moazami, N., & Mirhadizadeh, S. A. (2017). Review of organic Rankine cycle for small-scale applications. Energy Conversion and Management, 134, 135–155. https://doi.org/10.1016/j.enconman.2016.12.023

Rahman, M. A., Hasnain, S. M. M., Pandey, S., Tapalova, A., Akylbekov, N., & Zairov, R. (2024). Review on Nanofluids: Preparation, Properties, Stability, and Thermal Performance Augmentation in Heat Transfer Applications. ACS Omega. https://doi.org/10.1021/acsomega.4c03279

Rak, J., Błasiak, P., & Kolasiński, P. (2018). Influence of the Applied Working Fluid and the Arrangement of the Steering Edges on Multi-Vane Expander Performance in Micro ORC System. Energies, 11(4). https://doi.org/10.3390/EN11040892

Rashwan, S. S., Dincer, I., & Mohany, A. (2019). Analysis and assessment of cascaded closed loop type organic Rankine cycle. Energy Conversion and Management, 184. https://doi.org/10.1016/j.enconman.2018.12.089

REN21. (2020). Renewables 2020 Global Status Report. REN21 Secretariat.

Röder, M., Chong, K., & Thornley, P. (2022). The future of residue-based bioenergy for industrial use in Sub-Saharan Africa. Biomass and Bioenergy, 159, 106385. https://doi.org/10.1016/J.BIOMBIOE.2022.106385

Rostamnejad, H., & Zare, V. (2019). Performance improvement of ejector expansion refrigeration cycles employing a booster compressor using different refrigerants: Thermodynamic analysis and optimization. International Journal of Refrigeration, 101, 56–70. https://doi.org/10.1016/j.ijrefrig.2019.02.031

Saadatfar, B., Fakhrai, R., & Fransson, T. (2014). Conceptual Modeling of Nano Fluid ORC for Solar Thermal Polygeneration. Energy Procedia, 57, 2696–2705. https://doi.org/10.1016/j.egypro.2014.10.301

Safarian, S., & Aramoun, F. (2015). Energy and exergy assessments of modified Organic Rankine Cycles (ORCs). Energy Reports, 1. https://doi.org/10.1016/j.egyr.2014.10.003

Said, Z., Sabiha, M. A., Saidur, R., Hepbasli, A., Rahim, N. A., Mekhilef, S., & Ward, T. A. (2015). Performance enhancement of a Flat Plate Solar collector using

Titanium dioxide nanofluid and Polyethylene Glycol dispersant. Journal of Cleaner Production, 92, 343–353. https://doi.org/10.1016/J.JCLEPRO.2015.01.007

Said, Z., & Saidur, R. (2017). Thermophysical Properties of Metal Oxides Nanofluids. In Nanofluid Heat and Mass Transfer in Engineering Problems. InTech. https://doi.org/10.5772/65610

Said, Z., Saidur, R., & Rahim, N. A. (2016). Energy and exergy analysis of a flat plate solar collector using different sizes of aluminium oxide based nanofluid. Journal of Cleaner Production, 133. https://doi.org/10.1016/j.jclepro.2016.05.178

Saitoh, T., Yamada, N., & Wakashima, S. (2007). Solar Rankine Cycle System Using Scroll Expander. Journal of Environment and Engineering, 2(4). https://doi.org/10.1299/jee.2.708

Saleh, B., Koglbauer, G., Wendland, M., & Fischer, J. (2007). Working fluids for low-temperature organic Rankine cycles. Energy, 32(7), 1210–1221. https://doi.org/10.1016/j.energy.2006.07.001

Sami, S. (2020). Analysis of Nanofluids Behavior in a PV-Thermal-Driven Organic Rankine Cycle with Cooling Capability. Applied System Innovation, 3(1), 12. https://doi.org/10.3390/asi3010012

Shaligram, A. (2016). Improving Efficiency of ORC Power Generation. Tech Briefs Media Group. https://contest.techbriefs.com/2016/entries/sustainable-technologies/6990

Shao, L., Zhu, J., Meng, X., Wei, X., & Ma, X. (2017). Experimental study of an organic Rankine cycle system with radial inflow turbine and R123. Applied Thermal Engineering, 124, 940–947. https://doi.org/10.1016/j.applthermaleng.2017.06.042

Shi, L., Shu, G., Tian, H., & Deng, S. (2018). A review of modified Organic Rankine cycles (ORCs) for internal combustion engine waste heat recovery (ICE-WHR). Renewable and Sustainable Energy Reviews, 92, 95–110. https://doi.org/10.1016/j.rser.2018.04.023

Siddiqui, M. E., Almatrafi, E., & Saeed, U. (2023). Performance Analysis of Organic Rankine Cycle with Internal Heat Regeneration: Comparative Study of Binary Mixtures and Pure Constituents in Warm Regions. Processes, 11(8), 2267.

https://doi.org/10.3390/pr11082267
Sundar, L. S., Sharma, K. V., Naik, M. T., & Singh, M. K. (2013). Empirical and theoretical correlations on viscosity of nanofluids: A review. In Renewable and Sustainable Energy Reviews (Vol. 25). https://doi.org/10.1016/j.rser.2013.04.003

Sung, T., Yun, E., Kim, H. D., Yoon, S. Y., Choi, B. S., Kim, K., Kim, J., Jung, Y. B., & Kim, K. C. (2016). Performance characteristics of a 200-kW organic Rankine cycle system in a steel processing plant. Applied Energy, 183, 623–635. https://doi.org/10.1016/j.apenergy.2016.09.018

Tchanche, B. F., Pétrissans, M., & Papadakis, G. (2014). Heat resources and organic Rankine cycle machines. Renewable and Sustainable Energy Reviews, 39, 1185–1199. https://doi.org/10.1016/j.rser.2014.07.139

Tocci, L., Pal, T., Pesmazoglou, I., & Franchetti, B. (2017). Small Scale Organic Rankine Cycle (ORC): A Techno-Economic Review. Energies, 10(4), 413. https://doi.org/10.3390/en10040413

Topuz, A., Erdogan, B., & Aycan, O. (2021). Determination and measurement of some thermophysical properties of nanofluids and comparison with literature studies. Thermal Science, 25(5 Part A), 3579–3594. https://doi.org/10.2298/TSCI200704239T

Twomey, B., Jacobs, P. A., & Gurgenci, H. (2013). Dynamic performance estimation of small-scale solar cogeneration with an organic Rankine cycle using a scroll expander. Applied Thermal Engineering, 51(1–2), 1307–1316. https://doi.org/10.1016/J.APPLTHERMALENG.2012.06.054

Uusitalo, A., Honkatukia, J., Turunen-Saaresti, T., & Larjola, J. (2014). A thermodynamic analysis of waste heat recovery from reciprocating engine power plants by means of Organic Rankine Cycles. Applied Thermal Engineering, 70(1). https://doi.org/10.1016/j.applthermaleng.2014.04.073

Vallis, A. G., Zannis, T. C., Yfantis, E. A., Pariotis, E. G., Katsanis, J. S., & Asimakopoulou, K. D. (2020). Thermo-Economic Study of a Regenerative Dual-Loop ORC System Coupled to the Main Diesel Engines of a General Support Vessel. Energies, 13(11), 2991. https://doi.org/10.3390/en13112991

Vélez, F., Segovia, J. J., Martín, M. C., Antolín, G., Chejne, F., & Quijano, A. (2012). A technical, economical and market review of organic Rankine cycles for the conversion of low-grade heat for power generation. Renewable and Sustainable Energy Reviews, 16(6), 4175–4189. https://doi.org/https://doi.org/10.1016/j.rser.2012.03.022

Vicencio, R. B., & Aedo, E. C. (2017). A numerical model for boiling heat transfer coefficient of zeotropic mixtures. IOP Conference Series: Materials Science and Engineering, 278(1). https://doi.org/10.1088/1757-899X/278/1/012062

Vidhi, R., Kuravi, S., Yogi Goswami, D., Stefanakos, E., & Sabau, A. S. (2013). Organic fluids in a supercritical rankine cycle for low temperature power generation. Journal of Energy Resources Technology, Transactions of the ASME, 135(4). https://doi.org/10.1115/1.4023513/372207

Wang, E. H., Zhang, H. G., Fan, B. Y., Ouyang, M. G., Zhao, Y., & Mu, Q. H. (2011a). Study of working fluid selection of organic Rankine cycle (ORC) for engine waste heat recovery. Energy, 36(5), 3406–3418. https://doi.org/10.1016/j.energy.2011.03.041

Wang, E., & Peng, N. (2023). A Review on the Preliminary Design of Axial and Radial Turbines for Small-Scale Organic Rankine Cycle. Energies, 16(8), 3423. https://doi.org/10.3390/en16083423

Wang, E., Zhang, H., Fan, B., & Wu, Y. (2012). Optimized performances comparison of organic Rankine cycles for low grade waste heat recovery. Journal of Mechanical Science and Technology, 26(8), 2301–2312. https://doi.org/10.1007/s12206-012-0603-4

Wang, H., Peterson, R. B., & Herron, T. (2009). Experimental performance of a compliant scroll expander for an organic Rankine cycle. Proceedings of the Institution of Mechanical Engineers, Part A: Journal of Power and Energy, 223(7). https://doi.org/10.1243/09576509JPE741

Wang, J., Xu, P., Li, T., & Zhu, J. (2017). Performance enhancement of organic Rankine cycle with two-stage evaporation using energy and exergy analyses. Geothermics, 65, 126–134. https://doi.org/10.1016/J.GEOTHERMICS.2016.09.005

Wang, R., Kuang, G., Zhu, L., Wang, S., & Zhao, J. (2019). Experimental Investigation of a 300 kW Organic Rankine Cycle Unit with Radial Turbine for Low-Grade Waste Heat Recovery. Entropy 2019, Vol. 21, Page 619, 21(6), 619. https://doi.org/10.3390/E21060619

Wang, T., Zhang, Y., Peng, Z., & Shu, G. (2011b). A review of researches on thermal exhaust heat recovery with Rankine cycle. Renewable and Sustainable Energy Reviews, 15(6), 2862–2871. https://doi.org/10.1016/j.rser.2011.03.015

Wang, W., Deng, S., Zhao, D., Zhao, L., Lin, S., & Chen, M. (2020). Application of machine learning into organic Rankine cycle for prediction and optimization of thermal and exergy efficiency. Energy Conversion and Management, 210. https://doi.org/10.1016/j.enconman.2020.112700

Wang, W., Wu, Y. T., Ma, C. F., Liu, L. D., & Yu, J. (2011c). Preliminary experimental study of single screw expander prototype. Applied Thermal Engineering, 31(17–18), 3684–3688. https://doi.org/10.1016/J.APPLTHERMALENG.2011.01.019

Wang, Z., Zhao, Y., Xia, X., Pan, H., Zhang, S., & Liu, Z. (2023). Experimental evaluation of organic Rankine cycle using zeotropic mixture under different operation conditions. Energy, 264, 126188. https://doi.org/10.1016/j.energy.2022.126188

Wei, L., Ma, Z., Gong, X., & Guo, X. (2019). Experimental investigation and performance analysis of an Organic Rankine Cycle for low-temperature heat to electricity generation. International Journal of Low-Carbon Technologies, 14(4), 500–507. https://doi.org/10.1093/IJLCT/CTZ037

Weiß, A. P., Novotný, V., Popp, T., Streit, P., Špale, J., Zinn, G., & Kolovratník, M. (2020). Customized ORC micro turbo-expanders - From 1D design to modular construction kit and prospects of additive manufacturing. Energy, 209, 118407. https://doi.org/10.1016/J.ENERGY.2020.118407

Weng, R., Bory, D., & Berthou, M. (2013). A method to evaluate the waste heat recovery potential across the industrial sectors. Proceedings of the 26th International Conference on Efficiency, Cost, Optimization, Simulation and Environmental Impact of Energy Systems, ECOS 2013. France

Wu, Y., Zhu, Y., & Yu, L. (2016). Thermal and economic performance analysis of zeotropic mixtures for Organic Rankine Cycles. Applied Thermal Engineering, 96, 57–63. https://doi.org/10.1016/J.APPLTHERMALENG.2015.11.083

Xu, R. J., & He, Y. L. (2011). A vapor injector-based novel regenerative organic

Rankine cycle. Applied Thermal Engineering, 31(6–7). https://doi.org/10.1016/j.applthermaleng.2010.12.026

Xu, W., Zhao, R., Deng, S., Zhao, L., & Mao, S. S. (2021). Is zeotropic working fluid a promising option for organic Rankine cycle: A quantitative evaluation based on literature data. Renewable and Sustainable Energy Reviews, 148, 111267. https://doi.org/10.1016/j.rser.2021.111267

Yagoub, W., Doherty, P., & Riffat, S. B. (2006). Solar energy-gas driven micro-CHP system for an office building. Applied Thermal Engineering, 26(14–15). https://doi.org/10.1016/j.applthermaleng.2005.11.021

Yamamoto, T., Furuhata, T., Arai, N., & Mori, K. (2001). Design and testing of the organic rankine cycle. Energy, 26(3). https://doi.org/10.1016/S0360-5442(00)00063-3

Yang, F. Bin, Yang, F. F., Li, J., Hu, S. Z., Yang, Z., & Duan, Y. Y. (2021). Analysis of the thermodynamic performance limits of the organic Rankine cycle in low and medium temperature heat source applications. Science China Technological Sciences, 64(8), 1624–1640. https://doi.org/10.1007/S11431-020-1787-6/METRICS

Yang, F., Dong, X., Zhang, H., Wang, Z., Yang, K., Zhang, J., Wang, E., Liu, H., & Zhao, G. (2014). Performance analysis of waste heat recovery with a dual loop organic Rankine cycle (ORC) system for diesel engine under various operating conditions. Energy Conversion and Management, 80. https://doi.org/10.1016/j.enconman.2014.01.036

Yu, W., & Xie, H. (2012). A Review on Nanofluids: Preparation, Stability Mechanisms, and Applications. Journal of Nanomaterials, 2012(1), 435873. https://doi.org/10.1155/2012/435873

Yun, E., Kim, D., Yoon, S. Y., & Kim, K. C. (2015). Experimental investigation of an organic Rankine cycle with multiple expanders used in parallel. Applied Energy, 145, 246–254. https://doi.org/10.1016/j.apenergy.2015.02.022

Zanelli, R., & Favrat, D. (1994). Experimental investigation of a hermetic scroll expander-generator. 12th International Compressor Engineering Conference at Purdue.

Zhai, H., An, Q., Shi, L., Lemort, V., & Quoilin, S. (2016). Categorization and analysis of heat sources for organic Rankine cycle systems. Renewable and

Sustainable Energy Reviews, 64, 790–805. https://doi.org/10.1016/j.rser.2016.06.076

Zhang, B., Peng, X., He, Z., Xing, Z., & Shu, P. (2007). Development of a double acting free piston expander for power recovery in transcritical CO2 cycle. Applied Thermal Engineering, 27(8–9). https://doi.org/10.1016/j.applthermaleng.2006.05.034

Zhang, J., Zhang, W., Hou, G., & Fang, F. (2012). Dynamic modeling and multivariable control of organic Rankine cycles in waste heat utilizing processes. Computers and Mathematics with Applications, 64(5). https://doi.org/10.1016/j.camwa.2012.01.054

Zhang, X., Zhang, C., He, M., & Wang, J. (2019). Selection and Evaluation of Dry and Isentropic Organic Working Fluids Used in Organic Rankine Cycle Based on the Turning Point on Their Saturated Vapor Curves. Journal of Thermal Science, 28(4). https://doi.org/10.1007/s11630-019-1149-x

Zhang, X., Zhang, Y., Li, Z., Wang, J., Wu, Y., & Ma, C. (2020). Zeotropic Mixture Selection for an Organic Rankine Cycle Using a Single Screw Expander. Energies, 13(5), 1022. https://doi.org/10.3390/en13051022

Zhao, D., Deng, S., Zhao, L., Xu, W., Wang, W., Nie, X., & Chen, M. (2020a). Overview on artificial intelligence in design of Organic Rankine Cycle. Energy and AI, 1, 100011. https://doi.org/10.1016/j.egyai.2020.100011

Zhao, P., Wang, D., Zhou, D., Zhang, H., & Sun, Y. (2020b). Thermal Analysis of the Transcritical Organic Rankine Cycle Using R1234ze(E)/ R134a Mixtures as Working Fluids. Energy Engineering, 117(4), 209–224. https://doi.org/10.32604/EE.2020.010567

Zheng, N., Zhao, L., Wang, X. D., & Tan, Y. T. (2013). Experimental verification of a rolling-piston expander that applied for low-temperature Organic Rankine Cycle. Applied Energy, 112. https://doi.org/10.1016/j.apenergy.2012.12.030

Zhou, Y., Ruan, J., Hong, G., & Miao, Z. (2022). Multi-Objective Optimization of the Basic and Regenerative ORC Integrated with Working Fluid Selection. Entropy, 24(7). https://doi.org/10.3390/E24070902

Zhu, Q., Sun, Z., & Zhou, J. (2015). Performance analysis of organic rankine cycles using different working fluids. Thermal Science. https://doi.org/10.2298/TSCI120318014Z

Ziviani, D., James, N. A., Accorsi, F. A., Braun, J. E., & Groll, E. A. (2018). Experimental and numerical analyses of a 5 kWe oil-free open-drive scroll expander for small-scale organic Rankine cycle (ORC) applications. Applied Energy, 230, 1140–1156. https://doi.org/10.1016/j.apenergy.2018.09.025

Appendices

Appendix A – Simulation Parameters and Input Data

This appendix provides the complete set of simulation inputs and assumptions used to model the hybrid solar–biomass ORC system in ASPEN Plus V14. The details cover boundary conditions, component assumptions, module settings, property adjustments for nanofluids, and heat source management strategies.

A1. Boundary Conditions

Parameter	Value(s)	Remarks
Evaporator inlet temperature	140, 160, 180, 200 °C	Buffer outlet setpoints
Evaporator pressure	800 kPa (Set 1); 3.1–3.5 MPa (Set 2)	Adjusted for critical pressures
Condenser temperature	25 °C	Ambient air-cooled
Condenser pressure	200 kPa (Set 1); per Pc for Set 2	Cycle closing condition
HTF flow rate	0.05 kg/s and 0.1 kg/s	Solar loop flow rates

A2. Component Assumptions

Pump isentropic efficiency: default ASPEN thermodynamic calculation

Turbine isentropic efficiency: default ASPEN thermodynamic calculation

Pressure drops in pipes/heat exchangers: neglected

Evaporator and condenser: HXFlux module (counterflow)

Module Settings

Property method: Peng–Robinson EOS (PEOS)

Convergence criteria: tolerance 1e-6; max iterations = 200

Solver: Wegstein acceleration enabled

Nanofluid Property Adjustments

Nanoparticle-enhanced fluid properties were calculated using the following relations:

- Density:

$$\rho_{\text{nf}} = (1-\phi)\rho_f + \phi\rho_p$$

- Specific heat capacity:

$$c_{p,\text{nf}} = (1-\phi)c_{p,f} + \phi c_{p,p}$$

- Thermal conductivity (Maxwell relation):

$$k_{\text{nf}} = k_f \cdot \left(\frac{k_p + 2k_f - 2\phi(k_f - k_p)}{k_p + 2k_f + \phi(k_f - k_p)}\right)$$

- Viscosity (Brinkman model):

$$\mu_{\text{nf}} = \frac{\mu_f}{(1-\phi)^{2.5}}$$

Where:

- ϕ= nanoparticle volume fraction
- Subscripts $f$and $p$refer to base fluid and particle respectively

Heat Source Management

Solar energy prioritized; biomass engaged if buffer outlet < setpoint – 3 °C

Biomass efficiency: 80–85%

Fuel LHV: 15–18 MJ/kg

Appendix B – Thermophysical Properties of Working Fluids

This appendix summarizes the thermophysical and environmental properties of the working fluids and nanoparticles evaluated.

Zeotropic Mixtures – Set 1

Fluid	Tc (°C)	Pc (MPa)	GWP / ODP	Notes
R245fa	154.0	3.65	1030 / 0	Widely used in ORC studies; relatively high GWP
R1233zd(E)	165.6	3.63	~7 / 0	Low-GWP HFO; ASHRAE A1 classification
R123	183.7	3.67	77 / 0.012	Transitional refrigerant; phased out under the Montreal Protocol due to ODP

Zeotropic Mixtures – Set 2

Mixture	Tc (°C)	Pc (MPa)	GWP / ODP	Notes
R1224yd(Z)	153.7	3.62	~1/0	Low-GWP HFO; zero ODP; suitable for medium-T ORC
R1336mzz(Z)	171.3	2.90	~2/0	Very low GWP; high Tc; candidate for high-T ORC
R1233zd(E)	165.6	3.63	~7/0	Low GWP, zero ODP; ASHRAE A1 classification, stable

Nanoparticle Properties

Nanoparticle	k (W/m·K)	ρ (kg/m³)	cp (J/kg·K)
Ag	429	10,500	235
Al_2O_3	36	3970	765
CuO	20	6320	535
TiO_2	8.4	4230	692
ZnO	23	5600	495

Appendix C – Governing Equations and Derivations

This appendix presents the fundamental thermodynamic equations and derivations used in modeling the hybrid ORC systems described in Chapters 3 and 4. The equations underpin the simulation framework developed in Aspen Plus and support the performance analysis of zeotropic mixtures and nanoparticle-enhanced fluids.

Energy Balance Equations

Pump Work:

$$W_{\text{pump}} = \frac{v \cdot \Delta P}{\eta_{\text{pump}}}$$

Where:

v= specific volume of the working fluid

ΔP= pressure rise across the pump

η_{pump}= isentropic efficiency of the pump

Turbine Work:

$$W_{\text{turbine}} = \eta_{\text{turbine}} \cdot (h_{\text{in}} - h_{\text{out}})$$

Where:

$h_{\text{in}}, h_{\text{out}}$= specific enthalpies at turbine inlet and outlet

η_{turbine}= isentropic efficiency of the turbine

Net Work Output:

$$W_{\text{net}} = W_{\text{turbine}} - W_{\text{pump}}$$

Heat Input and Rejection:

$$Q_{\text{in}} = h_{\text{evap,out}} - h_{\text{evap,in}}; Q_{\text{out}} = h_{\text{cond,out}} - h_{\text{cond,in}}$$

Efficiency Metrics

Thermal Efficiency:

$$\eta = \frac{W_{\text{net}}}{Q_{\text{in}}}$$

Exergy Efficiency:

$$\eta_{\text{ex}} = \frac{W_{\text{net}}}{Q_{\text{in}} \cdot (1 - \frac{T_0}{T_{\text{source}}})}$$

Where:

T_0= ambient temperature

T_{source}= heat source temperature

Heat Transfer and Fluid Property Equations

Heat Transfer Rate:

$$Q = \dot{m} \cdot c_p \cdot \Delta T$$

Where:

$\dot{m}$= mass flow rate

c_p= specific heat capacity

ΔT= temperature difference across the heat exchanger

Nanofluid Property Adjustments:

Effective properties for nanoparticle-enhanced fluids were calculated using empirical correlations:

Effective Thermal Conductivity (Maxwell model):

$$k_{\text{eff}} = k_f \cdot (\frac{k_p + 2k_f - 2\phi(k_f - k_p)}{k_p + 2k_f + \phi(k_f - k_p)})$$

Effective Viscosity (Brinkman model):

$$\mu_{\text{eff}} = \mu_f \cdot (1 - \phi)^{-2.5}$$

Where:

k_f, μ_f= thermal conductivity and viscosity of base fluid

k_p= thermal conductivity of nanoparticle

ϕ= nanoparticle volume fraction

Equation of State (EOS) Modifications

The Peng–Robinson EOS was used to model fluid behaviour, with adjustments for nanofluid mixtures:

$$P = \frac{RT}{V - b} - \frac{a(T)}{V^2 + 2bV - b^2}$$

Where:

$a(T)$and $b$are fluid-specific parameters

Nanoparticle effects were incorporated by modifying $a(T)$based on effective heat capacity and dispersion stability.

Appendix D – Supplementary Results

This appendix presents additional simulation outputs, performance graphs, and sensitivity analyses that support the findings discussed in Chapters 3 and 4. These results offer deeper insight into system behaviour across varying fluid compositions, nanoparticle concentrations, and heat source conditions.

Mixture Set 1 Results Table

	R245fa/R123 (200 oC)											**Al2O3**					**CuO**					**Ag**				
	100/0	**90/10**	**80/20**	**70/30**	**60/40**	**50/50**	**40/60**	**30/70**	**20/80**	**10/90**	**0/100**	**0.01**	**0.001**	**0.0001**	**0.00001**	**0.000001**	**0.01**	**0.001**	**0.0001**	**0.00001**	**0.000001**	**0.01**	**0.001**	**0.0001**	**0.00001**	**0.000001**
W_tur	37.64	37.12	36.59	36.07	35.54	35.02	34.49	33.96	33.42	32.89	32.35	33.13	33.46	33.42	33.42	33.42	33.09	33.39	33.35	33.43	33.42	33.11	33.39	33.12	33.40	33.42
W_pump	0.46	0.45	0.45	0.45	0.44	0.44	0.44	0.43	0.43	0.43	0.43	0.47	0.44	0.43	0.43	0.43	0.44	0.43	0.43	0.43	0.43	0.43	0.43	0.43	0.43	0.43
Q_in	354.15	346.60	339.02	331.41	323.76	316.06	308.31	300.51	292.63	284.68	276.63	295.95	292.98	292.67	292.63	292.63	292.00	292.57	292.62	292.64	292.63	255.29	288.88	292.26	292.59	292.63
Q_out	316.97	309.94	302.88	295.79	288.66	281.48	274.26	266.98	259.64	252.22	244.70	263.29	259.96	259.68	259.64	259.64	259.34	259.61	259.70	259.65	259.65	222.62	255.92	259.57	259.63	259.64
W_net	37.18	36.66	36.14	35.62	35.10	34.58	34.05	33.52	32.99	32.46	31.93	32.66	33.03	32.99	32.99	32.99	32.65	32.96	32.92	32.99	32.99	32.68	32.96	32.69	32.96	32.99
Eff	10.50%	10.58%	10.66%	10.75%	10.84%	10.94%	11.04%	11.16%	11.27%	11.40%	11.54%	11.04%	11.27%	11.27%	11.27%	11.27%	11.18%	11.27%	11.25%	11.27%	11.27%	12.80%	11.41%	11.18%	11.27%	11.27%
	R245fa/R123 (150 oC)											**Al2O3**					**CuO**					**Ag**				
	100/0	**90/10**	**80/20**	**70/30**	**60/40**	**50/50**	**40/60**	**30/70**	**20/80**	**10/90**	**0/100**	**0.01**	**0.001**	**0.0001**	**0.00001**	**0.000001**	**0.01**	**0.001**	**0.0001**	**0.00001**	**0.000001**	**0.01**	**0.001**	**0.0001**	**0.00001**	**0.000001**
W_t	32.8	32.4	31.9	31.4	31.0	30.5	30.0	29.5	29.1	28.6	28.1	28.8	29.0	29.0	29.1	29.11	28.7	29.1	29.1	29.1	29.11	28.8	29.0	29.1	29.0	29.11

ur	8	1	4	7	0	3	6	8	1	3	5	5	9	9	1		9	2	1	1		3	8	1	8	
W_pump	0.46	0.45	0.45	0.45	0.44	0.44	0.44	0.43	0.43	0.43	0.43	0.47	0.44	0.44	0.43	0.43	0.44	0.43	0.43	0.43	0.43	0.43	0.43	0.43	0.43	0.43
Q_in	296.10	290.05	283.97	277.86	271.70	265.51	259.26	252.95	246.57	240.11	233.56	249.72	246.91	246.91	246.58	246.57	245.75	246.49	246.56	246.57	246.57	209.34	242.84	246.20	246.53	246.57
Q_out	263.68	258.09	252.48	246.83	241.14	235.41	229.64	223.80	217.90	211.91	205.84	221.34	218.25	218.25	217.90	217.90	217.40	217.80	217.88	217.89	217.89	180.93	214.19	217.52	217.89	217.90
W_net	32.42	31.96	31.49	31.03	30.56	30.09	29.62	29.15	28.68	28.20	27.72	28.38	28.66	28.66	28.68	28.68	28.35	28.69	28.68	28.68	28.68	28.40	28.65	28.67	28.64	28.67
Eff	10.95%	11.02%	11.09%	11.17%	11.25%	11.33%	11.43%	11.52%	11.63%	11.74%	11.87%	11.37%	11.61%	11.61%	11.63%	11.63%	11.54%	11.64%	11.63%	11.63%	11.63%	13.57%	11.80%	11.65%	11.62%	11.63%
	R245fa/R123 (120 oC)											**Al2O3**					**CuO**					**Ag**				
	100/0	**90/10**	**80/20**	**70/30**	**60/40**	**50/50**	**40/60**	**30/70**	**20/80**	**10/90**	**0/100**	**0.01**	**0.001**	**0.0001**	**0.00001**	**0.000001**	**0.01**	**0.001**	**0.0001**	**0.00001**	**0.000001**	**0.01**	**0.001**	**0.0001**	**0.00001**	**0.000001**
W_tur	29.91	29.48	29.04	28.61	28.17	27.73	27.29	26.85	26.41	25.96	25.51	26.16	26.39	26.46	26.41	26.41	26.05	26.39	26.44	26.41	26.41	26.16	26.38	26.40	26.41	26.41
W_pump	0.46	0.45	0.45	0.45	0.44	0.44	0.44	0.43	0.43	0.43	0.43	0.47	0.44	0.43	0.43	0.43	0.44	0.43	0.43	0.43	0.43	0.43	0.43	0.43	0.43	0.43
Q_in	262.91	257.68	252.41	247.11	241.77	236.38	230.94	225.44	219.88	214.23	208.49	222.80	220.19	219.91	219.88	219.88	218.59	219.75	219.86	219.87	219.88	182.68	216.14	219.50	219.84	219.87
Q_out	233.46	228.65	223.82	218.95	214.04	209.09	204.09	199.03	193.90	188.70	183.40	197.12	194.24	193.88	193.91	193.90	192.98	193.79	193.86	193.90	193.89	156.95	190.19	193.53	193.87	193.90
W_net	29.45	29.02	28.59	28.16	27.73	27.29	26.85	26.41	25.97	25.53	25.09	25.69	25.95	26.03	25.97	25.97	25.61	25.95	26.00	25.98	25.98	25.73	25.95	25.97	25.97	25.97
Eff	11.20%	11.26%	11.33%	11.40%	11.47%	11.55%	11.63%	11.72%	11.81%	11.92%	12.03%	11.53%	11.79%	11.84%	11.81%	11.81%	11.72%	11.81%	11.83%	11.81%	11.82%	14.08%	12.01%	11.83%	11.81%	11.81%
	R245fa/R1233zd (200 oC)											**Al2O3**					**CuO**					**Ag**				
	100/0	**90/10**	**80/20**	**70/30**	**60/40**	**50/50**	**40/60**	**30/70**	**20/80**	**10/90**	**0/100**	**0.01**	**0.001**	**0.0001**	**0.00001**	**0.000001**	**0.01**	**0.001**	**0.0001**	**0.00001**	**0.000001**	**0.01**	**0.001**	**0.0001**	**0.00001**	**0.000001**
W_tur	37.64	37.70	37.76	37.81	37.87	37.93	37.98	38.03	38.09	38.14	38.19	37.76	38.06	38.08	38.09	38.09	37.72	38.05	38.09	38.09	38.08	37.72	38.05	38.08	38.09	38.09

W_pump	0.46	0.46	0.46	0.47	0.47	0.47	0.48	0.48	0.48	0.49	0.49	0.52	0.49	0.48	0.48	0.48	0.49	0.48	0.48	0.48	0.48	0.48	0.48	0.48	0.48	0.48
Q_in	354.15	351.99	349.83	347.67	345.52	343.37	341.23	339.08	336.94	334.80	332.66	340.08	337.27	336.97	336.94	336.94	336.05	336.85	336.93	336.95	336.94	299.15	333.15	336.56	336.90	336.93
Q_out	316.97	314.75	312.54	310.33	308.12	305.92	303.72	301.53	299.33	297.14	294.96	302.84	299.70	299.37	299.34	299.33	298.82	299.28	299.33	299.34	299.34	261.90	295.58	298.96	299.30	299.33
W_net	37.18	37.24	37.29	37.35	37.40	37.45	37.50	37.56	37.60	37.65	37.70	37.24	37.57	37.60	37.60	37.60	37.23	37.57	37.60	37.61	37.60	37.24	37.57	37.60	37.60	37.60
Eff	10.50%	10.58%	10.66%	10.74%	10.82%	10.91%	10.99%	11.08%	11.16%	11.25%	11.33%	10.95%	11.14%	11.16%	11.16%	11.16%	11.08%	11.15%	11.16%	11.16%	11.16%	12.45%	11.28%	11.17%	11.16%	11.16%
	R245fa/R1233zd (150 oC)											**Al2O3**					**CuO**					**Ag**				
	100/0	**90/10**	**80/20**	**70/30**	**60/40**	**50/50**	**40/60**	**30/70**	**20/80**	**10/90**	**0/100**	**0.01**	**0.001**	**0.0001**	**0.00001**	**0.000001**	**0.01**	**0.001**	**0.0001**	**0.00001**	**0.000001**	**0.01**	**0.001**	**0.0001**	**0.00001**	**0.000001**
W_tur	32.88	32.92	32.97	33.01	33.05	33.10	33.14	33.18	33.22	33.26	33.29	32.93	33.19	33.22	33.22	33.22	32.88	33.18	33.21	33.23	33.22	32.90	33.19	33.25	33.19	33.22
W_pump	0.46	0.46	0.46	0.47	0.47	0.47	0.48	0.48	0.48	0.49	0.49	0.52	0.49	0.48	0.48	0.48	0.49	0.48	0.48	0.48	0.48	0.48	0.48	0.48	0.48	0.48
Q_in	296.10	294.55	293.00	291.45	289.91	288.37	286.83	285.30	283.76	282.23	280.70	286.84	284.09	283.80	283.77	283.76	282.84	283.67	283.75	283.76	283.76	246.14	279.99	283.80	283.77	283.76
Q_out	263.68	262.08	260.49	258.91	257.33	255.75	254.17	252.60	251.03	249.46	247.90	254.43	251.38	251.06	251.03	251.03	250.46	250.97	251.02	251.02	251.03	213.72	247.29	251.03	251.06	251.03
W_net	32.42	32.46	32.50	32.54	32.58	32.62	32.66	32.70	32.74	32.77	32.81	32.41	32.70	32.73	32.73	32.74	32.39	32.70	32.73	32.75	32.74	32.42	32.70	32.77	32.71	32.74
Eff	10.95%	11.02%	11.09%	11.17%	11.24%	11.31%	11.39%	11.46%	11.54%	11.61%	11.69%	11.30%	11.51%	11.53%	11.54%	11.54%	11.45%	11.53%	11.54%	11.54%	11.54%	13.17%	11.68%	11.55%	11.53%	11.54%
	R245fa/R1233zd (120 oC)											**Al2O3**					**CuO**					**Ag**				
	100/0	**90/10**	**80/20**	**70/30**	**60/40**	**50/50**	**40/60**	**30/70**	**20/80**	**10/90**	**0/100**	**0.01**	**0.001**	**0.0001**	**0.00001**	**0.000001**	**0.01**	**0.001**	**0.0001**	**0.00001**	**0.000001**	**0.01**	**0.001**	**0.0001**	**0.00001**	**0.000001**
W_tur	29.91	29.95	29.98	30.02	30.05	30.08	30.12	30.15	30.18	30.21	30.24	29.91	30.15	30.17	30.18	30.18	29.83	30.14	30.17	30.20	30.18	29.89	30.15	30.17	30.18	30.18
W_p	0.46	0.46	0.46	0.47	0.47	0.47	0.48	0.48	0.48	0.49	0.49	0.52	0.49	0.48	0.48	0.48	0.49	0.48	0.48	0.48	0.48	0.48	0.48	0.48	0.48	0.48

ump																										
Q_in	262.91	261.67	260.44	259.20	257.97	256.74	255.51	254.29	253.07	251.84	250.62	256.01	253.38	253.10	253.07	253.07	251.92	252.95	253.05	253.06	253.07	215.53	249.30	252.69	253.03	253.06
Q_out	233.46	232.19	230.92	229.65	228.39	227.13	225.87	224.62	223.37	222.12	220.88	226.62	223.71	223.40	223.37	223.37	222.58	223.29	223.36	223.35	223.36	186.11	219.63	223.00	223.33	223.37
W_net	29.45	29.49	29.52	29.55	29.58	29.61	29.64	29.67	29.70	29.72	29.75	29.39	29.66	29.69	29.70	29.70	29.34	29.66	29.69	29.71	29.70	29.41	29.67	29.69	29.70	29.70
Eff	11.20%	11.27%	11.33%	11.40%	11.47%	11.53%	11.60%	11.67%	11.73%	11.80%	11.87%	11.48%	11.71%	11.73%	11.73%	11.73%	11.65%	11.73%	11.73%	11.74%	11.74%	13.65%	11.90%	11.75%	11.74%	11.73%
	R1233zd/R123 (200 oC)											**Al2O3**					**CuO**					**Ag**				
	100/0	**90/10**	**80/20**	**70/30**	**60/40**	**50/50**	**40/60**	**30/70**	**20/80**	**10/90**	**0/100**	**0.01**	**0.001**	**0.0001**	**0.00001**	**0.000001**	**0.01**	**0.001**	**0.0001**	**0.00001**	**0.000001**	**0.01**	**0.001**	**0.0001**	**0.00001**	**0.000001**
W_tur	38.19	37.61	37.02	36.44	35.86	35.27	34.69	34.11	33.52	32.94	32.35	33.23	33.50	33.53	33.52	33.52	33.19	33.49	33.52	33.52	33.51	33.20	33.49	33.52	33.52	33.52
W_pump	0.49	0.48	0.48	0.47	0.46	0.46	0.45	0.45	0.44	0.43	0.43	0.48	0.44	0.44	0.44	0.44	0.45	0.44	0.44	0.44	0.44	0.44	0.44	0.44	0.44	0.44
Q_in	332.66	327.19	321.71	316.19	310.65	305.08	299.48	293.84	288.15	282.42	276.63	291.37	288.49	288.18	288.15	288.15	287.49	288.09	288.14	288.15	288.15	250.78	284.40	287.77	288.11	288.15
Q_out	294.96	290.07	285.16	280.22	275.26	270.27	265.24	260.17	255.07	249.91	244.70	258.62	255.43	255.09	255.07	255.07	254.75	255.04	255.07	255.07	255.08	218.02	251.35	254.69	255.03	255.06
W_net	37.70	37.12	36.55	35.97	35.39	34.82	34.24	33.66	33.08	32.50	31.93	32.75	33.06	33.09	33.08	33.08	32.75	33.05	33.08	33.08	33.07	32.77	33.05	33.08	33.08	33.08
Eff	11.33%	11.35%	11.36%	11.38%	11.39%	11.41%	11.43%	11.46%	11.48%	11.51%	11.54%	11.24%	11.46%	11.48%	11.48%	11.48%	11.39%	11.47%	11.48%	11.48%	11.48%	13.07%	11.62%	11.50%	11.48%	11.48%
	R1233zd/R123 (150 oC)											**Al2O3**					**CuO**					**Ag**				
	100/0	**90/10**	**80/20**	**70/30**	**60/40**	**50/50**	**40/60**	**30/70**	**20/80**	**10/90**	**0/100**	**0.01**	**0.001**	**0.0001**	**0.00001**	**0.000001**	**0.01**	**0.001**	**0.0001**	**0.00001**	**0.000001**	**0.01**	**0.001**	**0.0001**	**0.00001**	**0.000001**
W_tur	33.29	32.78	32.27	31.75	31.24	30.72	30.21	29.70	29.18	28.67	28.15	28.93	29.17	29.21	29.18	29.19	28.86	29.15	29.18	29.19	29.18	28.90	29.15	29.21	29.15	29.18
W_pump	0.49	0.48	0.48	0.47	0.46	0.46	0.45	0.45	0.44	0.43	0.43	0.48	0.44	0.44	0.44	0.44	0.45	0.44	0.44	0.44	0.44	0.44	0.44	0.44	0.44	0.44

Q_in	280.70	276.13	271.53	266.91	262.26	257.57	252.86	248.11	243.31	238.46	233.56	246.35	243.63	243.34	243.31	243.31	242.45	243.22	243.30	243.31	243.31	206.03	239.57	243.35	243.31	243.31
Q_out	247.90	243.83	239.74	235.62	231.48	227.31	223.10	218.86	214.57	210.23	205.84	217.90	214.90	214.57	214.57	214.55	214.03	214.51	214.55	214.55	214.57	177.57	210.86	214.58	214.60	214.57
W_net	32.81	32.30	31.79	31.28	30.77	30.27	29.76	29.25	28.74	28.23	27.72	28.45	28.73	28.77	28.74	28.75	28.42	28.71	28.75	28.75	28.74	28.46	28.71	28.77	28.71	28.74
Eff	11.69%	11.70%	11.71%	11.72%	11.73%	11.75%	11.77%	11.79%	11.81%	11.84%	11.87%	11.55%	11.79%	11.82%	11.81%	11.82%	11.72%	11.80%	11.81%	11.82%	11.81%	13.82%	11.98%	11.82%	11.80%	11.81%
	R1233zd/R123 (120 oC)											**Al2O3**					**CuO**					**Ag**				
	100/0	**90/10**	**80/20**	**70/30**	**60/40**	**50/50**	**40/60**	**30/70**	**20/80**	**10/90**	**0/100**	**0.01**	**0.001**	**0.0001**	**0.00001**	**0.000001**	**0.01**	**0.001**	**0.0001**	**0.00001**	**0.000001**	**0.01**	**0.001**	**0.0001**	**0.00001**	**0.000001**
W_tur	30.24	29.76	29.29	28.82	28.35	27.88	27.41	26.93	26.46	25.99	25.51	26.21	26.44	26.46	26.45	26.48	26.10	26.42	26.46	26.48	26.48	26.21	26.44	26.46	26.46	26.46
W_pump	0.49	0.48	0.48	0.47	0.46	0.46	0.45	0.45	0.44	0.43	0.43	0.48	0.44	0.44	0.44	0.44	0.45	0.44	0.44	0.44	0.44	0.44	0.44	0.44	0.44	0.44
Q_in	250.62	246.55	242.45	238.33	234.18	230.00	225.78	221.53	217.23	212.89	208.49	220.04	217.53	217.26	217.23	217.23	215.88	217.10	217.22	217.23	217.23	179.99	213.49	216.86	217.19	217.23
Q_out	220.88	217.27	213.64	209.98	206.29	202.58	198.83	195.04	191.21	187.33	183.40	194.30	191.53	191.24	191.22	191.19	190.23	191.11	191.20	191.19	191.19	154.21	187.50	190.84	191.17	191.21
W_net	29.75	29.28	28.82	28.35	27.89	27.42	26.95	26.49	26.02	25.55	25.09	25.73	26.00	26.02	26.01	26.04	25.65	25.98	26.02	26.04	26.04	25.78	26.00	26.02	26.02	26.02
Eff	11.87%	11.88%	11.89%	11.90%	11.91%	11.92%	11.94%	11.96%	11.98%	12.00%	12.03%	11.69%	11.95%	11.98%	11.97%	11.99%	11.88%	11.97%	11.98%	11.99%	11.99%	14.32%	12.18%	12.00%	11.98%	11.98%

Mixture Set 2 Results Table

R1224yd(Z)/R1336mzz(Z)

Nano Particle	NPF	COND	EVAPO	PUMP	TURBINE	Wtur	Wpump	Qevap	Qcond	Wnet	Efficiency
TiO	0.0001	654.67	-938.48	-941.02	801.60	146.93	2.54	1740.08	1595.69	144.39	8.30%
	0.001	649.50	-942.35	-944.89	796.27	146.76	2.54	1738.61	1594.39	144.22	8.30%
	0.01	598.60	-981.04	-983.56	744.07	145.47	2.52	1725.11	1582.16	142.95	8.29%
	0.1	89.78	-1368.03	-1370.41	222.08	132.30	2.38	1590.11	1460.19	129.92	8.17%
ZnO	0.0001	654.80	-938.25	-940.79	801.72	146.92	2.54	1739.96	1595.58	144.38	8.30%
	0.001	651.82	-940.01	-942.55	798.59	146.77	2.54	1738.60	1594.37	144.23	8.30%
	0.01	621.80	-957.65	-960.19	767.30	145.50	2.53	1724.95	1581.99	142.96	8.29%
	0.1	322.12	-1134.18	-1136.66	454.41	132.30	2.48	1588.59	1458.77	129.82	8.17%
Ag	0.0001	655.61	-937.76	-940.30	802.25	146.64	2.54	1740.01	1595.90	144.10	8.28%
	0.001	659.96	-935.11	-937.65	803.90	143.94	2.54	1739.01	1597.61	141.40	8.13%
	0.01	633.54	-908.65	-911.17	779.00	145.46	2.52	1687.65	1544.71	142.94	8.47%
	0.1	439.10	-646.42	-648.71	571.41	132.31	2.29	1217.82	1087.80	130.02	10.68%

R1224yd(Z)/R1233zd(E)

TiO	0.0001	645.59	-957.09	-959.64	795.17	149.58	2.55	1752.26	1605.23	147.04	8.39%
	0.001	640.56	-960.95	-963.49	789.96	149.40	2.55	1750.90	1604.05	146.85	8.39%
	0.01	589.73	-999.50	-1002.03	737.81	148.08	2.53	1737.31	1591.77	145.55	8.38%
	0.1	81.69	-1385.04	-1387.43	216.35	134.66	2.39	1601.39	1469.12	132.27	8.26%
ZnO	0.0001	645.86	-956.86	-959.40	795.41	149.55	2.55	1752.26	1605.26	147.00	8.39%
	0.001	642.87	-958.61	-961.15	792.28	149.41	2.55	1750.89	1604.03	146.86	8.39%
	0.01	612.98	-976.12	-978.66	761.04	148.07	2.54	1737.16	1591.63	145.53	8.38%
	0.1	314.03	-1151.18	-1153.67	448.68	134.65	2.48	1599.86	1467.70	132.16	8.26%
Ag	0.0001	646.28	-956.37	-958.91	795.52	149.24	2.55	1751.89	1605.20	146.69	8.37%
	0.001	647.15	-953.71	-956.25	793.45	146.30	2.55	1747.16	1603.40	143.76	8.23%
	0.01	624.68	-927.14	-929.66	772.75	148.07	2.52	1699.89	1554.34	145.55	8.56%
	0.1	431.05	-663.75	-666.05	565.72	134.67	2.29	1229.48	1097.10	132.38	10.77%

R1233zd(E)/R1336mzz(Z)

TiO	0.0001	106.32	-141.92	-142.33	128.82	22.50	0.41	270.74	248.65	22.09	8.16%
	0.001	101.73	-146.49	-146.90	124.20	22.47	0.41	270.69	248.62	22.06	8.15%
	0.01	55.75	-192.17	-192.58	78.02	22.27	0.41	270.20	248.34	21.86	8.09%
	0.1	-403.99	-647.18	-647.68	-383.73	20.26	0.50	263.45	243.69	19.76	7.50%
ZnO	0.0001	106.56	-141.69	-142.10	129.05	22.49	0.41	270.74	248.65	22.08	8.16%
	0.001	104.05	-144.15	-144.56	126.52	22.47	0.41	270.67	248.61	22.06	8.15%
	0.01	79.00	-168.79	-169.22	101.26	22.26	0.42	270.05	248.22	21.84	8.09%
	0.1	-171.65	-413.54	-414.10	-151.39	20.25	0.55	262.15	242.45	19.70	7.51%
Ag	0.0001	107.37	-141.20	-141.61	129.58	22.21	0.41	270.78	248.98	21.80	8.05%
	0.001	109.12	-139.25	-139.66	131.84	22.72	0.41	271.10	248.78	22.31	8.23%
	0.01	90.72	-119.94	-120.35	112.99	22.27	0.40	232.93	211.06	21.87	9.39%
	0.1	-54.36	58.41	58.04	-34.06	20.30	0.36	-92.46	-112.40	19.94	-21.56%